CALIFORNIA INSTITUTE OF TECHNOLOGY

EARTHQUAKE ENGINEERING RESEARCH LABORATORY

RESPONSE OF SIMPLE YIELDING STRUCTURES TO EARTHQUAKE EXCITATION

by

Paul C. Jennings

Pasadena, California

June 1963

RESPONSE OF SIMPLE YIELDING STRUCTURES TO EARTHQUAKE EXCITATION

Thesis by

Paul Christian Jennings

In Partial Fulfillment of the Requirements

For the Degree of

Doctor of Philosophy

California Institute of Technology

Pasadena, California

1963

TABLE OF CONTENTS

ACKNOWLEDGEMENTS

The author wishes to thank Professor G. W. Housner for his guidance and assistance in the preparation of the thesis. The interest and help of Professors T. K. Caughey, D. E. Hudson and J. N. Franklin also is appreciated.

The author is grateful for fellowships granted during the research by the Ford Foundation and the General Electric Foundation.

ABSTRACT

A method is developed for generating a random process that has the pertinent properties of recorded strong-motion earthquake accelerograms. The model accelerograms are sections of a stationary, Gaussian, random process with a power spectral density found from the average undamped velocity spectrum. Eight pseudo-earthquakes of thirty seconds duration are generated on the digital computer and the velocities, displacements, and velocity spectra calculated. The average velocity spectra of the real and pseudo-earthquakes correspond closely and the velocities, displacements, and velocity spectra of the real and pseudo-earthquakes exhibit similar statistical behavior. It is concluded that the pseudo-earthquakes are satisfactory models of strong-motion earthquakes for the purposes of structural analysis.

A general nonlinear hysteretic force-deflection relation for dynamic studies is presented. The relation is a continuous, smooth function and includes the linear and elasto-plastic relations as limiting cases. The steady-state response to sinusoidal excitation is studied in detail and the results presented. It is concluded that the hysteretic relation is general enough to be useful in structural analysis and that comparison of test results and theory may enable the dynamic force-deflection relations of real structures to be approximated.

A class of yielding structures suitable for earthquake response studies is defined by the geometry of the hysteresis curves and the law describing yielding behavior. The general yielding relation is included in this class as are the linear, the elasto-plastic and the bilinear hysteretic relations. The equation of motion and the energy equation

for the response of yielding structures to earthquake motion are examined and a typical yielding structure is subjected to the ensemble of pseudo-earthquakes.

I. INTRODUCTION

The response of a structure to earthquake motion is, in general, a complicated process that is impossible to analyze without making simplifying assumptions. The response of many relatively simple structures can be idealized as that of a one degree-of-freedom oscillator whose base is excited by the earthquake acceleration, as shown in figure 1. An understanding of the behavior of this structure during earthquake motion is valuable not only for its immediate application, but also because it is the basic element for analysis of more complicated structures. It is the response of this one degree-of-freedom structure to earthquake excitation that is the general subject of the thesis.

The response of the structure shown in figure 1 relative to its base is the same as that of a structure on an immovable base whose mass is excited by the force $-m\ddot{y}(t)$, where m is the mass of the structure and $\ddot{y}(t)$ is the earthquake acceleration. For this reason the acceleration is the most important measurement of earthquake motion for the purposes of structural analysis. Two strong-motion earthquake accelerograms are shown in figures 2 and 3, and other acceleration records can be found in reference 1. The statistical, rather than deterministic, nature of the earthquake excitation is apparent from examination of the figures. In figures 4 and 5 are shown the ground velocities and displacements associated with the accelerograms. These velocities and displacements were obtained by integrating the acceleration record and are taken from reference 2.

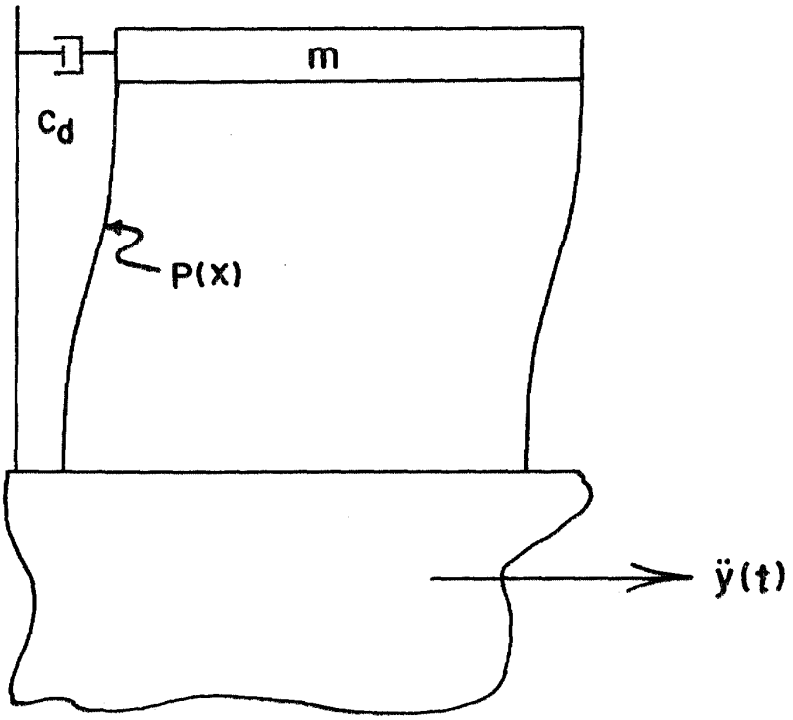

FIGURE NO. 1

A ONE DEGREE OF FREEDOM OSCILLATOR

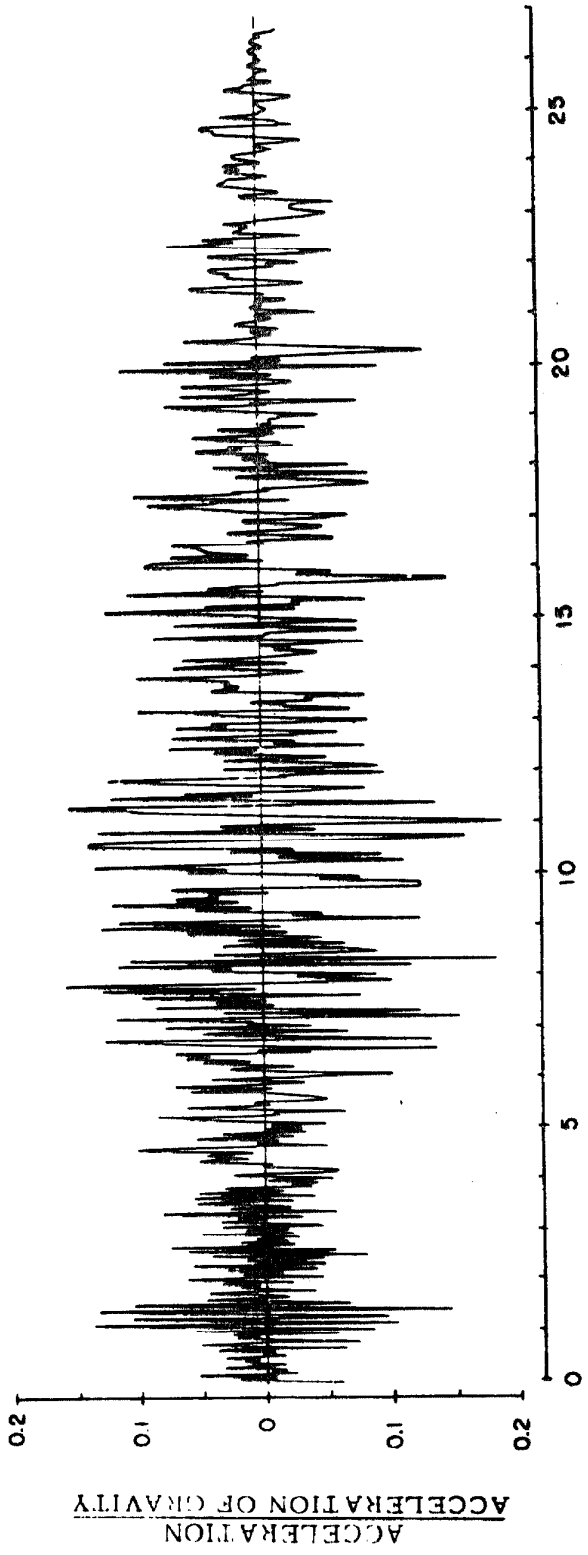

Figure No. 2

Accelerogram for the Olympia, Washington Earthquake of April 13, 1949, S 10^{o} E Component.

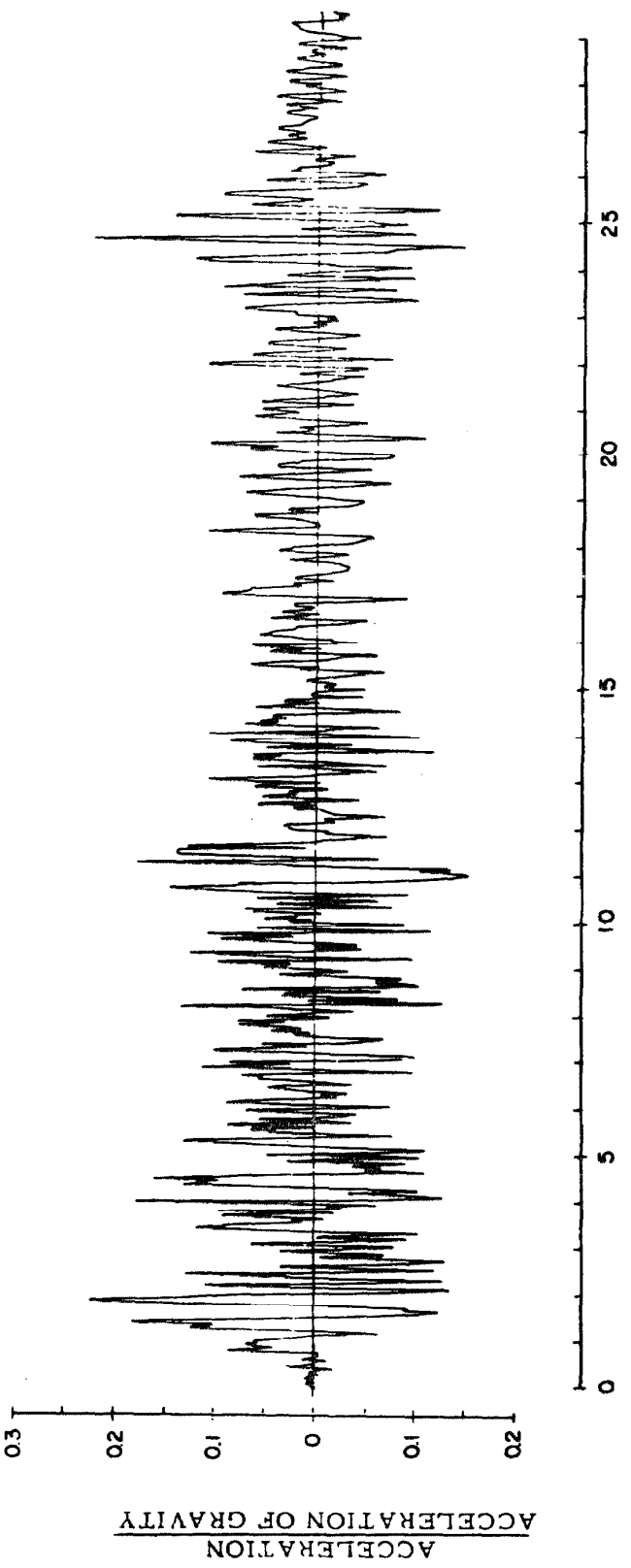

Figure No. 3

Accelerogram for the El Centro, California Earthquake of May 18, 1940, E-W Component.

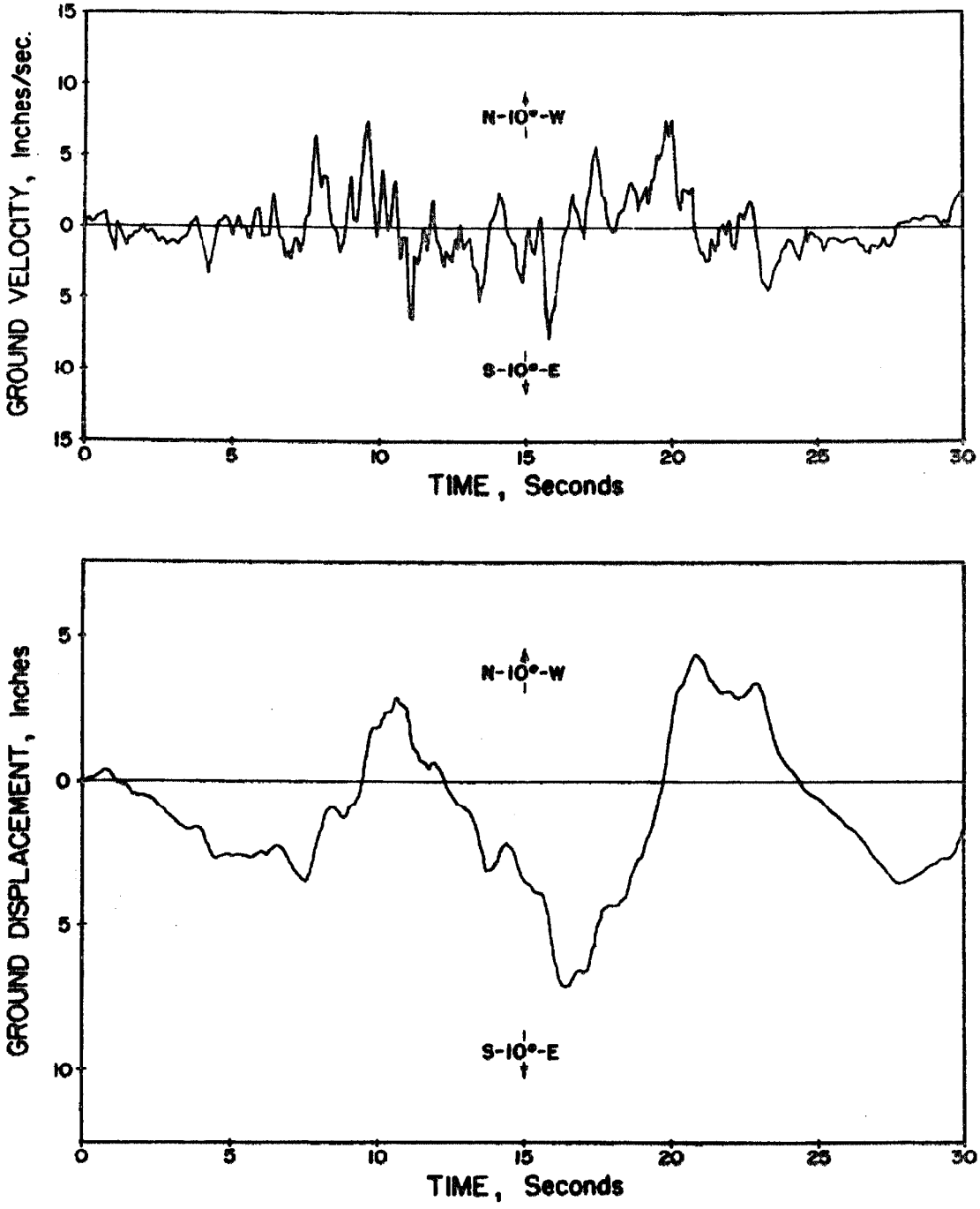

OLYMPIA, 1949 N-10°-W COMPONENT

Figure No. 4

Ground Velocity and Displacement, Olympia, 1949, S 10°E Component.

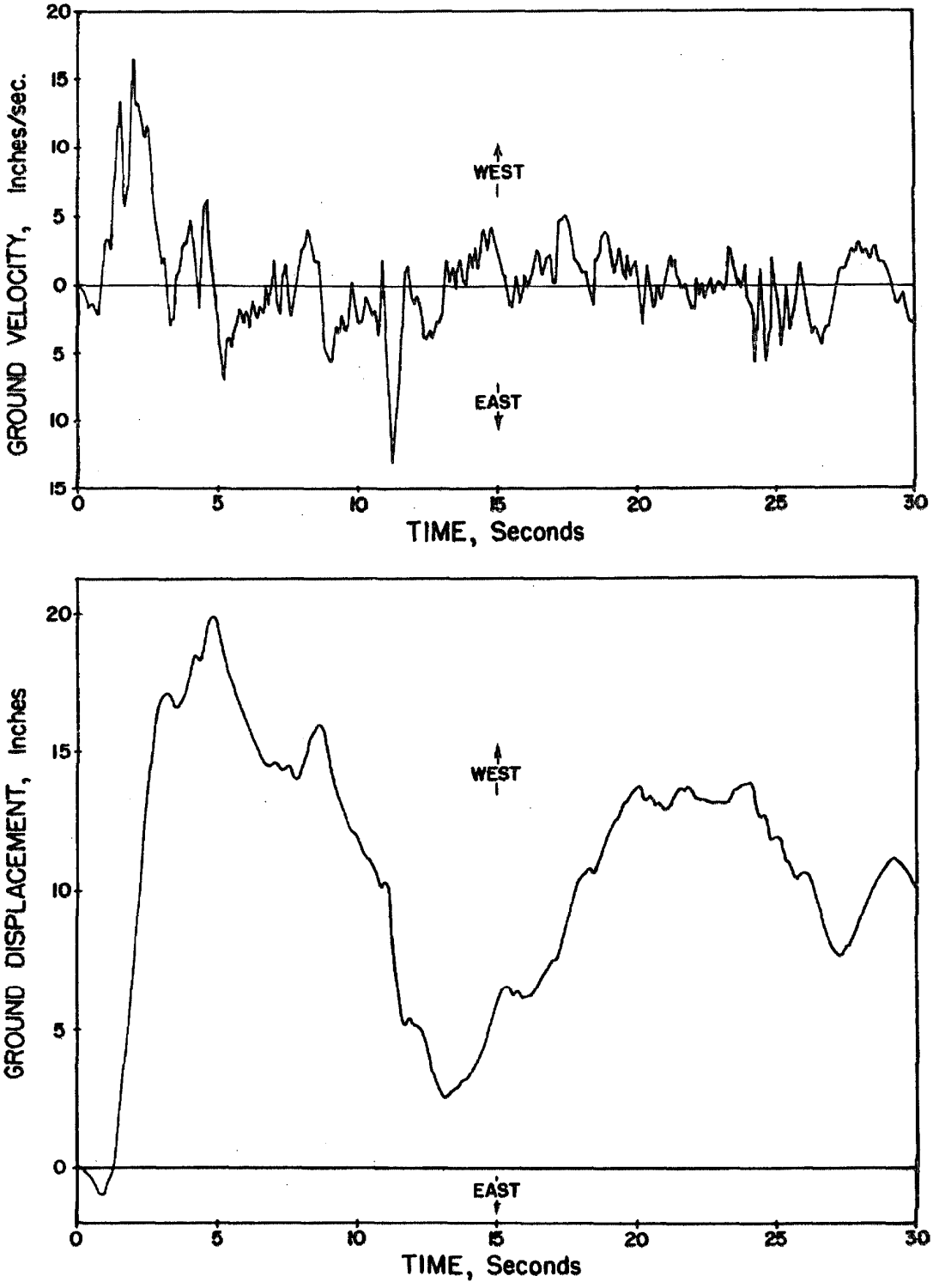

EL CENTRO, 1940 E-W COMPONENT

Figure No. 5

Ground Velocity and Displacement, El Centro, 1940, E-W Component.

To characterize the response of a linear one degree-of-freedom structure to earthquake ground motion, the response spectra are calculated.[1] The velocity response spectrum is defined as the maximum absolute value of the relative velocity of a linear structure subjected to the earthquake excitation. Similar definitions apply to the acceleration and displacement response spectra. The spectrum values are dependent upon the natural period and viscous damping of the structure and the nature of the response spectra has been the object of much study.[1, 3, 4, 5] By using the eight components of the four strongest ground motions recorded to date, G. W. Housner determined the average velocity spectrum shown in figure 6.[4] With this average the expected value of the response of a one degree-of-freedom linear structure can be estimated and by normal mode techniques the response of more complicated linear structures can be approximated. As a consequence of the statistical character of the response spectra the probability distribution of the response, as well as the expected value, is of interest and has been the subject of recent studies.[6-10] Because of the statistical nature of earthquake ground motions the information obtained from structural response studies using a single earthquake record is limited and it would be desirable to have a large sample of recorded strong earthquake accelerograms. However, since there are relatively few suitable instruments installed throughout the world it is only occasionally that ground motion is recorded. For this reason it is desirable to develop a practical method of constructing

FIGURE NO. 6

AVERAGE OF EARTHQUAKE VELOCITY SPECTRA

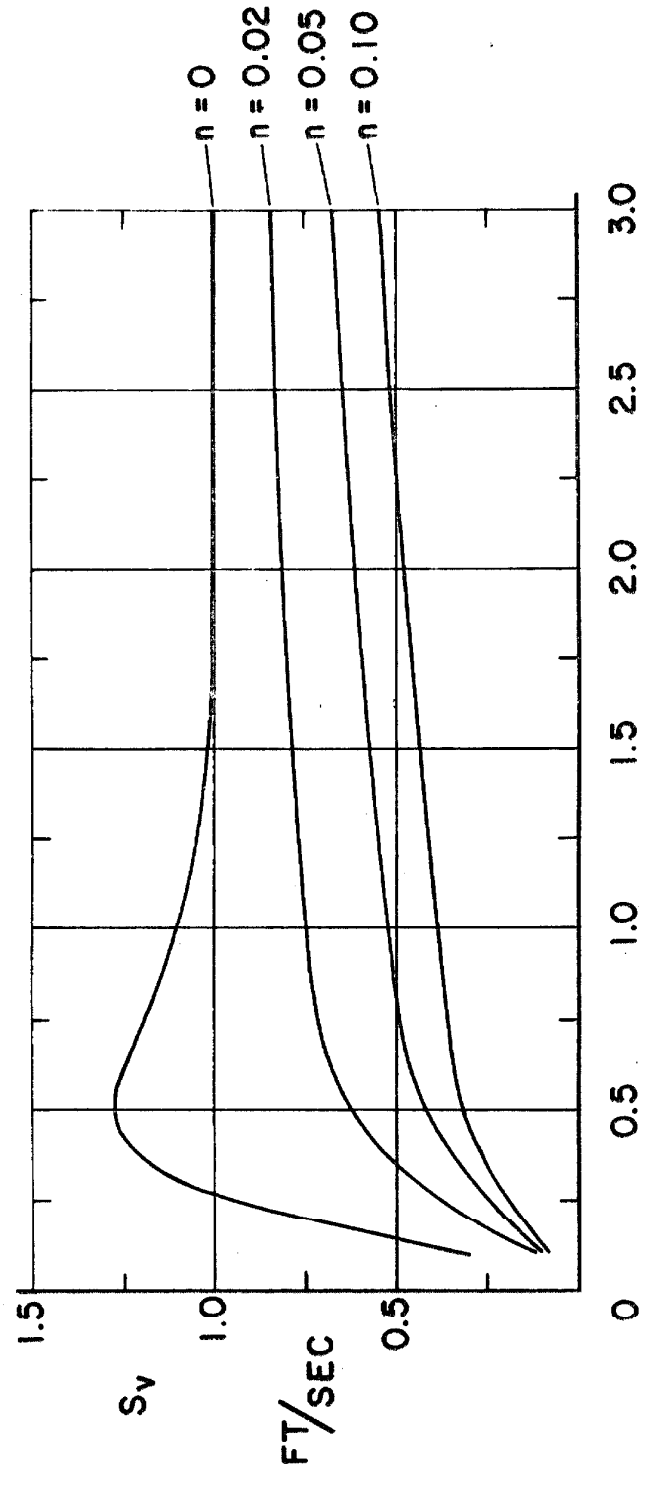

random functions that can be used in place of earthquake accelerograms in making studies of the response of structures.

The methods of linear analysis have not been able to satisfactorily describe the response of structures to strong earthquakes. As has been shown by R. W. Clough[11, 12] and S. S. Thomaides[13], linear analysis predicts forces in the structure significantly in excess of design code requirements, yet structures with less strength than required by building codes have withstood strong earthquakes with only moderate damage. It is apparent from examination of structures after strong earthquakes that yielding has occurred in structural elements and the study of nonlinear yielding structures has been undertaken in an effort to explain structural behavior during earthquakes. The earthquake response of a one degree-of-freedom elasto-plastic structure has been studied by many investigators including R. Tanabashi,[14, 15] A. S. Veletsos and N. M. Newmark,[16] J. Penzien,[17] S. S. Thomaides,[13] G. N. Bycroft[18, 19] and G. W. Housner.[20, 4, 21] The response of multistory structures with elasto-plastic elements has been the subject of research by G. V. Berg[22, 23, 24] and others.[25, 26]

The bilinear hysteretic force-deflection relation is a more general yielding relation than the elasto-plastic. It has been the object of detailed investigations by W. D. Iwan[27] and T. K. Caughey.[28, 29] The earthquake response studies using a bilinear hysteretic relation include references 30, 31, and 13. Other types of nonlinear hysteretic force-deflection relations have been studied by L. S. Jacobsen,[32, 33]

N. Ando,[31] and R. Tanabashi and K. Kaneta.[34] A detailed study of the steady-state response of a certain class of nonlinear hysteretic oscillators has been performed by G. S. Pisarenko.[35] The wide interest in the application of nonlinear hysteretic properties to earthquake response studies is shown by the recent work of Japanese investigators in this area.[34, 36-39]

The present study consists of three nearly independent parts. In the first part a simple statistical model for strong-motion earthquake accelerograms is derived with which pseudo-earthquakes can be generated on the digital computer. From comparison of the properties of the real and pseudo-earthquakes it is concluded that the pseudo-earthquakes are satisfactory representations of strong motion earthquakes for the purposes of structural analysis and may be used in lieu of the non-available true earthquake accelerograms.

The second chapter is concerned with the development and analysis of a general nonlinear hysteretic force-deflection relation. This relation covers a wide range of yielding structures and includes the linear and elasto-plastic as limiting cases. From the response to sinusoidal excitation it is concluded that the hysteretic formulation is general enough to be useful in structural analysis. In addition, by comparing test results with theory it may be possible to approximate the dynamic force-deflection relations of real structures.

In the third part of the thesis the response of yielding structures to earthquake excitation is studied. A class of nonlinear yielding structures, including the general yielding structure, is defined by

the law governing yielding response and by the geometry of the hysteresis curves. The equations describing the response of yielding structures are examined, and to illustrate the application of the pseudo-earthquakes in structural analysis and to demonstrate the behavior of the yielding structures, a typical member of the family of yielding oscillators is subjected to the ensemble of pseudo-earthquakes. From the results it is concluded that the class of hysteretic structures may provide a means for investigating the yielding response of actual structures.

It is hoped that this study furthers the understanding of the response of structures to strong-motion earthquakes and that the results will be useful to other investigators in this field.

II. A SIMPLE STATISTICAL MODEL OF STRONG-MOTION EARTHQUAKE ACCELEROGRAMS

A. Introduction

This chapter is concerned with the derivation of a simple statistical model of strong-motion earthquake accelerograms and with the generation of an ensemble of samples of this model on the digital computer. A formula for the average velocity spectra as a function of damping, natural frequency, and duration of the earthquake ensemble also is developed.

The first investigator to model earthquake acceleration as a random process was G. W. Housner.[40] He considered the acceleration as a series of pulses of a certain magnitude located randomly in time. With this model, spectra could be obtained similar to the velocity spectra available at that time (1947). In a later paper[41] he considered the accelerograms as the sum of full period sine wave pulses distributed randomly in time with frequency and amplitude taken from a calculated probability distribution. Using this model spectra similar to those shown in figure 6 could be obtained.

In more recent years several investigators, including D. E. Hudson,[3] G. N. Bycroft[19] and E. Rosenblueth[7, 10] have modeled earthquake accelerograms by white noise. Although white noise is physically impossible, the velocity spectra obtained by these investigators using this process are similar to those obtained from earthquake acceleration records, with the exception that the undamped

velocity spectrum is a constant, independent of the period.

J. L. Bogdanoff, J. E. Goldberg and M. C. Bernard[9] have modeled earthquake accelerograms by a non-stationary random process in which the accelerogram is composed of a sum of damped sinusoids. Their process appears to have the capability of modeling the weak tail as well as the strong primary phase of the ground motion.

In principle there is no difficulty in constructing random functions with specified ensemble average properties. From a practical point of view, however, if use is to be made of the sample functions it is virtually essential that the process be automated, that is, the process should be constructed so that all of the work is done on a digital computer without the necessity of doing hand labor at any stage of the process. The work described in this chapter has as its objective the development of such an automated process.

In this chapter earthquake accelerograms are modeled by sections of a stationary, Gaussian, random process with a power spectral density determined from an extension of an approximate theory developed by Rosenblueth.[10] An ensemble of eight 30 second long sections of a random process with this power spectral density are generated on the digital computer and the average of the velocity spectra of these pseudo-earthquakes is compared to the average earthquake spectra. The thirty second duration was chosen for the pseudo-earthquakes as it is estimated to be the duration of the strong phase of the accelerogram of a Magnitude 8 earthquake, and hence corresponds to the estimated length of the strongest possible ground

shaking. Because the duration of the accelerograms used to determine the average spectra is generally less than thirty seconds, an approximate formula is developed to determine the effect of the ensemble duration upon the spectrum averages. Using this formula it is possible to compare the ensemble of pseudo-earthquakes to the ensemble of real earthquakes and thereby produce an ensemble of eight model accelerograms which appear to possess, individually and on the average, the known properties of strong-motion earthquake records.

Graphs of the acceleration, velocity and displacement of two of the pseudo-earthquakes are presented along with individual velocity spectra of the entire ensemble. A comparison of the approximate spectrum formula with the average earthquake spectra and the average pseudo-earthquake spectra is presented also. Other results include an approximate expression for the power spectral density of strong-motion earthquakes and scale factors by which the ensemble should be multiplied to produce an ensemble typifying certain past earthquakes.

Some results from random vibration theory are assumed in the following presentation. General references in this subject include 42-47.

A list of the symbols to be used is given below and they are defined again where they first appear in the text.

LIST OF SYMBOLS

Symbol	Explanation or Definition
a, b, c	constants in the power spectral density formula
c_0, c_1, c_2	constants for least square fit of a cubic to ground velocity
c_d	viscous damping coefficient
$h(\tau)$	weighting function for a linear differential equation
i	$\sqrt{-1}$
i, j	subscripts
k	left superscript used to denote the k^{th} member of an ensemble or set
k_s	spring constant of a linear oscillator
m	mass of a linear oscillator
n	fraction of critical damping of a linear, viscously damped oscillator
q	intensity of a white noise as defined by E. Rosenblueth[10]
r	upper limit of a summation index
t	time
t'	duration of an acceleration record
t_o	equivalent duration of strong-motion earthquakes
v_i	magnitude of an acceleration impulse
x	relative displacement of a linear oscillator
$\ddot{y}(t)$	acceleration of an earthquake-type excitation
z	dummy variable

Symbol	Explanation or Definition
E	energy possessed by an oscillator
E_i	energy imparted by an acceleration impulse
E_D	energy dissipated by an oscillator
E_I	energy input to an oscillator
$F(t)$	acceleration
$G(\omega)$	power spectral density
$k_{N(t)}$	member of a white noise ensemble
SI_n	spectrum intensity for the damping value n
$S_v(n, \omega, t)$	velocity spectrum as a function of damping and natural period of the oscillator and of the duration of the excitation
T	natural period of a linear oscillator, $T=2\pi/\omega$
k_β, k_γ	uncorrelated numbers from a Gaussian distribution with mean zero and variance one
$\delta(t)$	Dirac delta function
λ	number of acceleration impulses per second
μ, ν	constants in the average spectra formula
σ^2	variance of the acceleration impulses
σ_N^2	variance of white numbers
τ	dummy time variable
ω	frequency, natural frequency of a linear oscillator
Δh	time interval
$\langle \quad \rangle_k$	symbol meaning the average with respect to k of the variable contained within the angles

B. Generation of the Random Process

Power Spectral Density of a Series of Pulses

Some previous studies of earthquake response[40, 3, 6, 7, 10] have assumed that the earthquake acceleration consisted of a series of impulses distributed randomly in time. The response of a linear, undamped, one degree-of-freedom oscillator, such as shown in figure 1, to this representation of the earthquake is described by

$$\ddot{x}(t) + \omega^2 x(t) = -\sum_{i=1}^{r} v_i \, \delta(t-t_i) \qquad (2.1)$$

where x is the displacement of the oscillator with respect to the base, ω is the natural frequency of the oscillator, t is time, v_i is the impulse magnitude and $\delta(t)$ is the Dirac delta function. The power spectral density of this type of random excitation may be derived by considering an ensemble of accelerograms:

$$\begin{aligned}
{}^1\ddot{y}(t) &= \sum_{i=1}^{r} {}^1v_i \, \delta(t-t_i) \\
{}^2\ddot{y}(t) &= \sum_{i=1}^{r} {}^2v_i \, \delta(t-t_i) \\
&\vdots \qquad\qquad \vdots \\
{}^k\ddot{y}(t) &= \sum_{i=1}^{r} {}^kv_i \, \delta(t-t_i) \qquad (2.2) \\
&\vdots \qquad\qquad \vdots
\end{aligned}$$

where ${}^{k}\ddot{y}(t)$ is the acceleration of the ground and the superscript on the left indicates the particular member of the ensemble. Let $\{{}^{k}v_i\} = {}^{1}v_i, \ldots, {}^{k}v_i, \ldots$ be the set of possible amplitudes of the pulses recurring at time t_i and let the ${}^{k}v_i$ be mutually independent random variables with mean zero and variance σ^2, the averages being taken over k. These properties can be written as

$$\begin{aligned} \left\langle {}^{k}v_i \right\rangle_k &= 0 \\ \left\langle {}^{k}v_i \, {}^{k}v_i \right\rangle_k &= \sigma^2 \\ \left\langle {}^{k}v_i \, {}^{k}v_j \right\rangle_k &= 0 \qquad i \neq j \end{aligned} \tag{2.3}$$

where the symbol $\langle \quad \rangle_k$ indicates that an average is taken over the ensemble of the variable within the angles. It is further assumed that the average number of impulses per second, denoted by λ, is the same for each member of the ensemble and that λ and the properties given by equation 2.3 are independent of time.

The phenomenon described by these assumptions is the well-known "shot effect".[45, 42] The power spectral density of this process is

$$G(\omega) = \frac{\lambda \sigma^2}{\pi} \tag{2.4}$$

Since the power spectral density is constant, excitations of this type are a form of white noise. Furthermore, if λ tends to infinity and σ^2 tends to zero in such a manner that $\lambda\sigma^2$ is constant, the process defined by equations 2.2 and 2.3 can be shown to be Gaussian by appealing to the central limit theorem.

E. Rosenblueth, of the University of Mexico, has used the process of equations 2. 2 and 2. 3 as a model for earthquake accelerations in some of his recent studies.[6, 7, 10] In these studies the intensity, q, of the acceleration is defined by

$$2q = \lim_{t_2 \to t_1} \frac{\left\langle \sum_{t=t_1}^{t_2} {}_k v_i^{\,2} \right\rangle_k}{t_2 - t_1} \qquad (2.5)$$

$$(t_2 > t_1)$$

It is seen that q is related to the power spectral density for the average value of the sum in equation 2. 5 is $\lambda \sigma^2 (t_2 - t_1)$. It thus follows that

$$2q = \lambda \sigma^2. \qquad (2.6)$$

Extension of Rosenblueth's Approximate Theory

Consider an ensemble of undamped one degree-of-freedom linear structures of the type shown in figure 1; the base of each structure being excited by an acceleration of the type discussed above. The equations of motion are

$$\begin{aligned}
&{}^1\ddot{x}(t) + \omega^2\, {}^1x(t) = -{}^1\ddot{y}(t) \\
&{}^2\ddot{x}(t) + \omega^2\, {}^2x(t) = -{}^2\ddot{y}(t) \\
&\quad\vdots \qquad\qquad\quad \vdots \qquad\quad \vdots \\
&{}^k\ddot{x}(t) + \omega^2\, {}^kx(t) = -{}^k\ddot{y}(t) \\
&\quad\vdots \qquad\qquad\quad \vdots \qquad\quad \vdots
\end{aligned} \qquad (2.7)$$

where ${}^{k}\ddot{y}(t)$ is defined by equations 2. 2 and 2. 3, and has the power spectral density given by equation 2. 4. These equations approximate the response of an undamped structure to a series of earthquakes; ${}^{1}x(t)$ is the relative displacement of the structure in response to the first acceleration ${}^{1}\ddot{y}(t)$, etc. In a recent paper[10] Rosenblueth has developed an approximate theory, based on a diffusion analogy, for the probability distribution of the response, and in a discussion of this paper T. K. Caughey and A. H. Gray* derive the basic equations of the theory from the Fokker-Planck equation and present an analysis of the errors involved in the approximations. One of the results of the theory relates the power spectral density of the white noise acceleration to a measure of the maximum energy of the oscillator:

$$\left\langle \sqrt{k_x^2 + \omega^2 k_x^2}_{\max} \right\rangle_k = 1.174 \sqrt{\lambda \sigma^2 t_o} \qquad (2.8)$$

where t_o is the duration of each member of the acceleration ensemble. With this result the power spectral density of strong-motion earthquake accelerograms can be approximated from the average undamped velocity spectrum shown in figure 6.

The deduction of the power spectral density requires that the following two assumptions be made:

1. ${}^{k}S_v = \sqrt{k_x^2 + \omega^2 k_x}_{\max}$, where ${}^{k}S_v$ is the undamped velocity spectrum value.

---

* To be published in the Proceedings of the American Society of Civil Engineers, Journal of the Engineering Mechanics Division.

2. The response, as measured by $\langle {}^{k}S_v \rangle_{k'}$ of an ensemble of linear structures with natural frequency ω to earthquake acceleration is the same as the response to white noise excitation provided that the power spectral density of the white noise is chosen equal to the power spectral density of earthquake acceleration at the frequency ω.

Since S_v is usually calculated as the maximum value of the relative velocity, assumption 1 introduces little error provided that $\omega^2 x^2$ is small when $\dot{x}$ is at its maximum. As the response of an undamped structure to earthquake acceleration is quasi-sinusoidal this provision usually holds. Rephrased, assumption 1 states that the maximum energy acquired by the structure is $1/2\ mS_v^2$, where m is the mass of the structure; this is the more common form of this assumption.[3, 4]

The second assumption is similar to that commonly made in noise theory in studying the response of a narrow band-pass filter to a broad spectrum noise. A mathematical examination of the second assumption is included in the discussion of reference 10 by Caughey and Gray, the physical reasoning behind the assumption is as follows. For the range of natural frequencies of greatest interest in the earthquake problem the duration of strong-motion earthquakes is at least several times as long as the period of the oscillator used to determine S_v, so the undamped velocity spectrum is essentially a measure of a resonance phenomenon. Although the earthquake delivers power at many frequencies, the response of the undamped

oscillator is determined mainly by the power delivered at or near its natural frequency and power delivered at frequencies far removed from the natural frequency has relatively little effect on the response. It follows that the response of the oscillator to the earthquake acceleration is approximately the same as the response to a white noise, provided that the power spectral density of the earthquake acceleration is sufficiently smooth and is equal to that of the white noise at the natural period of the oscillator.

The application of these assumptions to equation 2. 8 produces

$$\left\langle {}^{k}S_{v}(0,\omega,t_{o}) \right\rangle_{k} = 1.174\sqrt{\pi G(\omega)t_{o}} \qquad (2.9)$$

where equation 2. 4 has been used to replace the power spectral density of the white noise and the zero in the argument of S_v represents the damping factor. If t_o were known, this equation could be solved for $G(\omega)$ using the undamped velocity spectrum of figure 6 and standard techniques could be applied to generate samples of the random process. However, the accelerograms used to construct figure 6 vary in length, so for the application of this equation t_o must signify an equivalent duration, a constant as yet unknown. Solving equation 2. 9 for $G(\omega)$ one obtains

$$G(\omega) = \frac{0.2304}{t_{o}} \left[\left\langle {}^{k}S_{v}(0,\omega,t_{o}) \right\rangle_{k} \right]^{2} \qquad (2.10)$$

It is highly convenient to fit a simple, algebraic function to the relation given by equation 2. 10. The functional form used is that developed by H. Tajima[48] from the work of K. Kanai:[49]

$$G(\omega) = \frac{a\left(1 + 4b^2 \frac{\omega^2}{c^2}\right)}{\left(1 - \frac{\omega^2}{c^2}\right)^2 + 4b^2 \frac{\omega^2}{c^2}} \qquad (2.11)$$

where a, b and c are constants. To obtain agreement with equation 2.10 in the range from $\omega = 2.1$ (corresponding to a natural period T=3 seconds) to $\omega = 21$ (T=0.3 seconds) these constants are given values:

$$a = 0.2196/t_o$$
$$b^2 = 0.410 \qquad (2.12)$$
$$c^2 = 242$$

The agreement between equations 2.11 and 2.10, when t_o is given an arbitrary value, is shown in figure 7 and is considered to be satisfactory. It should be noted that the region where ω exceeds 21 corresponds to a natural period less than 0.3 seconds and the region where ω is less than 2.1 corresponds to a natural period exceeding 3.0 seconds. The average velocity spectra are not known accurately in these regions,[4] so the agreement in these areas is not considered critical. A better agreement could of course be obtained by using a more complicated expression in place of equation 2.11, but, as will be seen, this would be disadvantageous.

Procedure for Generating the Pseudo-Earthquake Ensemble

Consider any system described by a linear differential equation. Let $h(\tau)$ be the weighting function[42] for the system, i.e., the response of the system to an impulse τ time units in the past. In

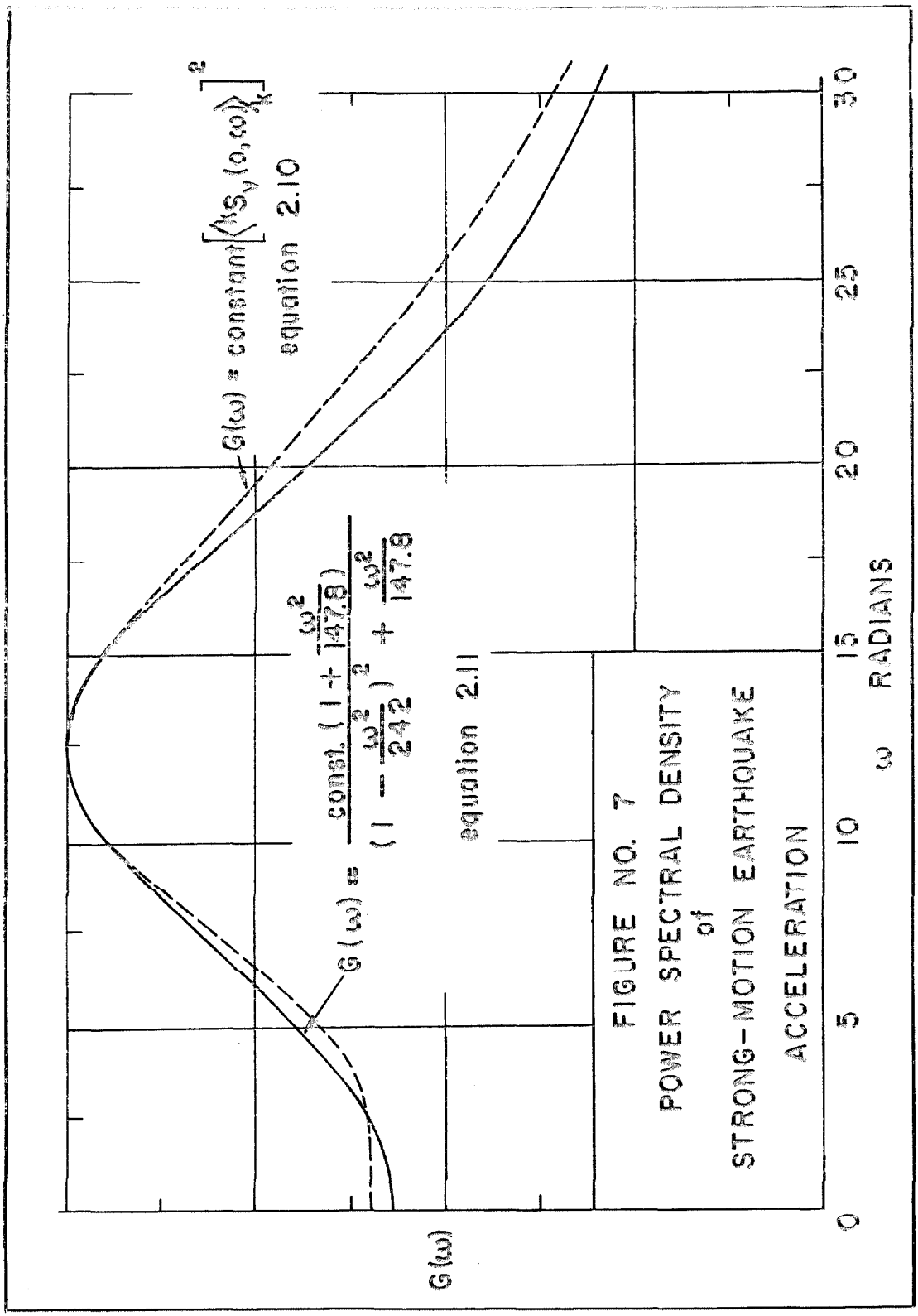

FIGURE NO. 7
POWER SPECTRAL DENSITY
of
STRONG-MOTION EARTHQUAKE
ACCELERATION

addition, let $Y(i\omega)$ be the Fourier transform of $h(\tau)$. If an ensemble of systems characterized by $h(\tau)$ is subjected to excitation by a random process with power spectral density $G_{in}(\omega)$, it is well-known that the power spectral density of the response $G_{out}(\omega)$ is related to $G_{in}(\omega)$ by

$$G_{out}(\omega) = \left|Y(i\omega)\right|^2 G_{in}(\omega) \tag{2.13}$$

It will be assumed that a Gaussian white noise with mean zero and power spectral density 1 is available. The generation procedure will be to let $G_{out}(\omega)$ be given by equation 2.11 and to solve for $Y(i\omega)$ and for $h(\tau)$; from $h(\tau)$ there can be determined the linear system that filters white noise to produce a random process with the required power spectral density. With $G_{in}(\omega) = 1$ and $G_{out}(\omega)$ given by equation 2.11 it is found that

$$Y(i\omega) = \frac{\sqrt{a}\left(1 + i\, 2b\frac{\omega}{c}\right)}{\left(1 - \frac{\omega^2}{c^2}\right) + i\frac{2b\omega}{c}} \tag{2.14}$$

and

$$h(\tau) = \sqrt{a}\left[\frac{c\sqrt{1-2b^2}}{\sqrt{1-b^2}}\; e^{-bc\tau}\; \sin c\sqrt{1-b^2}\,\tau + 2bc\, e^{-bc\tau}\cos c\sqrt{1-b^2}\,\tau\right] \tag{2.15}$$

If ${}^{k}N(t)$ represents a member of the white noise ensemble with power spectral density 1, then a sample of the pseudo-earthquake ensemble will be given by taking a segment of

$$ {}^{k}\ddot{y}(t) = \int_{-\infty}^{t} {}^{k}N(t)\, h(t-\tau)\, d\tau \qquad (2.16) $$

where ${}^{k}\ddot{y}(t)$ is the pseudo-earthquake acceleration. However, equation 2.16 is not in a form suitable for generating ${}^{k}\ddot{y}(t)$ on the digital computer; it would be more convenient to represent equation 2.16 by a differential equation which could be used more readily for producing samples of the process.

It will now be shown that the desired differential equation is

$$ \ddot{z} + 2bc\dot{z} + c^2 z = -F(t) \qquad (2.17) $$

where z is a variable and b and c are constants. This equation can describe the relative displacement of a linear, viscously damped oscillator whose base is excited by the acceleration F(t).[5] In integral form the relative displacement is

$$ z(t) = z(0) - \frac{1}{c\sqrt{1-b^2}} \int_{0}^{t} F(\tau)\, e^{-bc(t-\tau)} \sin c\sqrt{1-b^2}\,(t-\tau)\, d\tau \qquad (2.18) $$

Two differentiations produce the absolute acceleration of the mass

$$ \ddot{z} + F(t) = \frac{c\sqrt{1-2b^2}}{\sqrt{1-b^2}} \int_{0}^{t} F(\tau)\, e^{-bc(t-\tau)} \sin c\sqrt{1-b^2}\,(t-\tau)\, d\tau + 2bc \int_{0}^{t} F(\tau)\, e^{-bc(t-\tau)} \cos c\sqrt{1-b^2}\,(t-\tau)\, d\tau \qquad (2.19) $$

From the above equation it is seen that the weighting function for the

absolute acceleration is

$$h_{acc.}(\tau) = \frac{c\sqrt{1-2b^2}}{\sqrt{1-b^2}} e^{-bc\tau} \sin c\sqrt{1-b^2}\tau + 2bc\, e^{-bc\tau} \cos c\sqrt{1-b^2}\tau \tag{2.20}$$

This is identical with equation 2.15 except for a factor of $\sqrt{a}$. The differential equation to be used instead of equation 2.16 is thus given by replaceing F(t) by $\sqrt{a}\,{}^{k}N(t)$:

$$ {}^{k}\ddot{z} + 2bc\, {}^{k}\dot{z} + c^2\, {}^{k}z = -\sqrt{a}\, {}^{k}N(t) \tag{2.21}$$

The pseudo-earthquake accelerogram is:

$$ {}^{k}\ddot{y}(t) = {}^{k}\ddot{z} + \sqrt{a}\, {}^{k}N(t) = -(2bc\, {}^{k}\dot{z} + c^2\, {}^{k}z) \tag{2.22}$$

Rather than starting the integration of equation 2.21 with arbitrary initial conditions on z and $\dot{z}$ and carrying the integration for a long time to approximate the lower limit of the integral in equation 2.16, it is more convenient to choose z(0) and $\dot{z}(0)$ from the probability distributions of z(t) and $\dot{z}(t)$ and integrate equation 2.21 only as long as the duration of the accelerograms to be produced. Since N(t) is Gaussian with mean zero and power spectral density 1, it can be shown that z and $\dot{z}$ of equation 2.21 are Gaussian with means zero and variances given by

$$\begin{aligned} \left\langle {}^{k}z^2(t) \right\rangle_k &= \frac{\pi a}{4bc^3} \\ \left\langle {}^{k}\dot{z}^2(t) \right\rangle_k &= \frac{\pi a}{4bc} \end{aligned} \tag{2.23}$$

If ${}^{k}\beta$ and ${}^{k}\gamma$ are two uncorrelated numbers taken at random from a Gaussian distribution with mean zero and variance 1 then choosing ${}^{k}z(0)$ and ${}^{k}\dot{z}(0)$ as

$$\begin{aligned} {}^{k}z(0) &= \frac{1}{2c}\sqrt{\frac{a\pi}{bc}}\, {}^{k}\beta \\ {}^{k}\dot{z}(0) &= \frac{1}{2}\sqrt{\frac{a\pi}{bc}}\, {}^{k}\gamma \end{aligned} \tag{2.24}$$

will insure that the ensemble averages and variances of z and $\dot{z}$ are the same for all $t \geq 0$. Therefore, using these initial conditions it is necessary to integrate equation 2. 21 only for the length of accelerogram wanted.

At this point a convenient procedure has been established for constructing pseudo-earthquake accelerograms on a digital computer, only the duration of the pseudo-earthquakes must yet be specified. For the purposes of structural analysis it is desirable that all members of the ensemble have the same duration, and that this duration correspond to a large earthquake. For these reasons the duration of the ensemble of pseudo-earthquakes was chosen as 30 seconds.

The procedure for producing the pseudo-earthquakes is now completed. Equation 2. 21 is integrated for 30 seconds using the initial conditions of equation 2. 24. As the integration is performed $^{k}\ddot{y}(t)$ as defined by equation 2. 22 is produced. Because of the way it is generated $^{k}\ddot{y}(t)$ will have the power spectral density given by equation 2. 11 and the ensemble of records, each 30 seconds long, are samples of the random process that models the earthquake accelerograms.

To perform the calculation on the digital computer it is necessary to assign a numerical value to t_o, the equivalent duration of the strong-motion earthquakes used to construct the average earthquake spectra of figure 6. From equations 2. 11 and 2. 12 it is seen that the constant a which multiplies the approximate power spectral density of strong-motion earthquakes is inversely proportional to t_o. The linearity of equations 2. 21 and 2. 22 indicates that the

magnitude of the model accelerograms is proportional to $\sqrt{a}$. With this knowledge any convenient number can be used for t_o in the calculations and when an estimate for t_o or $\sqrt{a}$ becomes available, the accelerograms can be scaled accordingly. To perform the calculation t_o was taken as 30 seconds.

Calculation of the Pseudo-Earthquake Ensemble

In the preceding section a method for generating a pseudo-earthquake ensemble was developed assuming the availability of a Gaussian white noise. In the numerical integration of equation 2.21 an approximation of the white noise process is made by replacing the white noise by a noise whose power spectral density is approximately constant over the range of interest but falls to zero as ω tends to infinity. This approximation, which can be made to any degree of accuracy, is made necessary by the fact that true white noise is physically impossible to produce.

To form the approximate white noise, a white sequence of Gaussian numbers with mean zero and variance one was generated on the digital computer according to a procedure developed by J. N. Franklin of the California Institute of Technology.[50] By spacing these numbers at intervals Δh and then joining them by straight lines there is obtained a segmentally linear function that approximates white noise, the degree of approximation being dependent on the spacing Δh. It can be shown from the autocorrelation function that for small values of $\omega \Delta h$ the power spectral density is approximately given by

$$G(\omega) \approx \frac{\sigma_N^2 \Delta h}{\pi} \left[1 - \frac{(\omega \Delta h)^2}{6} \right] \qquad (2.25)$$

where σ_N^2 is the variance of the white numbers. Because the value of Δh used in the calculation is 0.025 seconds, equation 2.25 states that $G(\omega)$ is constant to within 10 percent for $\omega \leq 31$ ($T \geq 0.2$) and within 5 percent for $\omega \leq 21$ ($T \geq 0.3$). The analysis in the preceding section required that the power spectral density be unity; this is achieved by multiplying the numbers of the white sequence by $\sqrt{\pi/\Delta h}$ thus making $\sigma_N^2 = \pi/\Delta h$.

The integration of equation 2.21 using the approximate white noise was done on the IBM 7090 digital computer at the Computing Center of the California Institute of Technology using a program written by the author. A third order Runge-Kutta method was used and details of the calculation method can be found in Appendix I. The value of $^k\dot{y}(t)$ was determined at 0.025 second intervals and the numbers were joined by straight lines to produce a 30 second long model accelerogram. A total of eight such accelerograms were computed to make up an ensemble and plots of two of the accelerograms are shown later in the text.

The reader's attention is called to an alternate generating technique developed recently by J. N. Franklin[51] which would have been used had it been available at the time this work was done. This method uses the information contained in equations 2.11 and 2.22 and a white sequence of numbers from a Gaussian distribution to generate samples of the desired process $^k\dot{y}(t)$ to any degree of accuracy,

avoiding the errors associated with the approximate integration of any differential equations. In addition, this method is capable of handling with little difficulty more complicated processes than considered here. A report of this procedure will be published in a forthcoming Computing Center Technical Report.

C. Ensemble Calculations

The foregoing sections of this chapter have been devoted to the method of generating an ensemble of accelerograms. In the following section the generated accelerograms are processed in the same way as are those arising from real earthquakes, and the velocities, displacements and response spectra are calculated.

Velocity and Displacement Calculations

The first calculation performed on the ensemble of eight accelerograms was the determination of the velocity and displacement associated with the acceleration. The procedure adopted was that used by G. V. Berg and G. W. Housner[2] in finding the velocity and displacement of strong earthquake ground motion and only a brief resumé will be given here.

The integration of random functions is very sensitive to inaccuracies, particularly those of a secular type. The effect of these inaccuracies must be eliminated, at least to the extent that the ground velocity tends to zero at the end of the earthquake. To achieve this the accelerograms of the preceding sections are considered as ordinates with respect to a temporary base line which has the form $c_0 + c_1 t + c_2 t^2$ with respect to the true base line. The velocity of the ground is found

by integrating the acceleration as measured from this temporary base line and the constants c_0, c_1 and c_2 are determined so as to minimize the mean square value of the velocity, the initial velocity and displacement are taken to be zero. Then the acceleration ordinates are found with respect to the corrected base line, and the velocity and displacement are computed. Since the accelerogram is a series of straight line segments the integration for the velocity and displacement is an exact calculation and is easily done on a digital computer. The adjusted accelerations, velocities and displacements of pseudo-earthquakes number 1 and 4 are shown in figures 8, 9 and 10. Numbers one and four were chosen because they represent the extremes in statistical fluctuation of the velocity and displacement curves for members of the ensemble. The adjusted accelerations, velocities and displacements of strong-motion earthquakes are shown in figures 2-5. Comparison of the two sets of figures shows that the pseudo-earthquakes produce qualitatively similar curves.

Velocity Spectra of the Ensemble

As defined earlier, the velocity spectrum value is the maximum absolute value of the relative velocity of a single degree of freedom oscillator whose base is excited by the earthquake acceleration. The spectrum value is a function of the natural frequency and damping of the oscillator and of the duration of the earthquake acceleration. The equations determining the velocity spectrum value are

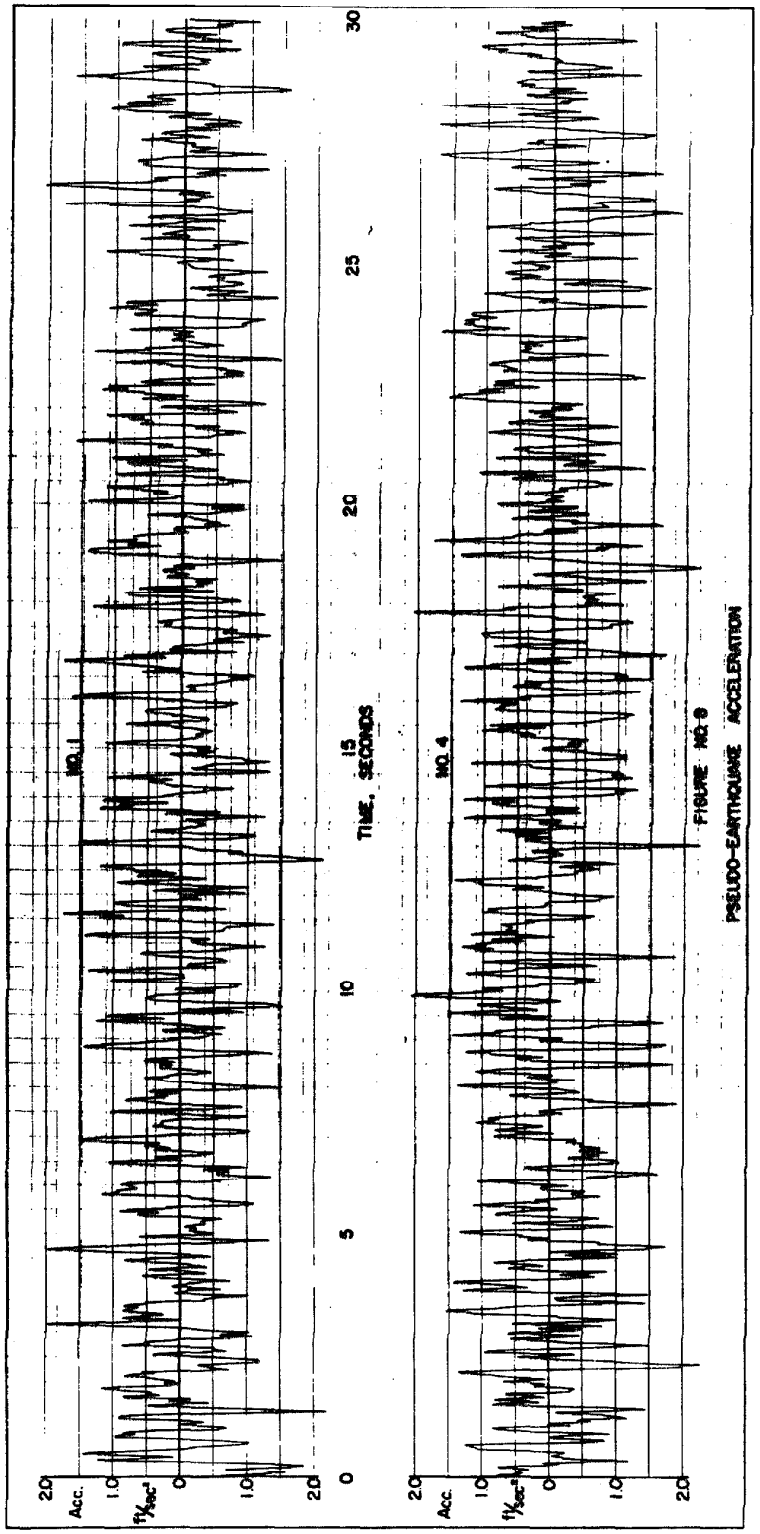

PSEUDO-EARTHQUAKE ACCELERATION

FIGURE NO. 8

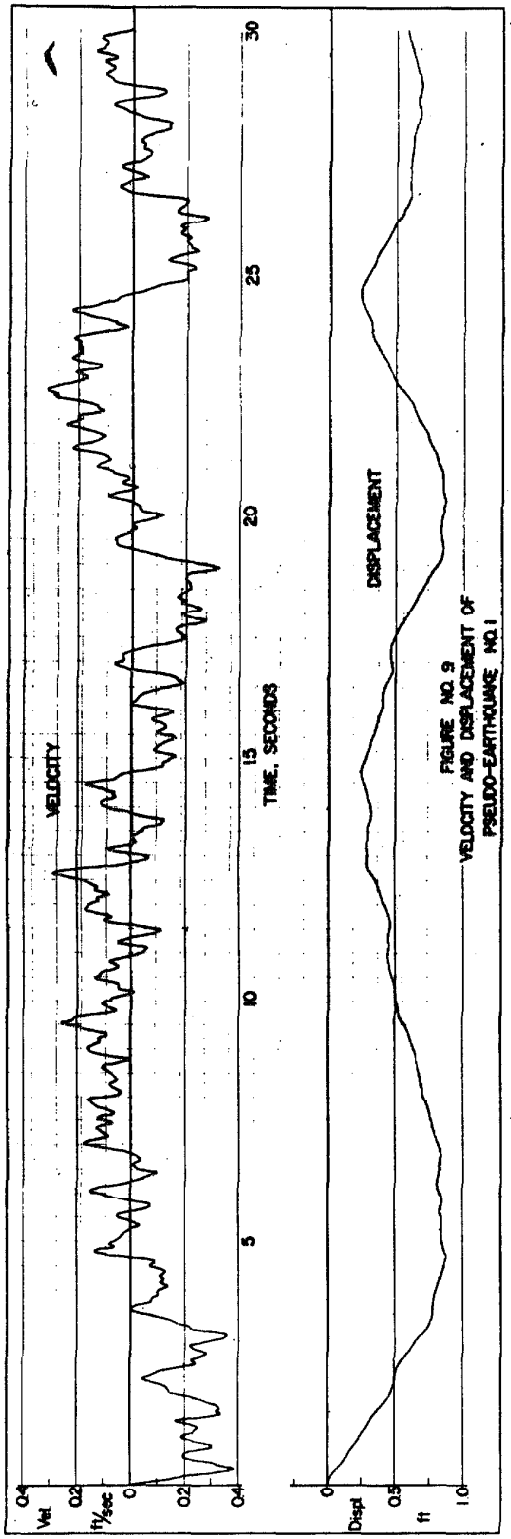

FIGURE NO. 9
VELOCITY AND DISPLACEMENT OF
PSEUDO-EARTHQUAKE NO. 1

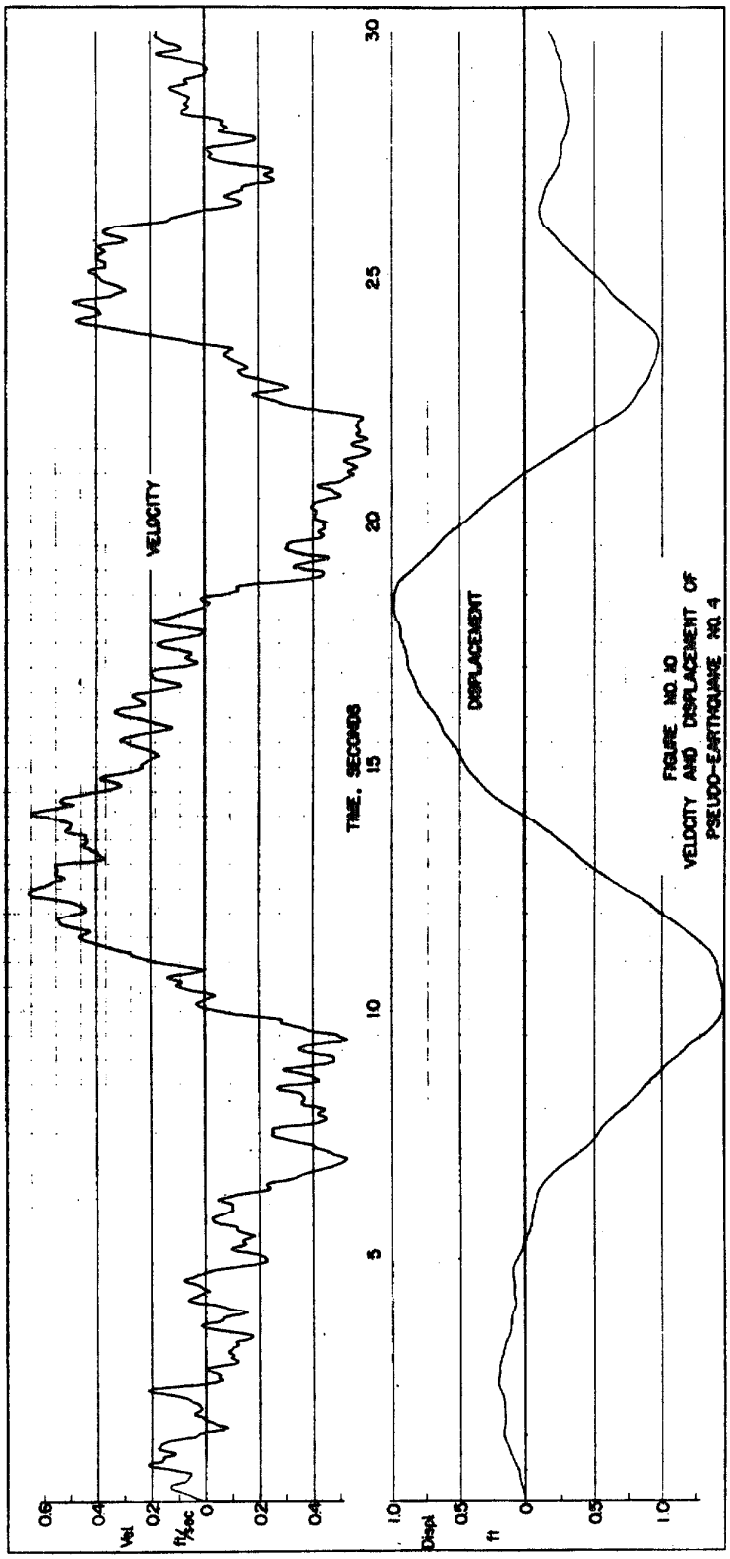

FIGURE NO. 10
VELOCITY AND DISPLACEMENT OF
PSEUDO-EARTHQUAKE NO. 4

$$\ddot{z} + 2n\omega\dot{z} + \omega^2 z = -\ddot{y}(t) \qquad (2.26)$$

$$S_v(n, \omega, t') = \left|\dot{z}\right|_{max}$$

where z is the relative displacement of the oscillator, n the fraction of critical damping, ω the natural frequency, and t' the length of the acceleration record.

The velocity spectra of the adjusted model accelerograms were calculated on the IBM 7090 computer at the C. I. T. Computing Center, and details are presented in Appendix I. The spectrum values were found for twenty natural frequencies (listed in Appendix I) and four values of damping (n=0, 0.02, 0.05, 0.10) for each of the eight members of the pseudo-earthquake ensemble. The individual spectra are shown in figures 11-18 and the ensemble average of the spectra is shown in figure 19. Also presented in figure 19 is the average of the undamped velocity spectra of real earthquakes from figure 6. It should be noted that this curve is a smoothed version of a curve qualitatively similar to the average undamped pseudo-earthquake spectrum.

Because t_o was chosen equal to the length of the ensemble of pseudo-earthquakes that were generated, the two undamped average spectra can be compared directly. That this is the case can be seen as follows: with the average undamped earthquake spectrum given, equation 2.9 was applied to find $G(\omega)$; this $G(\omega)$ then was used to generate samples of a stationary random process whose undamped spectra also should be described by equation 2.9; from this equation

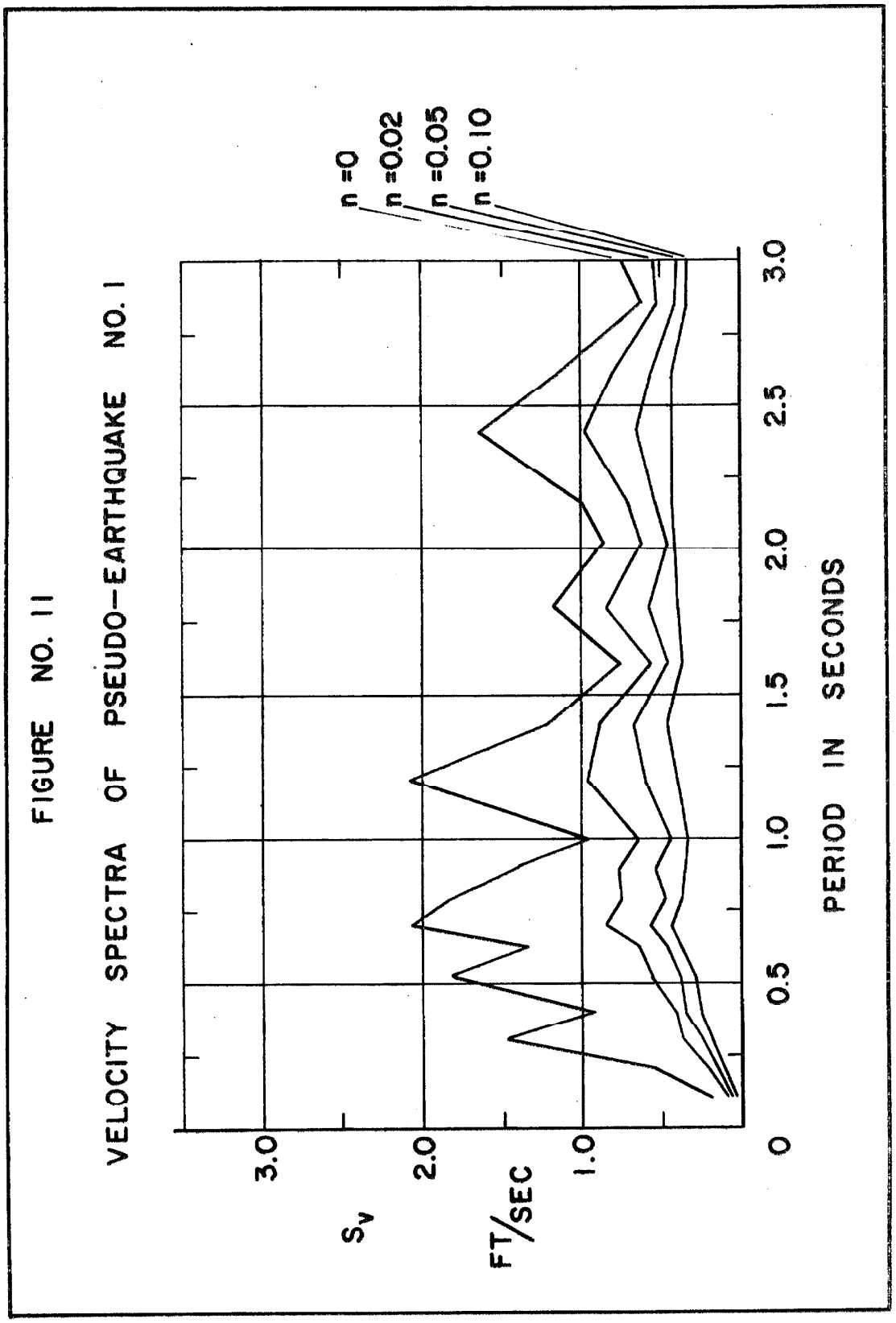
FIGURE NO. 11
VELOCITY SPECTRA OF PSEUDO-EARTHQUAKE NO. 1
n =0
n =0.02
n =0.05
n =0.10
3.0
2.0
1.0
0
S_v
FT/SEC
0.5
1.0
1.5
2.0
2.5
3.0
PERIOD IN SECONDS

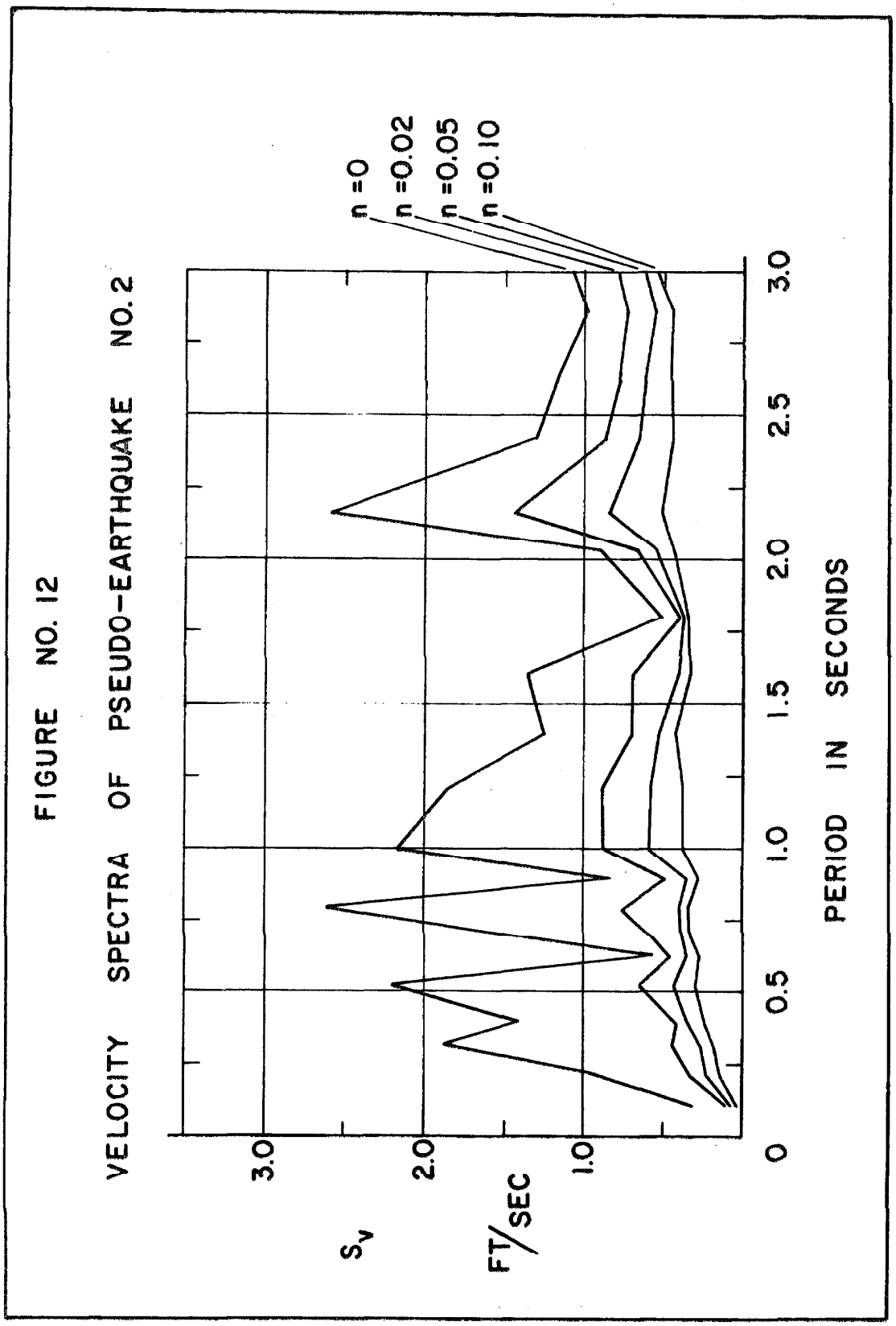
FIGURE NO. 12
VELOCITY SPECTRA OF PSEUDO-EARTHQUAKE NO. 2
n =0
n =0.02
n =0.05
n =0.10
S_v
FT/SEC
3.0
2.0
1.0
0
0.5
1.0
1.5
2.0
2.5
3.0
PERIOD IN SECONDS

FIGURE NO. 13

VELOCITY SPECTRA OF PSEUDO-EARTHQUAKE NO. 3

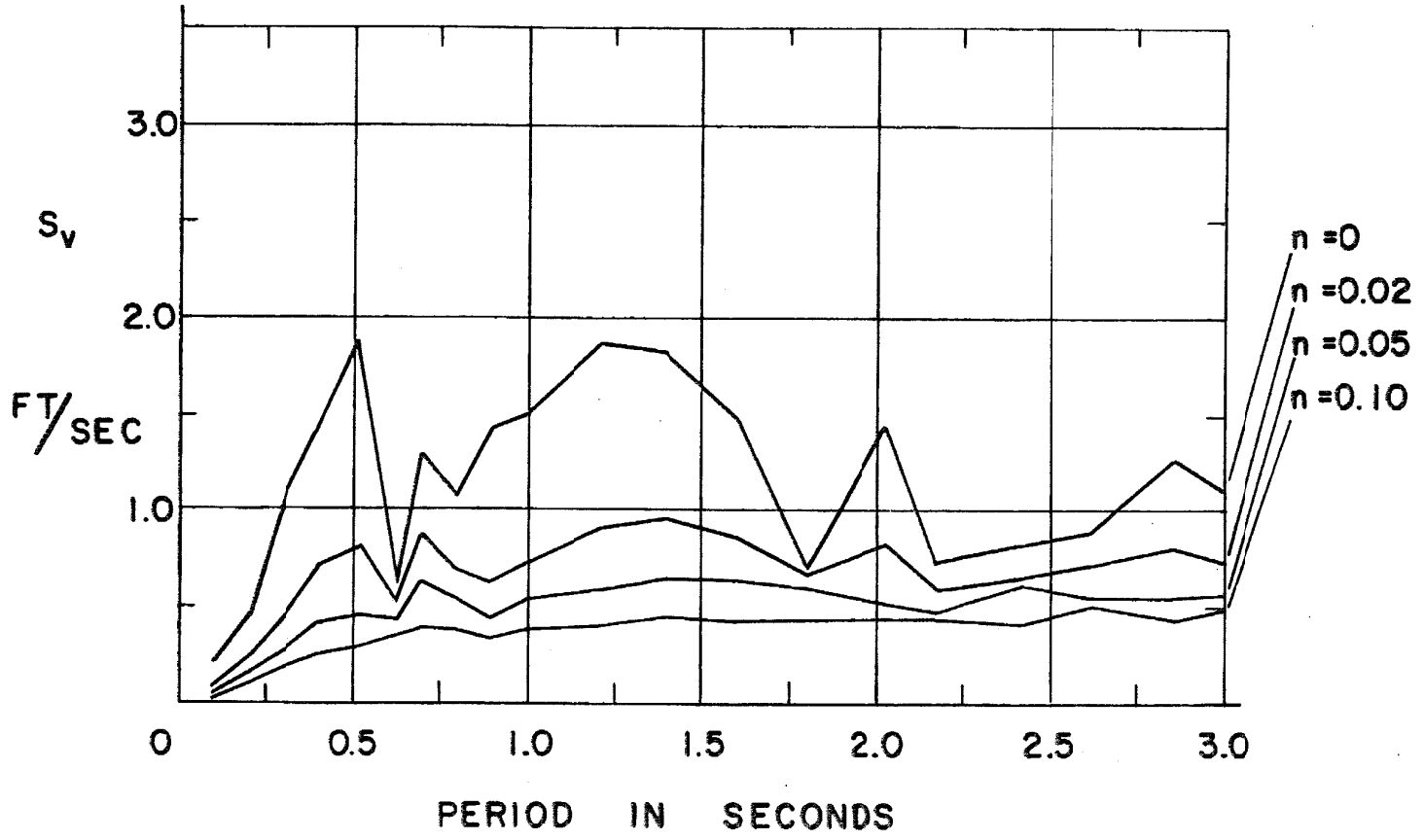

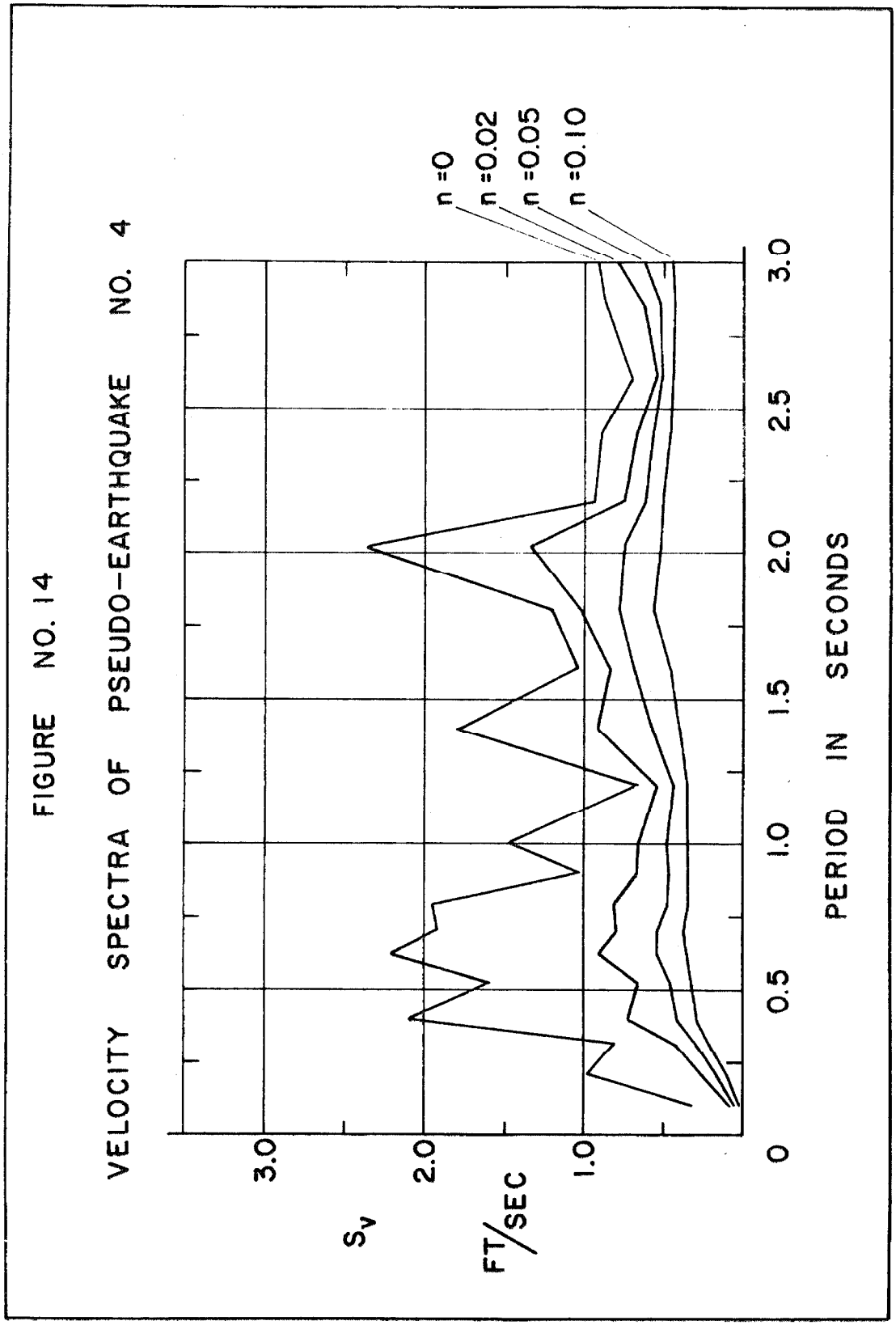
VELOCITY SPECTRA OF PSEUDO-EARTHQUAKE NO. 4
n =0
n =0.02
n =0.05
n =0.10
3.0
2.0
1.0
S_v
FT/SEC
0
0.5
1.0
1.5
2.0
2.5
3.0
PERIOD IN SECONDS

FIGURE NO. 14

FIGURE NO. 15

VELOCITY SPECTRA OF PSEUDO-EARTHQUAKE NO. 5

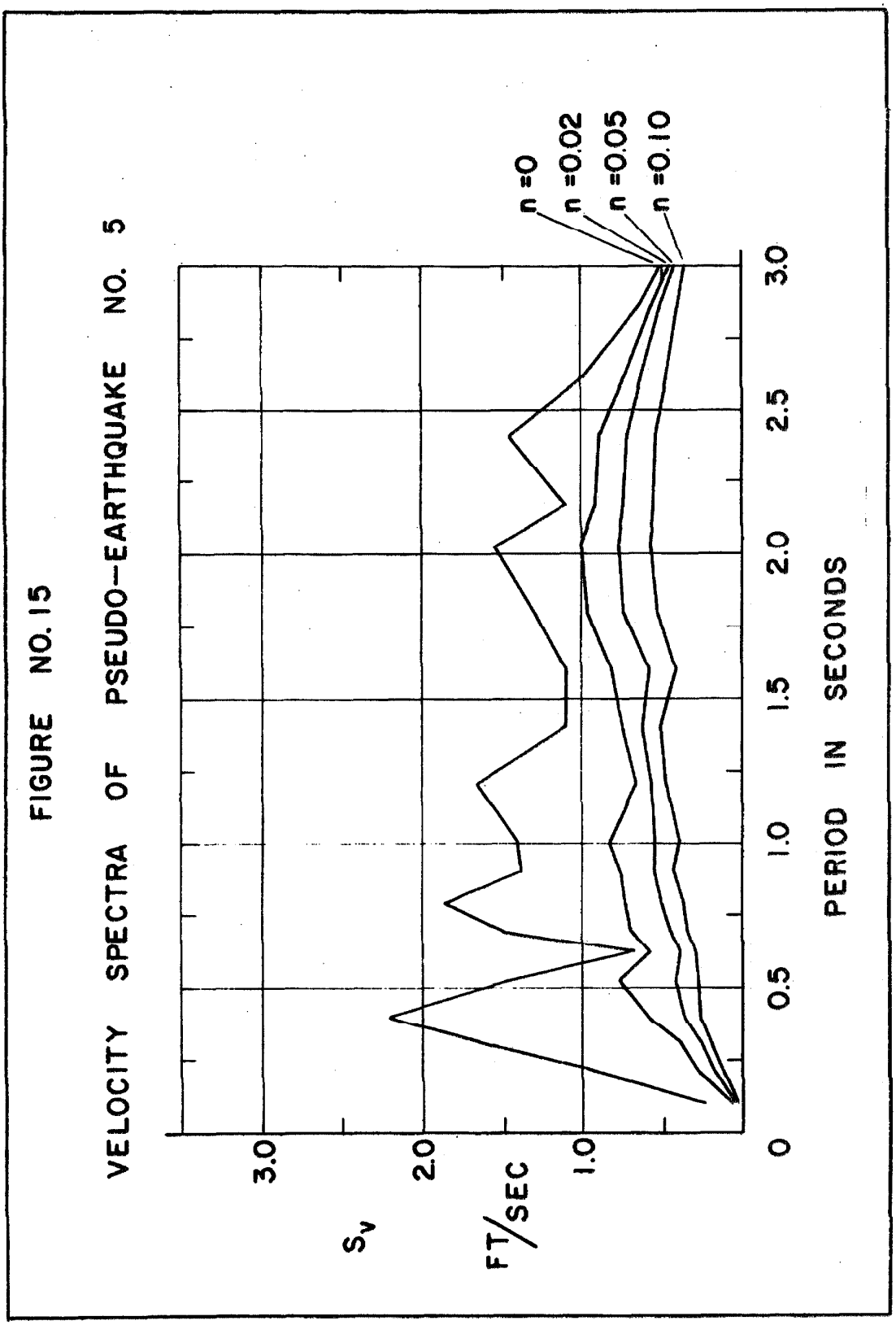

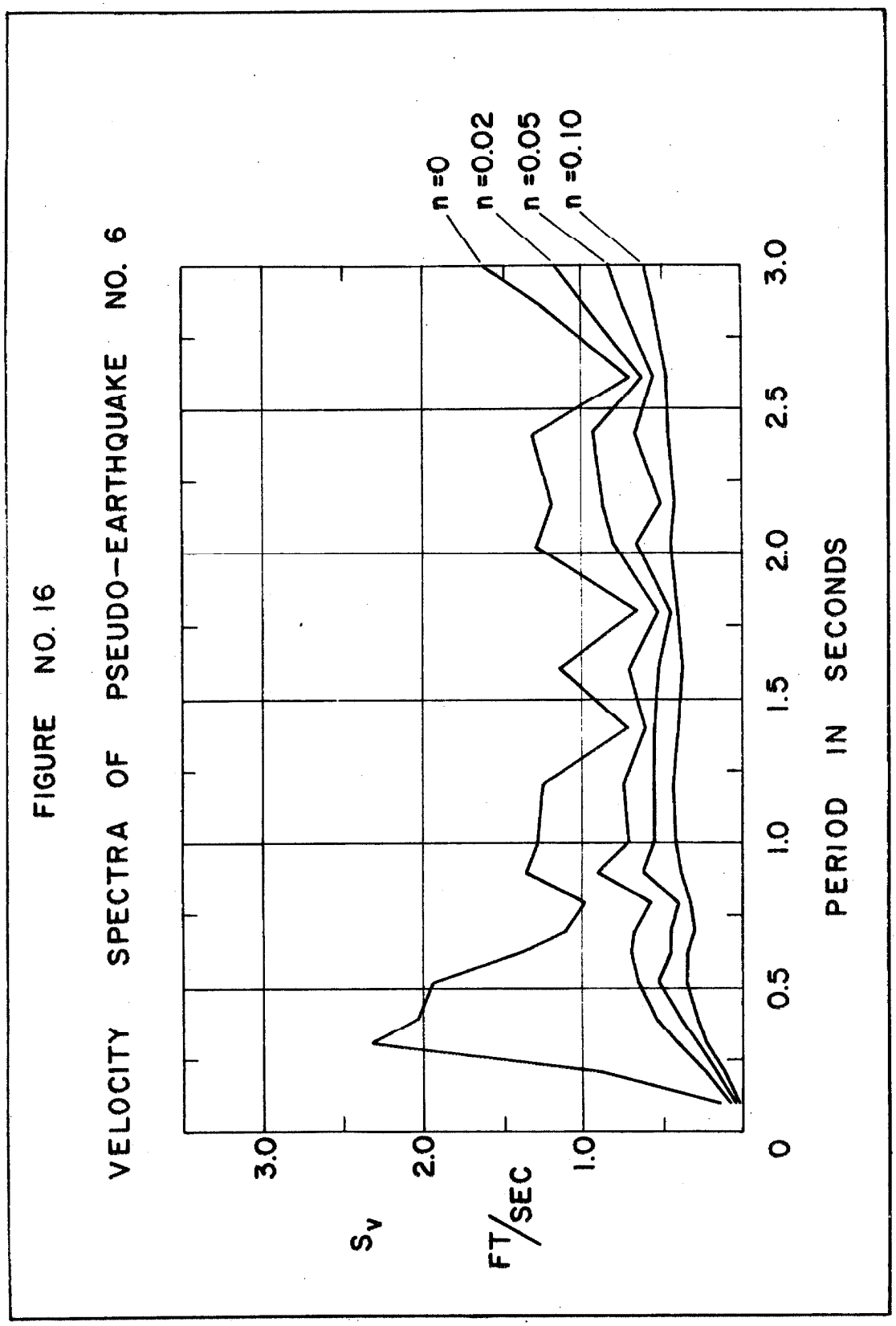

FIGURE NO. 16

VELOCITY SPECTRA OF PSEUDO-EARTHQUAKE NO. 6

FIGURE NO. 17

VELOCITY SPECTRA OF PSEUDO-EARTHQUAKE NO. 7

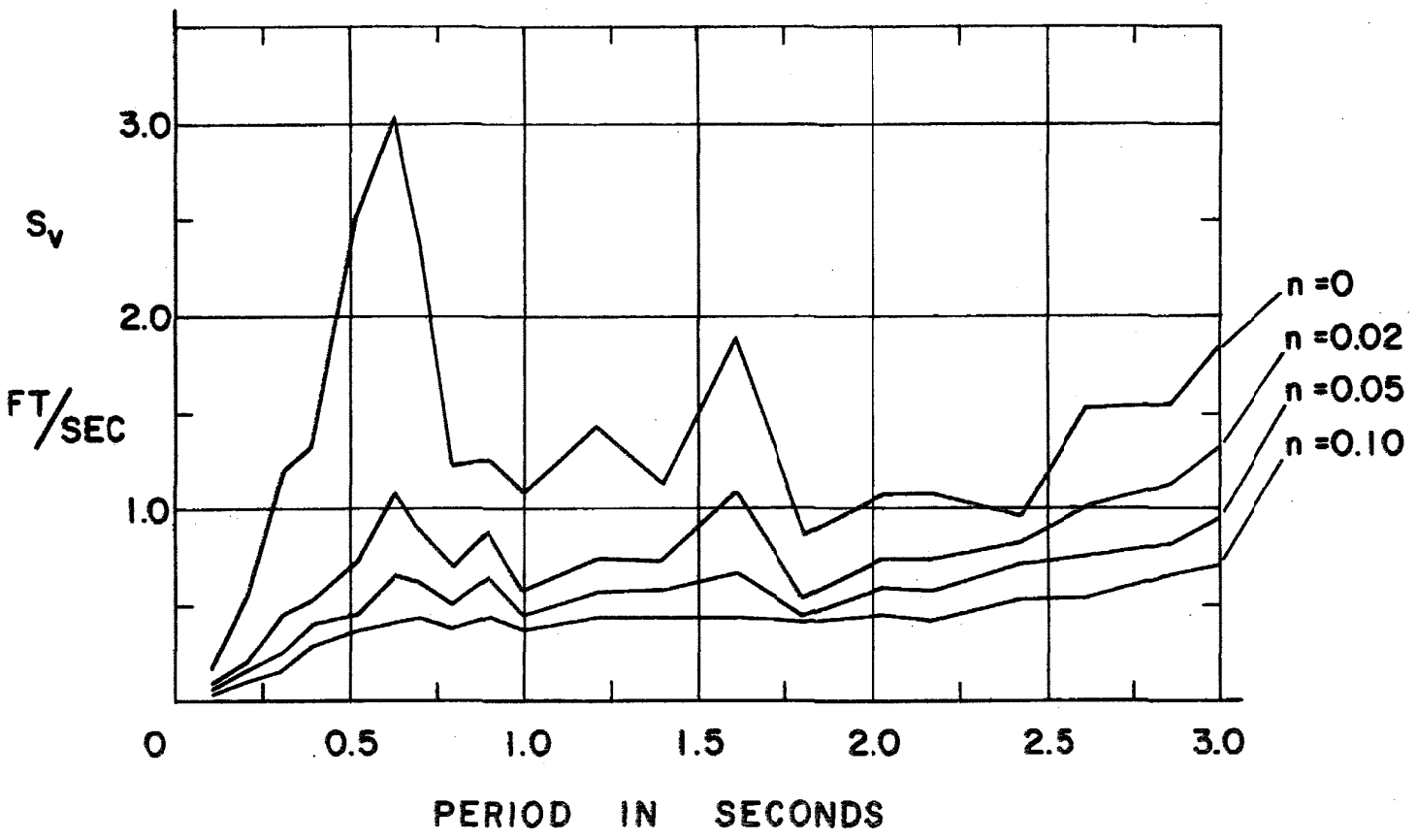

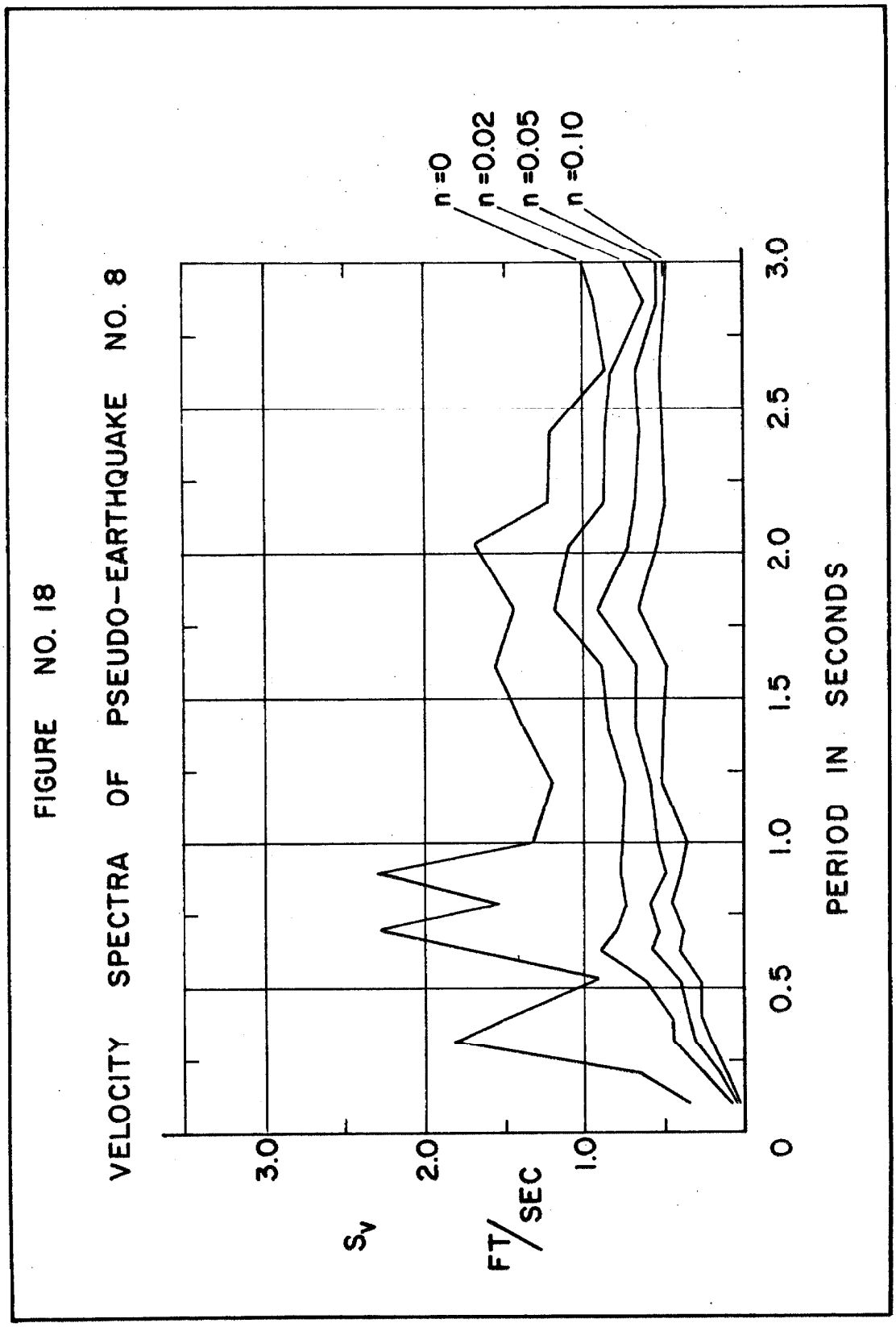

FIGURE NO. 18

VELOCITY SPECTRA OF PSEUDO-EARTHQUAKE NO. 8

FIGURE NO. 19

---- AVERAGE OF UNDAMPED EARTHQUAKE VELOCITY SPECTRA

—— AVERAGE OF 8 PSEUDO-EARTHQUAKE SPECTRA

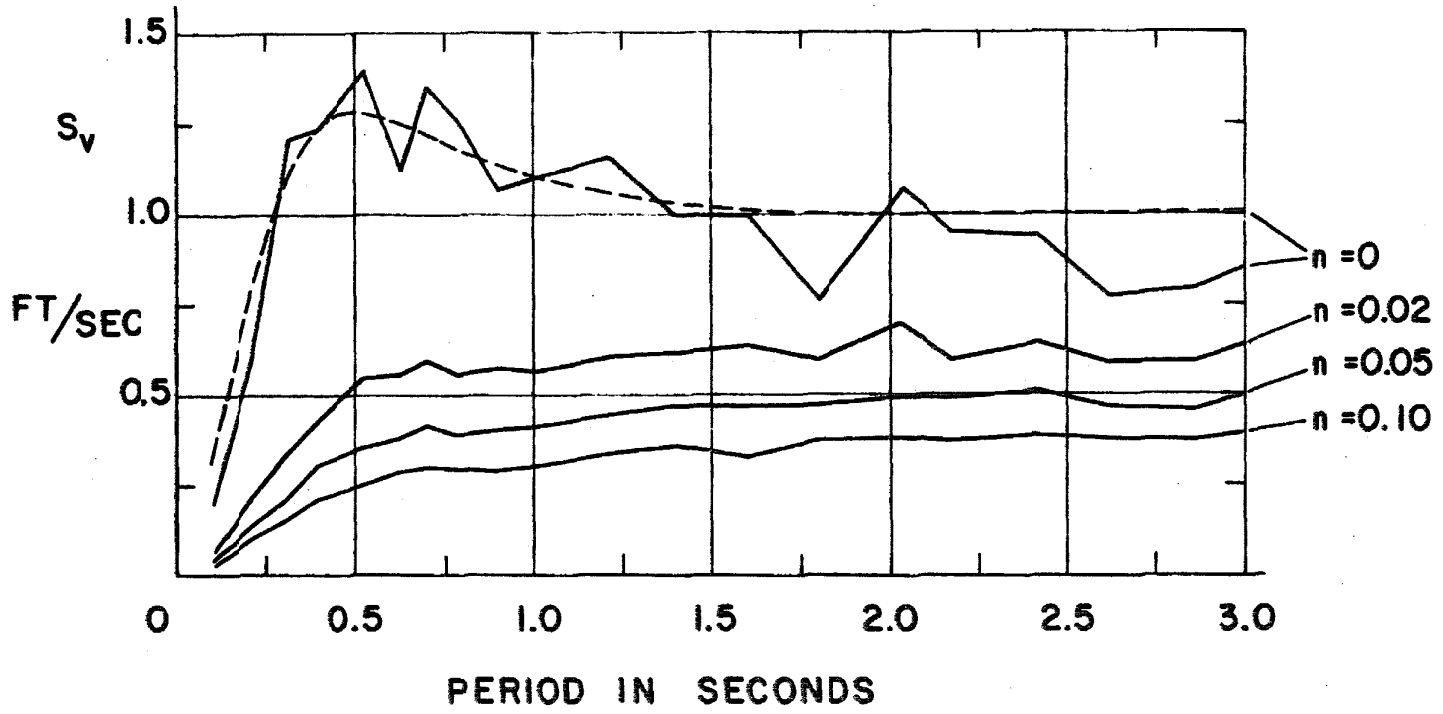

it follows that if the value of t_o is 30 seconds in each application the spectra should coincide. The comparison of the undamped spectra in figure 19 is therefore an example of the application of the approximate theory for a particular t_o. Considering the large variance of the individual undamped pseudo-earthquake spectra and the small size of the sample the agreement shown in figure 19 is considered good, although a precise comparison of the scales of the two average spectra is not possible. This agreement tends to confirm the applicability of equation 2.9 to stationary processes and indicates that a stationary process exists whose undamped spectra resemble those of strong-motion earthquakes. However, if this process is to model strong-motion earthquakes successfully, the damped velocity spectra of the earthquakes and of the random process must be examined.

A comparison of the damped curves of figures 6 and 19 indicates that the damped curves of the pseudo-earthquake ensemble, while qualitatively similar to those of real earthquakes, are considerably below their real counterparts. Part of this discrepancy can be ascribed to the fact that the length of the pseudo-earthquake ensemble, because of the way it was chosen, is longer than the equivalent duration of real earthquakes. If the effect of the ensemble duration on the spectra were known and an estimate of t_o were available, the effect on the pseudo-earthquake spectra of having used 30 seconds instead of the proper t_o could be estimated and a more meaningful comparison made. For this reason an approximate spectra formula is sought.

D. Approximate Velocity Spectra Formula

Introduction

In this section an approximate velocity spectra formula of a type first proposed by D. E. Hudson in reference 3 is derived and extended to include equation 2.9 as a special case. From this formula it is possible to approximate the effect of the ensemble duration upon the average spectra and by applying the formula to the spectra of both the real and pseudo-earthquakes it is seen that the damped curves should be used as the basis of comparison of the two sets of spectra. From this comparison the appropriate scale factor for the model accelerograms is determined.

Average Velocity Spectra

Figure 6 is the average velocity spectra as calculated by G. W. Housner.[4] Table I shows some of the properties of the eight strong-motion accelerograms that were used in constructing these average spectra. Most of the table is as reported in reference 4. The spectrum intensity SI_n is the area under the spectrum curve for the damping factor n from a natural period of 0.1 seconds to a natural period of 2.5 seconds and is a measure of the average ordinate of the spectrum curve. It is noted that the undamped spectrum intensity varies more from earthquake to earthquake than does the 20 per cent damped spectrum intensity. The last two columns have been added to indicate the effect of the duration of the earthquakes on the spectrum curves. The strong-motion duration was determined by inspection of the accelerograms as published in reference 1. As the end of the

TABLE I

Strong-Motion Earthquake Properties

Location and Date	Magnitude	Component	SI_o	SI_o-ave.	$SI_{0.2}$-ave.	$SI_o/SI_{0.2}$	Strong-Motion Duration
El Centro, Calif. 18 May 1940	6.7	N.S.	8.94	8.35	2.71	3.08	25-30
		E.W.	7.77				
El Centro, Calif. 30 Dec. 1934	6.5	N.S.	5.93	5.88	2.09	2.81	17-25
		E.W.	5.83				
Olympia, Wash. 13 April 1949	7.1	S80W	6.05	5.82	2.21	2.63	21-25
		S10E	5.59				
Taft, Calif. 21 July 1952	7.7	S69E	4.84	4.69	1.91	2.46	14-17
		N21E	4.53				
							Ave. 19-24

Magnitude is that reported by the Seismological Laboratory of the California Institute of Technology.

strong motion is hard to define,two numbers are given, the end of the strong motion having been judged to be between these numbers. From the averages of these numbers it is expected that the equivalent duration of the eight accelerograms would be between 19 and 24 seconds. The ratios of the undamped and 20 per cent damped intensities were formed in an attempt to find an objective measure of the relative magnitude of the damped and undamped spectrum curves. No definite conclusion can be drawn from such a small sample, but it does appear plausible from examining the last two columns that in the longer earthquakes the undamped spectrum values are proportionately larger than those for 20 per cent damping.

To form the average velocity spectra of the earthquake accelerograms, the spectra of the eight components first were normalized so that the undamped spectrum intensities were all the same. These normalized spectra then were averaged and curves were obtained for 0, 2, 5, 10, 20 and 40 per cent damping. No effect of the duration of the earthquakes was considered. An example of what the effect of the duration of the earthquake on the spectra might be is illustrated by figure 20. This figure shows the spectra as calculated from the first 15 seconds, the first 22. 5 seconds, and the full 30 seconds of pseudo-earthquake 6. It is seen that the undamped curve is much more sensitive to the duration of this pseudo-earthquake than is the 10 per cent damped curve. Or, in other words, as the length of the accelerogram is increased the undamped spectrum curve becomes proportionately larger.

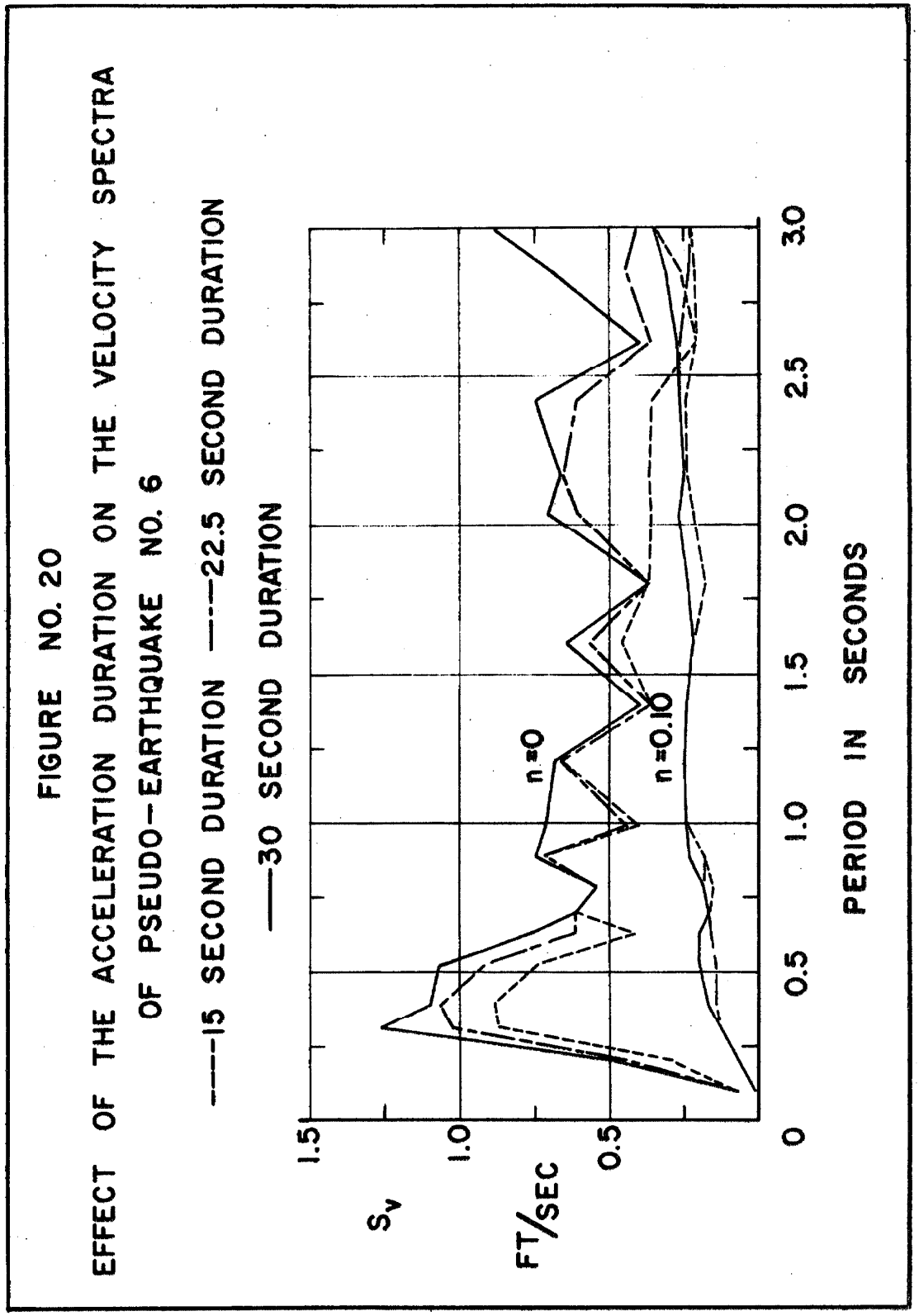
FIGURE NO. 20
EFFECT OF THE ACCELERATION DURATION ON THE VELOCITY SPECTRA
OF PSEUDO-EARTHQUAKE NO. 6
----15 SECOND DURATION ——22.5 SECOND DURATION
——30 SECOND DURATION
S_v
FT/SEC
1.5
1.0
0.5
0
n=0
n=0.10
0.5
1.0
1.5
2.0
2.5
3.0
PERIOD IN SECONDS

Derivation of the Spectra Formula

To derive the average spectra formula the earthquake acceleration again will be modeled by a white noise consisting of a large number of small impulses and when an equation is established the power spectral density of the white noise will be replaced by that of earthquakes as was done in the derivation of equation 2.9.

Consider an ensemble of identical, linear, viscously damped oscillators whose bases are subjected to accelerograms composed of large numbers of small impulses described by equations 2.2 and 2.3. The equation of motion of the kth member of this ensemble is

$$ {}^{k}\ddot{x}(t) + 2n\omega\, {}^{k}\dot{x}(t) + \omega^2\, {}^{k}x(t) = -\sum_{i=1}^{r} {}^{k}v_i\, \delta(t-t_i) \qquad (2.27) $$

Just before time t_i the average energy in the ensemble is

$$ \left\langle {}^{k}E(t_i^-) \right\rangle_k = \frac{1}{2} m \left\langle {}^{k}\dot{x}^2 \right\rangle_k + \frac{1}{2} k_s \left\langle {}^{k}x^2 \right\rangle_k \qquad (2.28) $$

where ${}^{k}E$ is the energy contained in the k^{th} oscillator, m the mass and k_s the spring constant of the oscillators. Similarly, just after the impulses at t_i have occurred

$$ \left\langle {}^{k}E(t_i^+) \right\rangle_k = \frac{1}{2} m \left\langle \left({}^{k}\dot{x} + {}^{k}v_i\right)^2 \right\rangle_k + \frac{1}{2} k_s \left\langle {}^{k}x^2 \right\rangle_k \qquad (2.29) $$

Because the velocity of the oscillators is uncorrelated with the impulses of the accelerogram $\left\langle {}^{k}\dot{x}\, {}^{k}v_i \right\rangle_k$ is zero and the average amount of energy imparted by the impulses is

$$\left\langle {}^{k}E_{i} \right\rangle_{k} = \frac{1}{2} m \left\langle {}^{k}v_{i}^{2} \right\rangle_{k} \tag{2.30}$$

where ${}^{k}E_{i}$ denotes the energy imparted to the k^{th} member of the ensemble by the impulse occurring at t_i. Since λ is the number of impulses per second the average rate of energy input to the ensemble of oscillators is

$$\frac{d\left\langle {}^{k}E_{I} \right\rangle_{k}}{dt} = \frac{1}{2} m \lambda \left\langle {}^{k}v_{i}^{2} \right\rangle_{k} \tag{2.31}$$

where ${}^{k}E_{I}$ is the total energy input to the k^{th} oscillator of the ensemble. Using equation 2.3 equation 2.31 becomes

$$\frac{d\left\langle {}^{k}E_{I} \right\rangle_{k}}{dt} = \frac{1}{2} m \lambda \sigma^{2} \tag{2.32}$$

On the other hand, a linear, viscously damped oscillator is capable of dissipating energy at a rate proportional to the velocity with respect to the base

$$d\,{}^{k}E_{D} = c_{d}\,{}^{k}\dot{x}\,dx \tag{2.33}$$

where c_d is the damping coefficient and E_D is the energy dissipated. In terms of n, the fraction of critical damping, this can be written as

$$\frac{d\,{}^{k}E_{D}}{dt} = 2n\omega m\,{}^{k}\dot{x}^{2} \tag{2.34}$$

taking the ensemble average of this relation one obtains

$$\frac{d\left\langle {}^{k}E_{D} \right\rangle_{k}}{dt} = 2n\omega m \left\langle {}^{k}\dot{x}^{2} \right\rangle_{k} \tag{2.35}$$

The average square of the displacement of an oscillator starting from rest in response to white noise with mean zero has been reported by T. K. Caughey and H. J. Stumpf;[8] neglecting a periodic term which is small for small values of damping it can be written as

$$\left\langle {}^{k}x^{2} \right\rangle_{k} = \frac{\lambda \sigma^{2}}{4n\omega^{3}} \left(1-e^{-2\omega nt}\right) \qquad (2.36)$$

where t is the time since the beginning of the excitation. For small damping the average square of the velocity is approximately ω^{2} times the average square of the displacement and using the value of $\left\langle {}^{k}x^{2} \right\rangle_{k}$ from equation 2. 36 equation 2. 35 becomes

$$\frac{d\left\langle {}^{k}E_{D} \right\rangle_{k}}{dt} = \frac{m\lambda\sigma^{2}}{2} \left(1-e^{-2\omega nt}\right) \qquad (2.37)$$

The average rate at which energy accumulates in the oscillators of the ensemble is the rate of energy input minus the rate of energy dissipation. Using equations 2. 32 and 2. 37 the rate of energy accumulation is

$$\frac{d\left\langle {}^{k}E \right\rangle_{k}}{dt} = \frac{m\lambda\sigma^{2}}{2} e^{-2\omega nt} \qquad (2.38)$$

where ${}^{k}E$ is the energy contained in the k^{th} oscillator at time t. Equation 2. 38 states that on the average the energy in the oscillators is always increasing but that the rate of increase goes to zero exponentially as the time increases. Integration of equation 2. 38 assuming the ensemble starts from rest produces

$$\left\langle {}^{k}E \right\rangle_{k} = \frac{m\lambda\sigma^{2}}{4\omega n}\left(1-e^{-2\omega nt}\right) \qquad (2.39)$$

As a theoretically sound formula for the average spectra of white noise excitation could be obtained from equations 2.38 and 2.39 if $\left\langle {}^{k}E \right\rangle_{k}$ could be related to $\left\langle {}^{k}S_{v}(n,\omega,t) \right\rangle_{k}$ these quantities are examined. $\left\langle {}^{k}E \right\rangle_{k}$ as a function of time is the average energy in the ensemble of oscillators at time t whereas $\left\langle {}^{k}S_{v}(n,\omega,t)\right\rangle_{k}$ represents the average over the ensemble of the maximum velocity that has occurred in each oscillator for all time from zero to t. It is seen that these two expressions have a very fundamental difference in that $\left\langle {}^{k}E \right\rangle_{k}$ is an average of quantities all evaluated at the same time t while $\left\langle {}^{k}S_{v}(n,\omega,t)\right\rangle_{k}$ is an ensemble average of quantities that do not occur at the same time. Because of the difficulties associated with this difference only an approximate relationship between the two averages is attempted here.

Since ${}^{k}S_{v}$ is the maximum velocity that has occurred in the k^{th} oscillator, $\frac{1}{2}\, m\, {}^{k}S_{v}{}^{2}$ is the maximum kinetic energy that the oscillator has obtained and $\frac{1}{2}\, m \left[\left\langle {}^{k}S_{v}(n,\omega,t) \right\rangle_{k} \right]^{2}$ is an approximate measure of the average maximum energy contained in the oscillators (it is not the average maximum kinetic energy of the ensemble because of the order of the averaging and squaring operations). It is assumed that

$$\frac{d}{dt}\left(\frac{m}{2}\left[\left\langle {}^{k}S_{v}(n,\omega,t) \right\rangle_{k} \right]^{2} \right) = \mu^{2}\, \frac{m\lambda\sigma^{2}}{2}\, e^{-2n\omega\frac{t}{\nu}} \qquad (2.40)$$

where μ^{2} and ν are positive constants. The integration of equation 2.40 with the condition that the oscillators of the ensemble start from

rest yields

$$\frac{m}{2}\left[\left\langle {}^{k}S_{v}(n,\omega,t)\right\rangle_{k}\right]^{2} = \mu^{2}\nu\,\frac{m\lambda\sigma^{2}}{4\omega n}\,(1-e^{-2n\omega\frac{t}{\nu}}) \qquad (2.41)$$

The meaning attached to the constants μ^2 and ν can be found by comparing equations 2.40 and 2.41 with equations 2.38 and 2.39. In the case of zero damping equations 2.39 and 2.41 can be evaluated by expanding the exponential in a series and taking the limit as n tends to zero. If this is done for these two equations the results are

$$\left\langle {}^{k}E\right\rangle_{k} = \frac{m\lambda\sigma^{2}}{2}\,t$$

$$\frac{m}{2}\left[\left\langle {}^{k}S_{v}(n,\omega,t)\right\rangle_{k}\right]^{2} = \mu^{2}\,\frac{m\lambda\sigma^{2}}{2}\,t \qquad (2.42)$$

The first of these equations states that the average energy of the undamped ensemble of oscillators grows linearly with time; the second states that the average maximum energy also grows linearly but at a different rate. Because the average energy contained in the undamped ensemble is always increasing, the average energy at t is nearly the same as the average of the maximum energy in each member of the ensemble for all time. For this reason it is expected that μ^2 should have a value near one.

By comparing equations 2.38 and 2.40 it is seen that the constant ν embodies the assumption that the rate of change of the average maximum energy is governed by a different time scale than is the rate of change of the average energy. This assumption is made in order to take into account in a simple manner the aforementioned fact that

the average maximum energy is not a function of time in the same way as is the average energy. Equation 2. 39 shows that if n and ω are finite the average energy in the ensemble increases to a constant value, indicating that on the average the response of the oscillators increases until a steady state is achieved. However, on the average, it is more likely that the maximum velocity of an oscillator will occur after this steady state has been achieved than before. Therefore equation 2. 39 reaches its stationary value before equation 2. 41 and it follows that the velocity spectra are governed by a slower time scale. This is achieved by making ν greater than one.

From equation 2. 41 the average spectra is

$$\left\langle {}^{k}S_{v}(n,\omega,t)\right\rangle_{k} = \mu\sqrt{\frac{\nu\lambda\sigma^{2}}{2n\omega}\left(1-e^{-2n\omega\frac{t}{\nu}}\right)} \qquad (2.43)$$

The power spectral density of the white noise, given by equation 2. 4, is now replaced by the power spectral density of strong-motion earthquakes:

$$\left\langle {}^{k}S_{v}(n,\omega,t)\right\rangle_{k} = \mu\sqrt{\frac{\nu\pi G(\omega)}{2n\omega}\left(1-e^{-2n\omega\frac{t}{\nu}}\right)} \qquad (2.44)$$

In the case where the damping is zero equation 2. 44 becomes

$$\left\langle {}^{k}S_{v}(0,\omega,t)\right\rangle_{k} = \mu\sqrt{\pi G(\omega)t} \qquad (2.45)$$

and it is seen that equation 2. 45 is identical with equation 2. 9 if μ is chosen as 1. 174.

Application of the Spectra Formula

The constant ν was estimated by making a comparison of the relative amplitude of the damped and undamped spectrum curves. From equations 2. 44 and 2. 45 it follows that

$$\frac{\left\langle {}^{k}S_{v}(n, \omega, t) \right\rangle_{k}}{\left\langle {}^{k}S_{v}(0, \omega, t) \right\rangle_{k}} = \sqrt{\frac{1-e^{-2n\omega\frac{t}{\nu}}}{2n\omega t/\nu}} \qquad (2.46)$$

where it is noted that this ratio is independent of the power spectral density and of μ^2. The estimate of ν was found by applying equation 2. 46 to the spectrum curves of figure 19. Because it was implicitly assumed that earthquake accelerograms were a stationary process in the derivation of equation 2. 44, this approximate formula should describe the pseudo-earthquake spectra better than it does the earthquake spectra, for the pseudo-earthquake accelerograms are samples of a stationary process and the earthquake accelerograms are only approximately so. Using a smoothed version of the spectra of figure 19 the ratio indicated by the left side of equation 2. 46 was formed for several values of n and ω and then the right side of the equation was applied. By this procedure it was estimated that $\nu = 2.5 \pm 10$ per cent. Although this estimate is not precise it will be adequate to establish a criterion for comparing the pseudo-earthquake spectra with those of real earthquakes in a manner that takes into account the difference in duration of the two ensembles. Later equation 2. 44 will be fitted to both sets of spectra to determine ν and μ^2 more precisely.

From Table I it was seen that the equivalent duration of strong-motion earthquakes might be expected to lie between 19 and 24 seconds.

Using the smaller of these two values for reasons that will become apparent, the magnitudes of spectra from a 30 second ensemble and from a 19 second ensemble with identical power spectral densities will be compared by means of equations 2.44 and 2.45. First the ratio of the average undamped spectra is formed by the use of equation 2.45

$$\frac{\left\langle {}^{k}S_v(0,\omega,30)\right\rangle_k}{\left\langle {}^{k}S_v(0,\omega,19)\right\rangle_k} = \sqrt{\frac{30}{19}} = 1.25 \qquad (2.47)$$

In a similar manner the ratio of the averaged damped spectra is formed from equation 2.44.

$$\frac{\left\langle {}^{k}S_v(n,\omega,30)\right\rangle_k}{\left\langle {}^{k}S_v(n,\omega,19)\right\rangle_k} = \sqrt{\frac{1-e^{-2n\omega\frac{30}{2.5}}}{1-e^{-2n\omega\frac{19}{2.5}}}} \qquad (2.48)$$

For 2 per cent damping the maximum value of this ratio is 1.16 in the range considered and occurs when $\omega = 2.1$ (T=3); when $\omega = 3.14$ (T=2) the ratio is 1.12; and when $\omega = 6.28$ (T=1) it is 1.06. For 5 per cent damping the value of the ratio is 1.08 at $\omega = 2.1$ and 1.03 at $\omega = 3.14$. When the damping is 10 per cent the ratio has a value of 1.02 at $\omega = 2.1$, and as is the case with the other values of damping, the value of the ratio approaches closer to 1 as ω is increased. From the form of equation 2.48 it is seen that if a value of t_o greater than 19 had been assumed the ratios mentioned above would have been closer to 1, this would have happened also if a value of ν less than 2.5 had been used. If ν were to exceed 2.5 by 10 per cent the ratios for 2 per cent damping would be slightly larger than those above but the 5 and 10 per cent damping ratios would be affected

by less than 1 per cent.

From this discussion it is concluded that if the ensemble of pseudo-earthquakes are to be equivalent to real earthquakes for the purposes of structural analysis the damped spectra, rather than the undamped, should be used as a basis of comparison. From the above ratios it follows that the 10 per cent damped spectra of the two ensembles should coincide for all values of natural period; the 5 per cent spectra for periods less than about 2 seconds; and the 2 per cent for periods less than about 1 second. Using these criteria the scale of the pseudo-earthquake ensemble was adjusted until the agreement with the average earthquake spectra shown in figure 21 was obtained. The agreement between the average damped spectra of the two ensembles is considered satisfactory over the major portion of the range of natural periods considered. The discrepancy between the averages for $T < 0.3$ seconds is attributed to the fact that the power spectral density of the model accelerograms, equation 2.11, is less than that required by equation 2.10 in this region ($\omega > 21$) as can be seen in figure 7. In the period range from 2.5 to 3.0 seconds the spectra of the model accelerograms are below the values that were expected from the discussion of the preceding paragraph. It is possible that this is just a local variation due to the small sample size like that occurring near 1.75 seconds, but this supposition cannot be verified without calculating more members of the ensemble. In figure 21 it is seen that the ratio of the undamped curves of the two sets of spectra

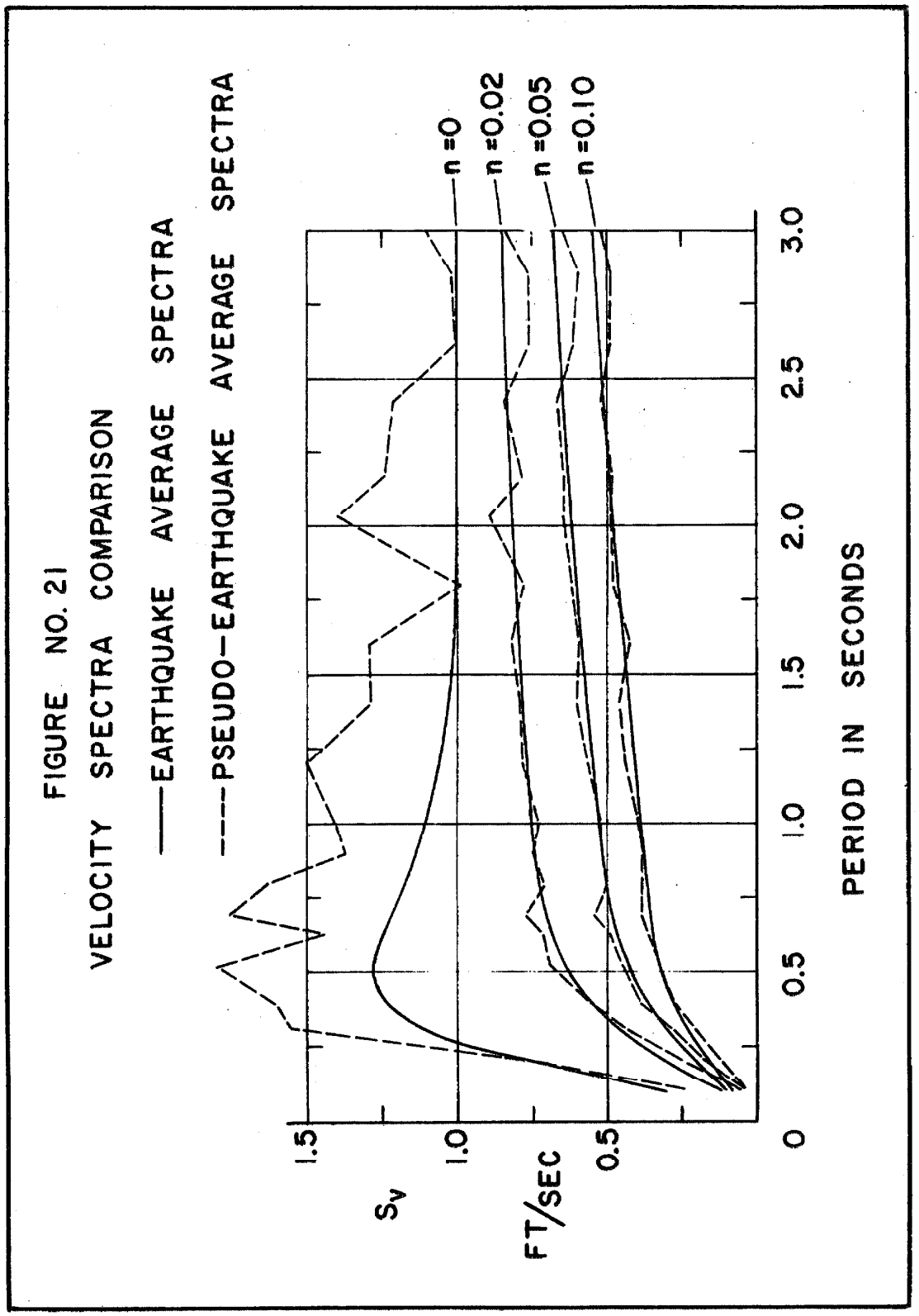
FIGURE NO. 21
VELOCITY SPECTRA COMPARISON
——EARTHQUAKE AVERAGE SPECTRA
- - - -PSEUDO-EARTHQUAKE AVERAGE SPECTRA
n =0
n =0.02
n =0.05
n =0.10
S_v
FT/SEC
1.5
1.0
0.5
0
0.5
1.0
1.5
2.0
2.5
3.0
PERIOD IN SECONDS

reflect a difference in duration of about the magnitude predicted by equation 2. 47.

To obtain the agreement shown in figure 21 it was necessary to increase the ordinates of figure 19 by a factor of 1. 30. From the linearity of the generating process with $\sqrt{a}$ as noted previously this increase in size of the accelerograms (and hence the velocity spectra) would have been achieved if the power spectral density had been 1. 69 times as large as that used to produce figure 19. Since the value of a used in the calculations was 0. 2196/30, the agreement shown in figure 21 would have been achieved if a had been 0. 01238. A refined estimate of the power spectral density of strong-motion earthquakes then follows directly from equations 2. 11 and 2. 12.

$$G(\omega) = \frac{0.01238\left(1 + \frac{\omega^2}{147.8}\right)}{\left(1 - \frac{\omega^2}{242}\right)^2 + \frac{\omega^2}{147.8}} \tag{2.49}$$

This function is shown in figure 22.

Using the power spectral density given by equation 2. 49 the approximate spectra formula of equation 2. 44 was fitted to the average earthquake spectra and to the average pseudo-earthquake spectra in order to obtain more precise estimates of the values of μ , ν , and t_o. The resulting formula is

$$\left\langle {}^{k}S_v(n, \omega, t) \right\rangle_k = 1.796 \sqrt{\frac{\pi G(\omega)}{2n\omega}\left(1 - e^{-2n\omega t/2.44}\right)} \tag{2.50}$$

which for zero damping reduces to

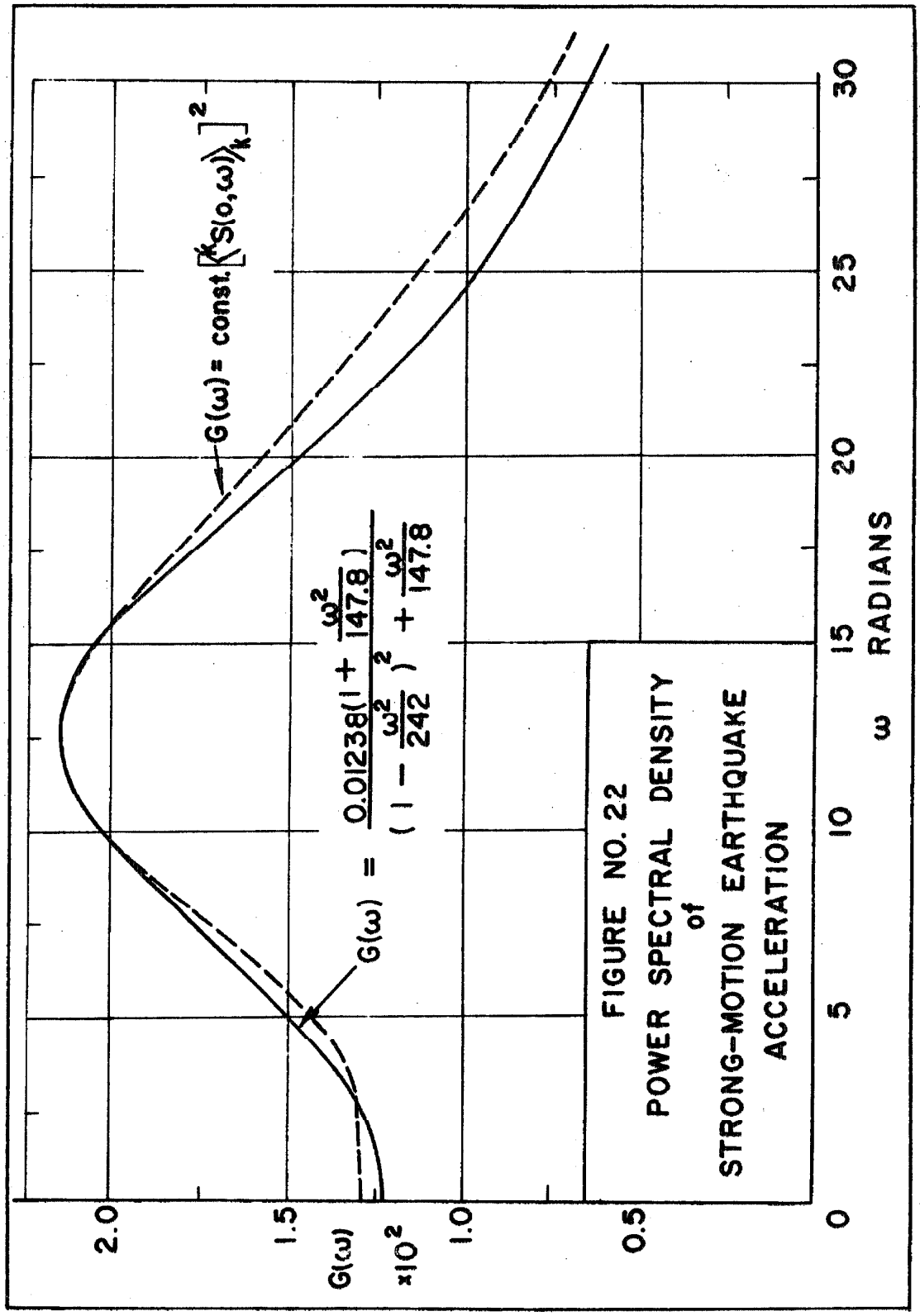

FIGURE NO. 22
POWER SPECTRAL DENSITY
of
STRONG-MOTION EARTHQUAKE
ACCELERATION

$$\left\langle {}^{k}S_{v}(0,\omega,t)\right\rangle_{k} = 1.150\sqrt{\pi G(\omega)t} \qquad (2.51)$$

where $G(\omega)$ is given by equation 2.49 and t is the duration of the acceleration ensemble. The agreement of this approximate spectra formula with the earthquake spectra is shown in figure 23; the value used for the equivalent duration was 18.6 seconds. The agreement of this formula with the spectra of the pseudo-earthquake ensemble is shown in figure 24. From figure 23 it is concluded that equation 2.50 describes the earthquake spectra satisfactorily as a function of period and damping. Most of the discrepancy in the region $T < 0.3$ seconds is again attributed to the fact that the function that was assumed for $G(\omega)$ is too small in this range ($\omega > 21$). The agreement of equation 2.50 with the pseudo-earthquake spectra as shown in figure 24 is not as good as that in figure 23 although better agreement could have been obtained at the expense of that shown in figure 23. Considering the figures together it is concluded that equation 2.50 satisfactorily approximates the behavior of the spectra as a function of the duration of the acceleration ensemble.

As mentioned above, the accelerograms producing figure 19 had to be increased by 1.30 to produce the desired ensemble. The spectra shown in figures 11-18 are shown to this corrected scale as are the accelerations, velocities and displacements shown in figures 8, 9 and 10. Thus all these figures correspond to the ensemble of accelerograms whose average spectra are shown in figure 21 and whose power spectral density is given by equation 2.49.

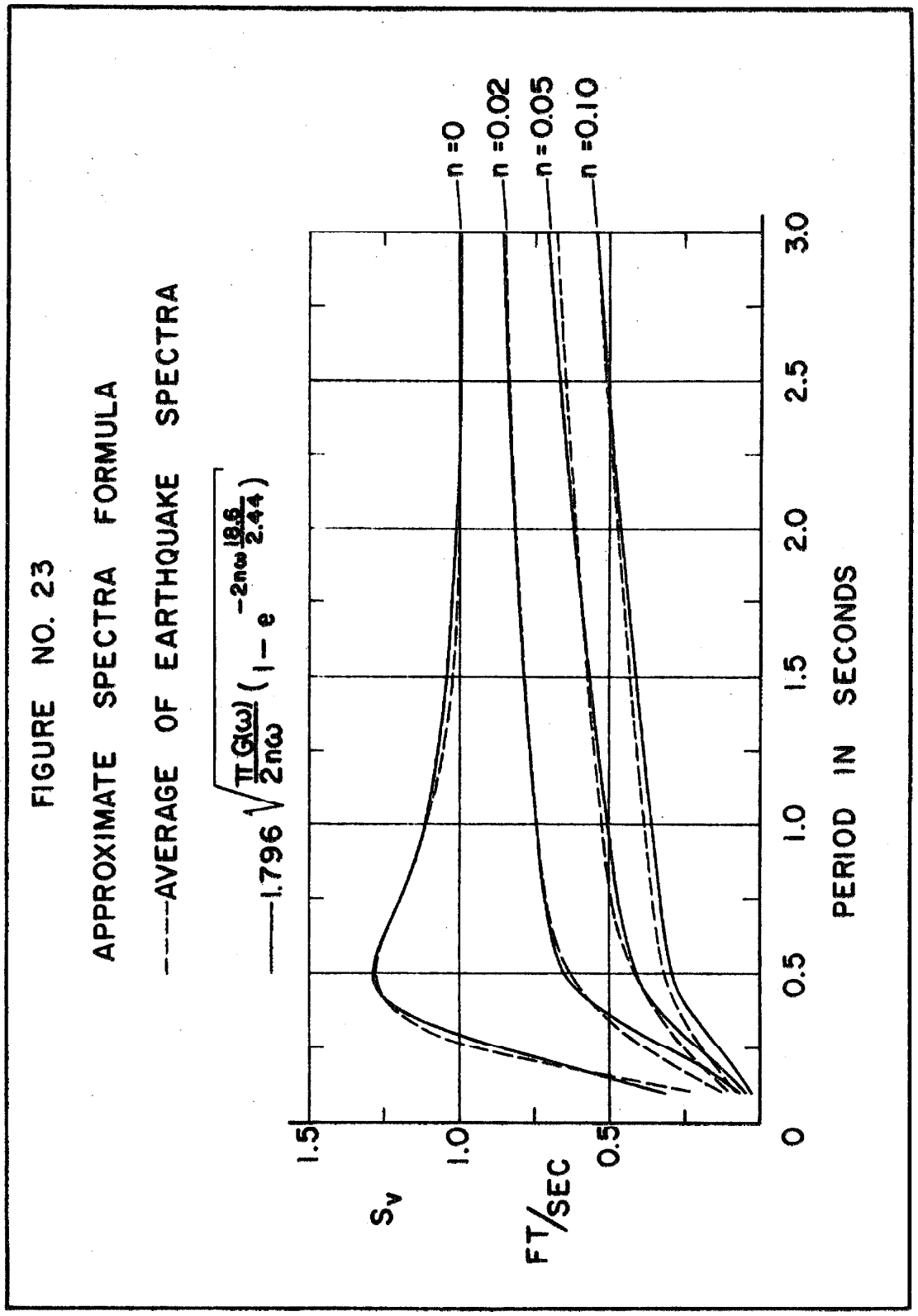
FIGURE NO. 23
APPROXIMATE SPECTRA FORMULA
----AVERAGE OF EARTHQUAKE SPECTRA
——1.796 $\sqrt{\frac{\pi G(\omega)}{2n\omega}\left(1-e^{-2n\omega\frac{19.6}{2.44}}\right)}$
n =0
n =0.02
n =0.05
n =0.10
S_v
FT/SEC
1.5
1.0
0.5
0
0.5
1.0
1.5
2.0
2.5
3.0
PERIOD IN SECONDS

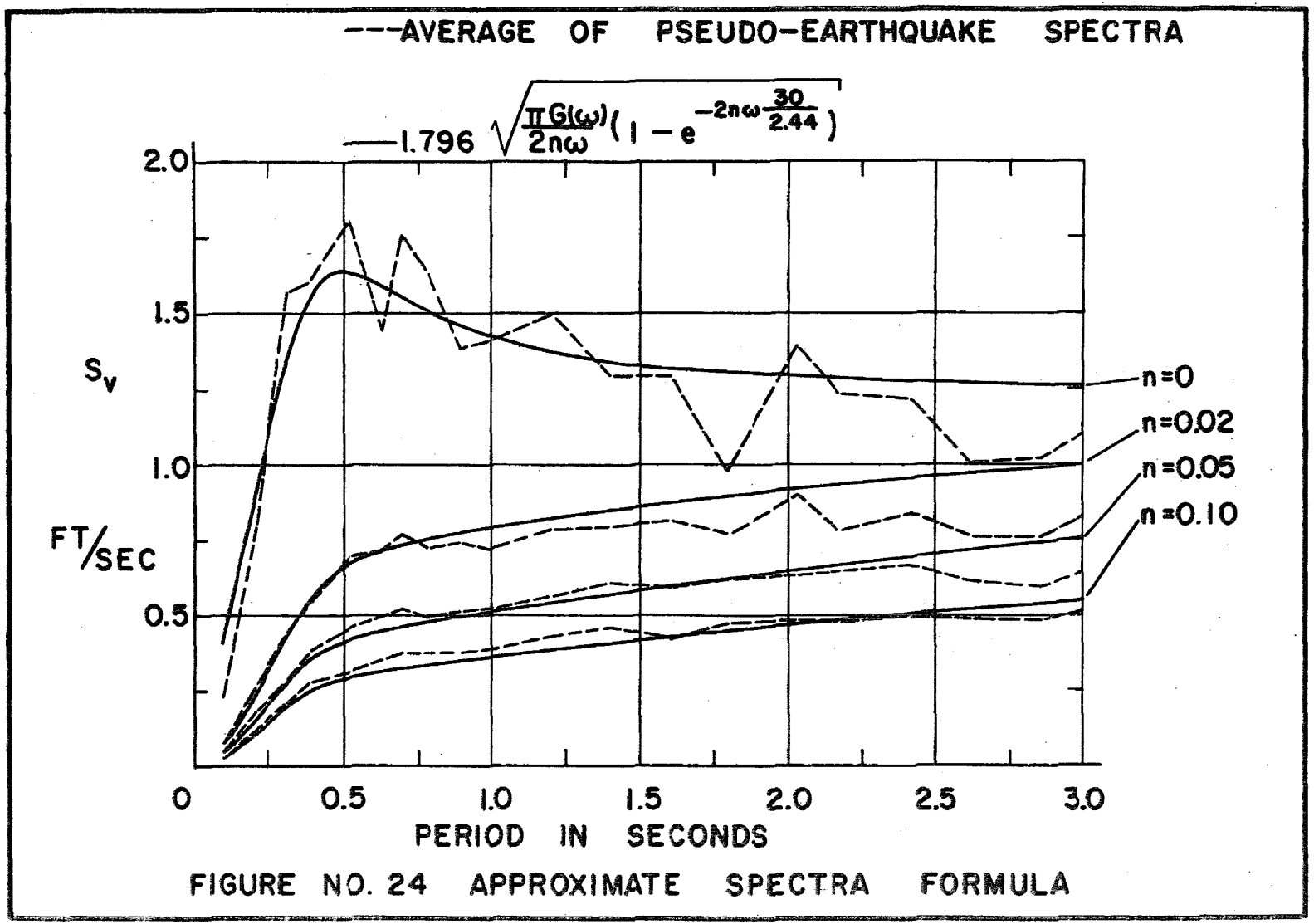

FIGURE NO. 24 APPROXIMATE SPECTRA FORMULA

A summary of some of the properties of the model accelerograms is given in Table II. The first row of this table is the root mean square of the adjusted acceleration. Since the acceleration record is composed of straight line segments the average value of the square of this function is calculated easily and was determined in a subroutine of the velocity spectra calculations. The second row is the average of the r. m. s. values and the third row indicates the departure of each particular r. m. s. value from the mean. The next three rows contain similar information about the undamped spectrum intensities of the model accelerograms. The spectrum intensity is the area under the spectrum curve from T=0. 1 to T=2. 5 seconds and was evaluated with a planimeter. The seventh row contains the average square of the 1200 numbers of the white sequence used to construct each accelerogram.

From the table it is seen that the r. m. s. values and undamped spectrum intensities of the accelerograms are relatively constant, although the individual undamped spectra vary markedly as can be seen in figures 11-18. The r. m. s. values of the accelerograms are all within about 5 per cent of the mean, while the spectrum intensities are within about 10 per cent of their mean. The deviations from the mean of these two quantities appear to be independent of each other.

E. Modeling of Earthquakes of Different Strengths

It was found in the preceding section that the equivalent duration of strong-motion earthquakes was near the average of the lower estimates of strong-motion duration given in Table I. To determine

TABLE II

Model Accelerogram Properties

Item	Accelerogram Number							
	1	2	3	4	5	6	7	8
r. m. s. $= \left[\frac{1}{30}\int_0^{30} k\ddot{y}^2(t)dt\right]^{\frac{1}{2}}$	0. 665	0. 684	0. 698	0. 734	0. 689	0. 709	0. 700	0. 694
Average r. m. s.			0. 697					
Percentage of average r. m. s.	95. 5	98. 1	100. 3	105. 3	98. 9	101. 8	100. 5	99. 6
Spectrum intensity								
$SI_o = \int_{0.1}^{2.5} S_v(0,\omega,30)d\left(\frac{2\pi}{\omega}\right)$	3. 02	3. 49	2. 99	3. 22	3. 23	2. 89	3. 18	3. 38
Average spectrum intensity			3. 18					
Percentage of average intensity	95. 4	110. 1	94. 2	101. 5	101. 9	91. 0	100. 2	106. 4
White sequence variance	0. 9677	0. 9913	1. 0202	1. 0064	0. 9962	0. 9978	0. 9709	1. 0172

scale factors by which the ensemble of pseudo-earthquakes can be multiplied to produce ensembles typifying past earthquakes, the r. m. s. values of the eight strong-motion earthquake components listed in Table I were found using as durations the lower estimates of that table. The calculations were performed on the IBM 7090 computer by Mr. A. G. Brady of the C. I. T. Civil Engineering Department. The results and the scale factors are given in Table III. The scale factors are the ratios of the average r. m. s. acceleration of the two components of the earthquake to the average r. m. s. of the model accelerogram ensemble. Also presented are similar scale factors determined from the undamped spectrum intensities by G. W. Housner.[4] The relative magnitudes of the 20 per cent damped spectra are taken from Table I. They were normalized by letting the El Centro 1940 factor be 2. 9 and are included to show the behavior of scale factors determined from the damped spectrum intensities.

It is seen that the factors determined from the r. m. s. acceleration and the undamped spectrum intensity agree closely for the two El Centro shocks but are different for the other two earthquakes. Because of the effect of duration upon the undamped spectrum and because the undamped spectrum intensity was seen to vary more across the ensemble of pseudo-earthquakes than did the r. m. s. acceleration, it is considered that the scale factors determined from the r. m. s. values are slightly better measures of the strength of the earthquake acceleration. The relative magnitudes of the 20 per cent damped spectra indicate that a scaling made from damped spectra

TABLE III

Strong-Motion Earthquake r. m. s. Values and Scale Factors

Location and Date	Strong-Motion Duration (seconds)	Component	Acceleration r. m. s. ft/sec^2	Average r. m. s.	Scale Factor from Average r. m. s.	Scale Factor from SI_0 [4]	Relative Magnitude of $SI_{0.2}$
El Centro, Calif. 18 May, 1940	25	N. S. E. W.	2. 20 1. 82	2. 01	2. 9	2. 7	2. 9
El Centro, Calif. 30 Dec. 1934	17	N. S. E. W.	1. 43 1. 27	1. 35	1. 9	1. 9	2. 2
Olympia, Wash. 13 April 1949	21	S80°W S10°E	1. 95 1. 57	1. 76	2. 5	1. 9	2. 3
Taft, Calif. 21 July 1952	14	S69°E N21°E	1. 45 1. 42	1. 44	2. 1	1. 6	2. 0

would give the same general results and also would have the advantage of being relatively independent of the duration of the acceleration. The approximate nature of these scale factors is emphasized by the differences between r. m. s. accelerations and spectrum intensities for different components of the same shock.

The purpose of the scale factor is illustrated by the following example. If the ensemble of pseudo-accelerograms is multiplied by 2.9 the resulting ensemble will have an average r. m. s. acceleration equal to the average of the strong-motion portions of the two components of the El Centro 1940 earthquake. The velocity spectra and results of structural investigations using this ensemble will be such that the results are approximately the same statistically as those that would be obtained from an ensemble of earthquakes of the strength of the El Centro 1940 shock.

F. Summary and Conclusions

A result of an approximate theory developed by E. Rosenblueth has been extended to find, within a constant, the power spectral density of strong-motion earthquakes from the average undamped velocity spectra. The constant factor is related to the equivalent duration of the four earthquakes used to construct the average velocity spectra. An integral expression for pseudo-earthquake accelerograms in terms of the power spectral density was found and this integral expression was then replaced by a differential equation with appropriate initial conditions to produce a generating procedure convenient for use on a digital computer. The constant in the power spectral density was

fixed conveniently and an ensemble of eight 30 second accelerograms was generated on an IBM 7090 computer. The accelerograms were adjusted by a least square fit to the velocity and the adjusted acceleration, velocity, and displacement were computed. The velocity spectra also were calculated from the adjusted accelerations. The average undamped velocity spectra of the real and pseudo-earthquakes compared well but the undamped did not, part of the difference being attributed to the difference in duration of the two acceleration ensembles. To find the effect of the ensemble duration an approximate average spectra formula was developed which includes Rosenblueth's result for the case of zero damping. Using this formula it was found that it was more meaningful to compare the average damped spectra of the real and pseudo-earthquake ensembles. From this comparison the constant in the power spectral density expression was determined, and since the generation process and other calculations were linear, the model accelerograms and results could be scaled appropriately to produce the desired ensemble. This scaled ensemble produces average damped spectra corresponding to those of the four strong-motion earthquakes and the difference in the average undamped spectra is approximately that predicted by the average spectra formula as a consequence of the difference in duration. The approximate spectra formula was then fitted more precisely to the average spectra of both ensembles and the results presented. The results implied that the equivalent duration of the earthquakes was near 19 seconds, the average of the lower estimates of the end of strong motion made from examination of the acceleration records.

The r. m. s. accelerations of the eight earthquake components were found using the lower estimates of duration, and from these values approximate scale factors were determined by which the model accelerograms can be multiplied to produce ensembles typifying past strong-motion earthquakes.

From the work of this chapter it is concluded that for purposes of structural analysis, strong-motion earthquake accelerograms can be modeled successfully by sections of a stationary random process with a power spectral density determined from the average undamped velocity spectrum. This conclusion is based on the fact that the averaged damped spectra of the pseudo-earthquake ensemble generated here correspond closely to those of strong-motion earthquakes, and also because the pseudo-earthquake accelerations, velocities, displacements and velocity spectra exhibit behavior similar to that of real earthquakes. It is considered that the difference in the average undamped spectra of the real and pseudo-earthquakes is a consequence of the difference in duration of the two ensembles.

It is further concluded that the average velocity spectra formula, equation 2. 50, describes the average strong-motion earthquake spectra satisfactorily as a function of period and damping. This formula also approximates the influence of the earthquake duration on the spectra.

From the derivation of the average spectrum formula it is indicated that the damped spectra, rather than the undamped, are a more reliable basis for comparison of velocity spectra of strong-

motion earthquakes. When future data warrant a recalculation of the average velocity spectra it is suggested that one of the damped spectrum intensities or the acceleration r. m. s. be considered for normalizing the individual spectra as these measures have a smaller range than the undamped spectra and are more nearly independent of the duration of the earthquakes.

III. DYNAMIC PROPERTIES OF A GENERAL NONLINEAR STRUCTURE

A. Introduction

In this chapter a general nonlinear hysteretic force-deflection relation for a one degree-of-freedom structure is developed. This relation is a continuous, smooth function and describes yielding behavior varying between the limits of the linear and elasto-plastic cases. The steady-state response of a structure having these properties to sinusoidal excitation is investigated by energy methods and by the method of slowly varying parameters and the resonant amplitude and frequency response curves are obtained. A typical family of these curves is verified by direct numerical integration of the equation of motion. The equivalent viscous damping factor for the general structure is determined and it is found to be strongly dependent on the amplitude of the vibrations and to have a maximum value of $1/2\pi$ of critical damping. The question of infinite resonance is investigated and it is found that this phenomenon does not occur for members of the general relation, but does occur for the elasto-plastic and linear structures at force levels determined in other studies. From these results it is concluded that the relation is practical and is general enough to be useful as a model for dynamic behavior. By comparing test results to the theoretical results it may be possible to approximate the dynamic force-deflection relations of real structures.

An explanation of the symbols used in this chapter of the thesis is given below and they are defined also where they first appear in the text. Wherever possible the symbols of the previous chapter are used.

Symbol	Explanation or Definition
a	subscript used to designate the ascending branch of the hysteresis loop
d	subscript used to designate the descending branch of the hysteresis loop
j	index in a Fourier Series
m	mass of a one degree-of-freedom structure
n	fraction of critical damping of a linear, viscously damped structure
n_{eq}	equivalent viscous damping factor for a yielding structure
p	restoring force of a one degree-of-freedom structure
p_y	characteristic restoring force
p_o	steady-state restoring force amplitude
r	positive odd integer
s	subscript used to designate the skeleton curve
t	time
w	subscript used as an iteration index
x	displacement of a one degree-of-freedom structure
x_o	steady-state displacement amplitude
x_y	characteristic displacement
y, z	dummy variables
A_j	Fourier series coefficient
$C(x_o)$	integral expression defined in equation 3.49

E_c	energy input per cycle of vibration
E_d	energy dissipated per cycle of vibration
F_o	force amplitude
$F(t)$	time dependent force
$S(x_o)$	integral expression defined in equation 3.49
a	positive constant
β	ratio of A_1 to x_o
η	frequency ratio = ω / ω_o
θ	angle = $\omega t + \phi$
ϕ	phase angle
ϕ_j	phase angle in a Fourier series
τ	dimensionless time variable = $\omega_o t$
ω	frequency of sinusoidal excitation
ω_o	natural frequency of a linear structure, natural frequency of small oscillations of a yielding structure
$\left(\frac{x_i}{x_y}, \frac{p_i}{p_y}\right)$	point at which the loading on a structure is reversed

B. The Skeleton Curve and Hysteresis Loop

Skeleton Curve

The skeleton curve is the name given to the force-deflection relation obtained by increasing from zero the magnitude of the load acting upon a structure. A one degree-of-freedom structure and various skeleton curves are illustrated in figure 25. In this chapter a general formula is presented for skeleton curves of the softening

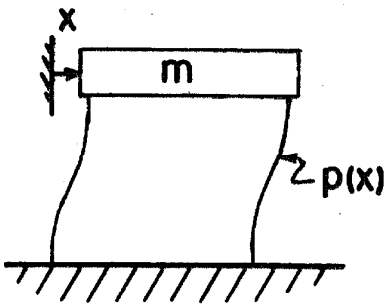

ONE D.O.F.
STRUCTURE

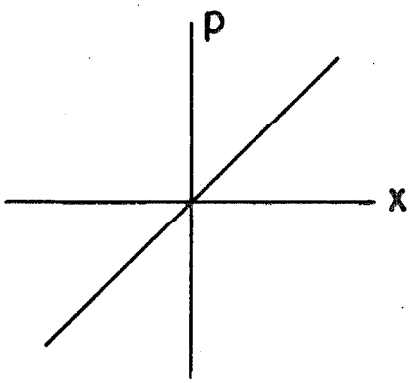

A. LINEAR

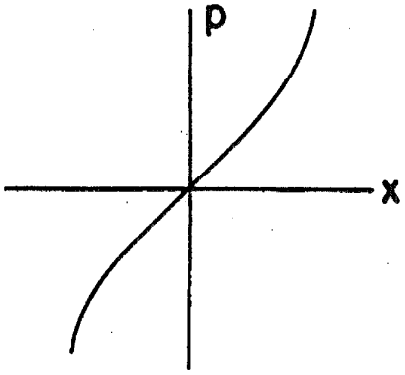

B. HARDENING SPRING

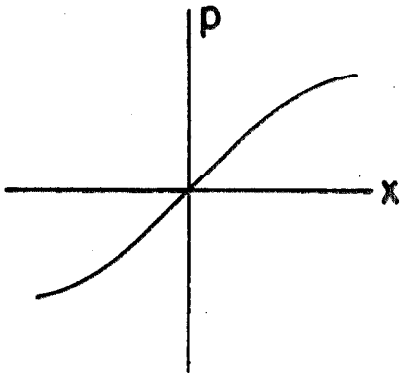

C. SOFTENING SPRING

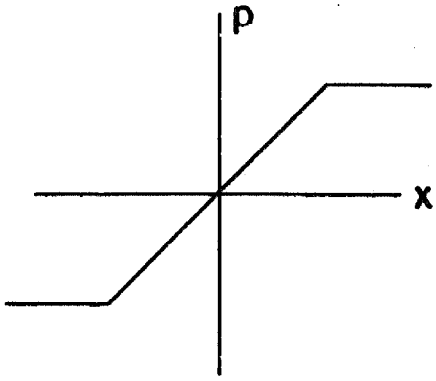

D. ELASTO–PLASTIC

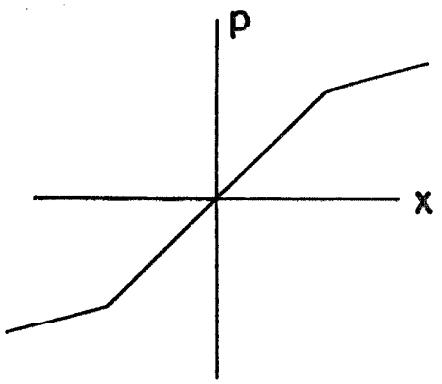

E. BILINEAR HYSTERETIC

FIGURE NO. 25
SKELETON CURVES
OF VARIOUS TYPES

type which are symmetric about the origin, and which can be considered linear for small deflections. Curves A, C, D and E of figure 25 fall into this classification, but hardening relations of the type shown as curve B do not. The skeleton curves of the general force-deflection relation presented here are described by the equation

$$\frac{x}{x_y} = \frac{p}{p_y} + \alpha \left(\frac{p}{p_y}\right)^r \tag{3.1}$$

where x is the displacement of the structure, x_y is a characteristic displacement, p is the restoring force, p_y is a characteristic force, α is a positive constant, and r is a positive odd integer greater than one. If only real numbers are considered there is always a one-to-one correspondence between force and displacement in equation 3.1. To allow the use of non-integer values of r, equation 3.1 can be written as

$$\frac{x}{x_y} = \frac{p}{p_y}\left|1 + \alpha \frac{p}{p_y}\right|^{r-1} \tag{3.2}$$

However, this refinement complicates the analysis and will not be used here.

Some of the curves described by equation 3.1 are shown in figure 26; in view of the symmetry about the origin only the positive portions of the curves are given. From the figure and from equation 3.1 it is seen that a wide range of softening systems can be represented by this relation. In particular, a linear structure is described by $\alpha = 0$ and an elasto-plastic structure is approached as r tends to ∞. Examination of equation 3.1 shows that this tendency to an elasto-plastic structure for large r occurs for all values of α greater than zero.

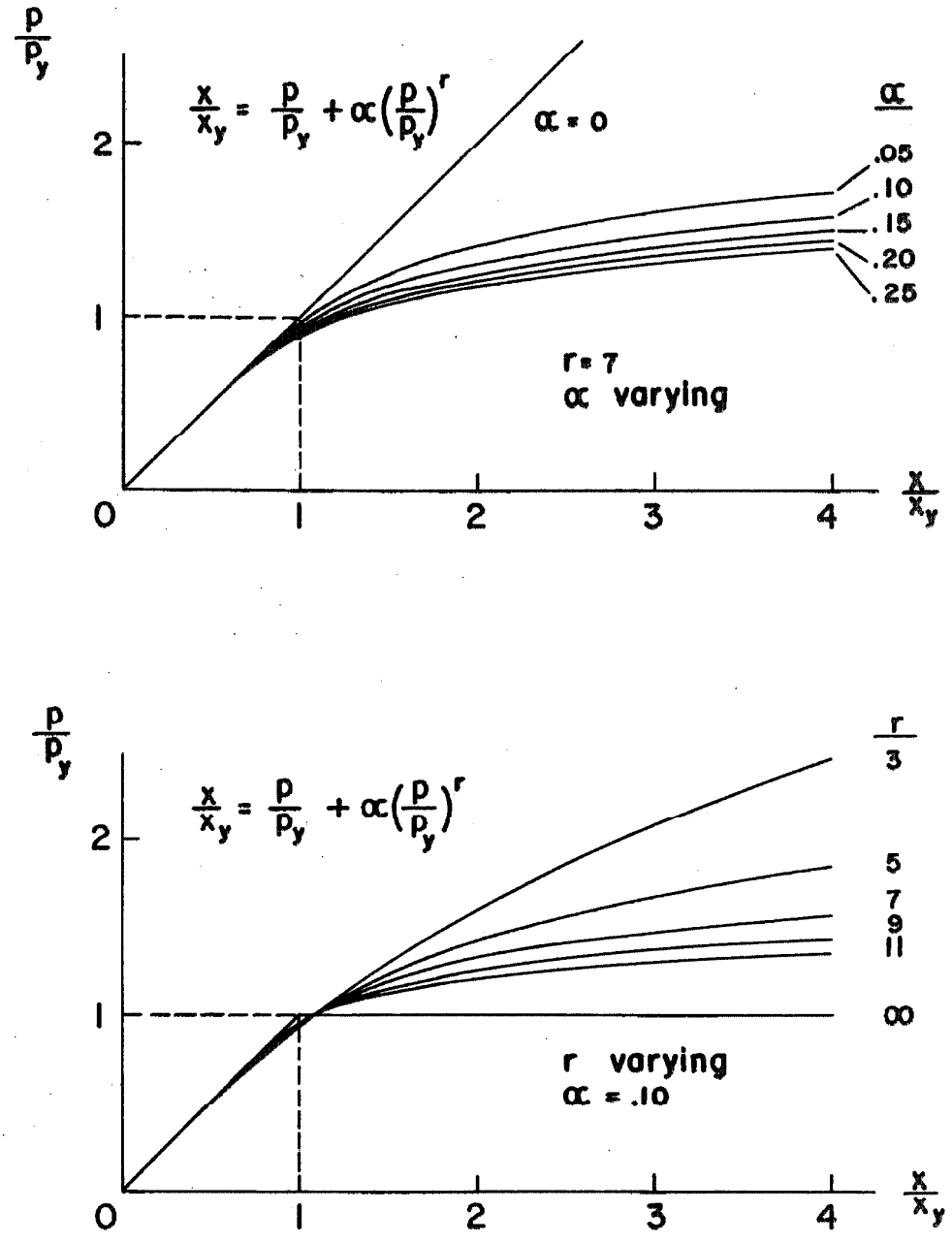

FIGURE NO. 26
EXAMPLES OF SKELETON CURVES
DESCRIBED BY EQUATION 3.1

A formula similar to equation 3.1 was first proposed by W. Ramberg and W. R. Osgood to describe relations between stress and strain[52] and similar expressions have been used for static analysis of structures loaded into the plastic range.[53] The general shape of the curves given by equation 3.1 compares favorably with the results of proportional loading tests of steel frames.[54, 55, 56] To find the values of r and α that give the best fit between equation 3.1 and experimental data Ramberg and Osgood have suggested a procedure that is applicable here. A logarithmic plot is made of the departure from linearity of the deflection versus the applied force. From equation 3.1 it is seen that the logarithm of the departure from linearity is $\log \alpha + r \log(p/p_y)$. Thus α and r are the intercept and the slope of the straight line which fits best the data of this logarithmic plot. In cases where integer values of r are not sufficient to obtain the desired fit equation 3.2 may be used.

A more informative interpretation of the parameters with reference to many structures is as follows. Let x_y be the calculated yield deflection of the structure and p_y the yield force. In theory, x and p are linearly related for values less than these yield points, but tests of actual structures show a departure from linearity before the calculated yield level is achieved. Evaluating equation 3.1 when p/p_y is 1 indicates that under this interpretation α is the fractional departure from linearity of the deflection at the calculated yield level. The value of r may then be chosen to determine the behavior of the

structure near the yield level, greater values of r giving more sharply defined knees in the force-deflection curve as shown in figure 26.

Hysteresis Loop

When an elastic structure is loaded and then unloaded the force-deflection values are described by the same curve. This is not the case in a yielding structure, where the force-deflection curve departs from the skeleton curve upon unloading. The force-deflection relation associated with alternating the loading between two extremes is called a hysteresis loop and the area of the loop is the energy dissipated by the structure during the loading cycle. Hysteresis loops for a variety of structures and the loading paths which produce these loops are shown in figure 27. Also indicated in this figure are the skeleton curves associated with the structures. If there is no deterioration of the material of the structure, repetition of the loading cycle will cause the hysteresis loop to be retraced.

The hysteretic behavior of the structure with a skeleton curve given by equation 3.1 is described by

$$\frac{x-x_i}{2x_y} = \frac{p-p_i}{2p_y} + \alpha\left(\frac{p-p_i}{2p_y}\right)^r \qquad (3.3)$$

where the point $(x_i/x_y,\ p_i/p_y)$ is the most recent point at which the direction of the loading has been reversed. Applying this equation to a hysteresis loop describing cyclic loading between $(x_o/x_y,\ p_o/p_y)$ and $(-x_o/x_y,\ -p_o/p_y)$ gives for the ascending branch of the loop

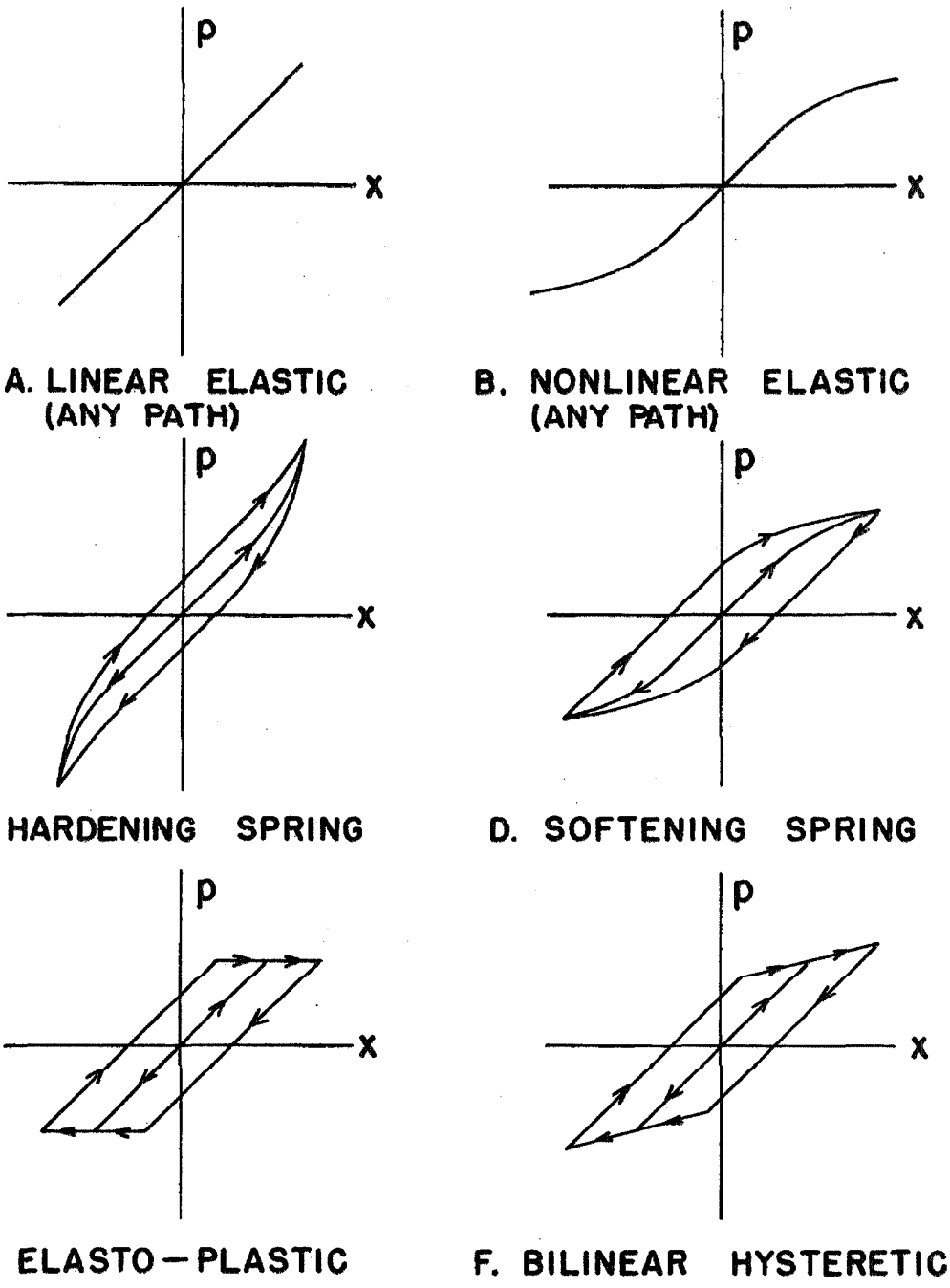

FIGURE NO. 27
HYSTERESIS LOOPS
OF VARIOUS TYPES

$$\frac{x + x_o}{2x_y} = \frac{p + p_o}{2p_y} + a\left(\frac{p + p_o}{2p_y}\right)^r \qquad (3.4)$$

where, in the region where equation 3.4 applies, $x + x_o$ and $p + p_o$ are never negative. The descending branch of the hysteresis loop is given by

$$\frac{x - x_o}{2x_y} = \frac{p - p_o}{2p_y} + a\left(\frac{p - p_o}{2p_y}\right)^r \qquad (3.5)$$

and in the region of application $x-x_o$ and $p-p_o$ are never positive. The general hysteresis loop described by equations 3.4 and 3.5 and the skeleton curve (equation 3.1) are shown in figure 28. Examples of hysteresis loops given by different values of r and a are shown in figures 29 and 30. In figure 29 all of the loops have the same r value and the same force amplitude but have different values of a. The loops in figure 30 have the same value of a and deflection amplitude but the value of r is varied. Figure 31 illustrates the effect of the deflection amplitude upon the shape of the hysteresis loop. It is seen that for small amplitudes the loop is narrow with its major axis aligned with the linear portion of the skeleton curve. As the amplitude increases the loop broadens and the major axis is seen to rotate clockwise, a characteristic of softening systems.

As noted above, equations 3.4 and 3.5 are the same basic equation with origins located at $(-x_o/x_y, -p_o/p_y)$ and $(x_o/x_y, p_o/p_y)$, respectively. Furthermore, equation 3.1 is the same equation with origin at (0, 0) but with variables to a scale such that its graph is only half as large as that obtained from equation 3.4 or 3.5. The fact

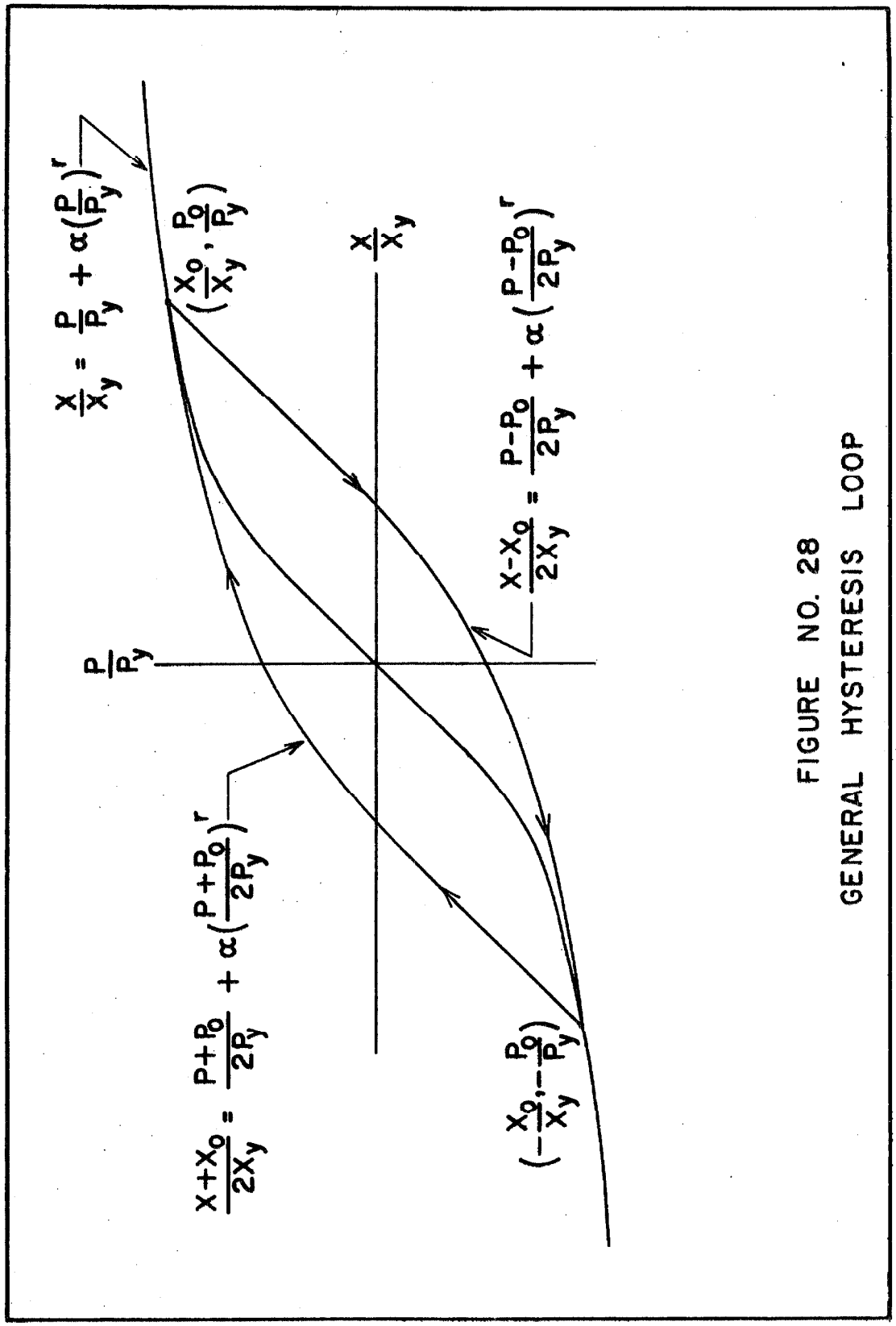

FIGURE NO. 28
GENERAL HYSTERESIS LOOP

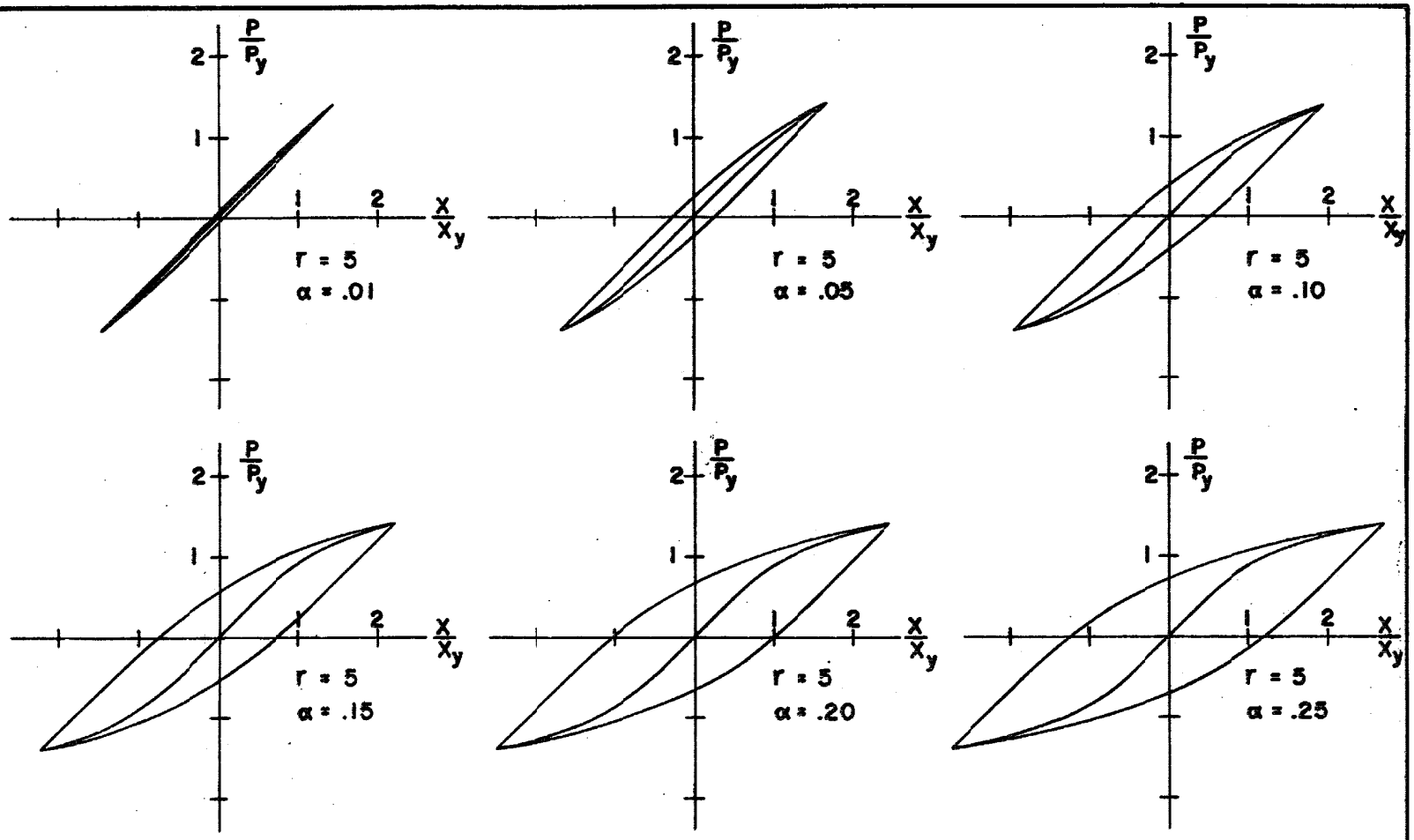

FIGURE NO. 29

THE EFFECT OF α ON THE HYSTERESIS LOOP

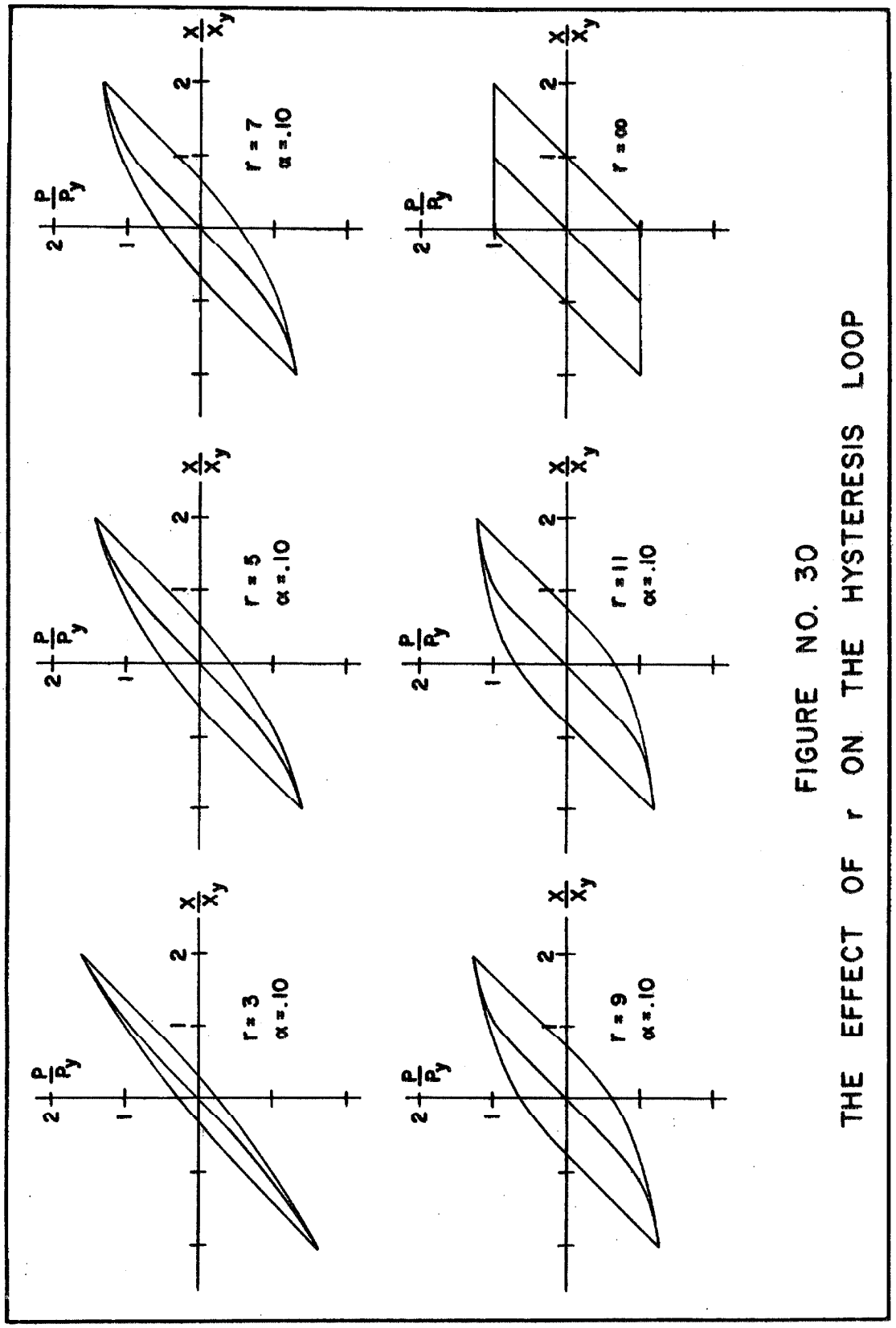

FIGURE NO. 30

THE EFFECT OF r ON THE HYSTERESIS LOOP

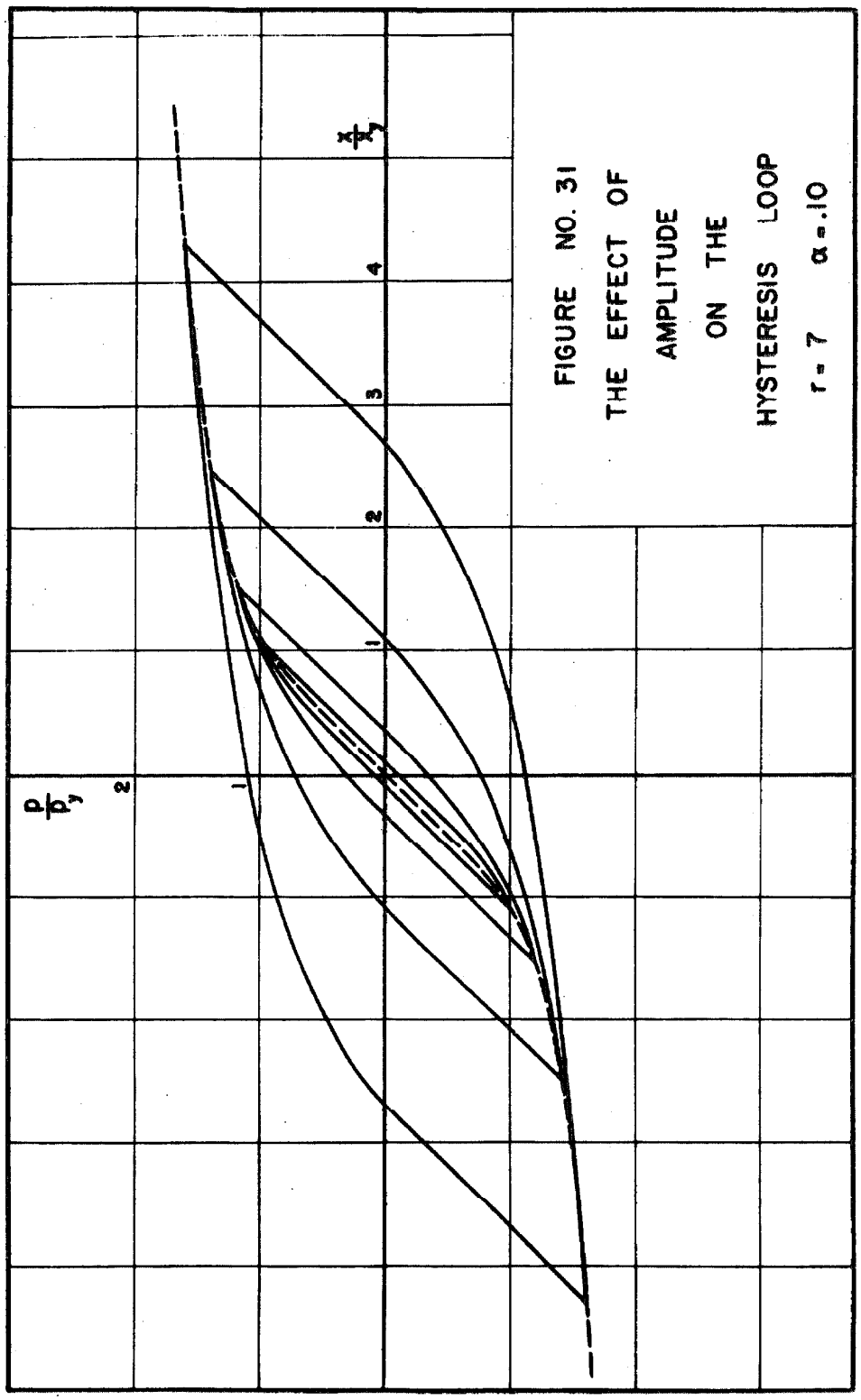

FIGURE NO. 31
THE EFFECT OF
AMPLITUDE
ON THE
HYSTERESIS LOOP
r = 7 α = .10

that the skeleton curve and both the ascending and descending branches of the hysteresis loop are described by the same basic equation has significant computational advantages. The formulation of a model for hysteretic behavior using the idea that the branches of the hysteresis loop are described by the same basic equation as the skeleton curve has been attributed to Masing.[34]

Properties of the Hysteresis Loops

Since it is intended to use the general hysteresis loop described by equations 3.4 and 3.5 to determine the steady-state response of a yielding structure to sinusoidal excitation, it will be useful to note some of the properties of the hysteresis loop.

By recalling that r is an odd integer, it is seen from examination of equation 3.1 that if $(x_o/x_y, p_o/p_y)$ is a point on the skeleton curve then $(-x_o/x_y, -p_o/p_y)$ is also on the skeleton curve. Equation 3.4 is used to describe the loop as it ascends from $(-x_o/x_y, -p_o/p_y)$ to $(x_o/x_y, p_o/p_y)$ and it is seen that the first of these two points satisfies equation 3.4 identically and that the second point satisfies the equation if it is a point on the skeleton curve. By applying similar reasoning to the descending branch of the loop it is concluded that equations 3.4 and 3.5 can describe a closed hysteresis loop whose upper and lower points lie on the skeleton curve.

It is clear from equations 3.4 and 3.5 and figure 28 that the initial slopes of the ascending and descending branches of the hysteresis loop are parallel to the linear portion of the skeleton

curve. At their other points of contact with the skeleton curve, it can be shown that the ascending and descending branches are tangent to the skeleton curve. The slope of the ascending curve is given by the derivative of equation 3. 4:

$$\frac{d(p/p_y)}{d(x/x_y)_a} = \frac{1}{1 + \alpha r \left(\frac{p+p_o}{2p_y} \right)^{r-1}} \tag{3.6}$$

The slope of the skeleton curve is determined from equation 3. 1:

$$\frac{d(p/p_y)}{d(x/x_y)_s} = \frac{1}{1 + \alpha r \left(\frac{p}{p_y} \right)^{r-1}} \tag{3.7}$$

Evaluation of equations 3. 6 and 3. 7 at their common point $(x_o/x_y, p_o/p_y)$ shows that the two curves are indeed tangent. A similar argument shows the tangency of the descending and skeleton curves at $(-x_o/x_y, -p_o/p_y)$.

As the constant α approaches zero the curves described by equations 3. 4 and 3. 5 can be made arbitrarily close to straight lines (assuming x/x_y and p/p_y are bounded). Thus the hysteresis loop degenerates into the straight line of the linear undamped oscillator as α approaches zero. Examples of the effect on the hysteresis loop of decreasing α are shown in figure 29. Moreover, as r approaches infinity the hysteresis loop approaches that of the elasto-plastic structure as is illustrated in figure 30. Therefore, it is seen that the hysteresis loops as well as the skeleton curves include the linear and elasto-plastic models as limiting cases.

Solution of the Basic Equation

Many of the results of this chapter will be expressed in terms of force amplitude rather than displacement amplitude. This is a consequence of the fact that equation 3.1 specifies the deflection as a function of the force instead of the force in terms of the deflection as is the usual case. Because there is a one-to-one correspondence between force and deflection in equations such as 3.1, 3.4 and 3.5, no error is made by presenting the results in terms of either variable. However, it is often more convenient to express the results in terms of the deflection level; thus requiring the solution of the equation

$$y = z + \alpha z^r \tag{3.8}$$

where y and z are variables which may have different meanings depending on which equation is being discussed. If z is given and y is to be found there is no problem, but when z is desired, given y, iterative solutions must be used for in general there is no explicit solution to the r^{th} degree polynomial of equation 3.8.

The iterative method used to solve equation 3.8 is that due to Newton and Raphson and is explained in reference 57, pp. 443-450. The application of the method to equation 3.8 produces the following formula for the $w+1^{st}$ iteration for z.

$$z_{w+1} = \frac{\alpha(r-1)z_w^r + y}{1 + \alpha r z_w^{r-1}} \tag{3.9}$$

Because r-1 is an even integer the denominator is always finite so convergence is guaranteed. The convergence is very fast, the error

in each iteration tends to be proportional to the square of the previous error. In slide rule use two or three iterations are sufficient if a well chosen first value is used. For digital computer application rapid convergence is obtained if z_o has absolute value larger than that of the final solution and has the same sign as y. Although convergence is assured in theory, for large values of r round off and truncation errors may occasionally cause difficulties when the answer z is very close to unity.

C. Discussion of the Hysteretic Formulation

L. S. Jacobsen has emphasized in a recent study[33] that almost no determination of structural damping properties has been made so that studies must be based upon static tests and there are few of these that include several cycles of loading in alternate directions. Some examples of work in cyclic loading are reported in references 33, 58, 30 and 55. In particular, the appendix of reference 33 gives some examples and references to work by Japanese investigators in this area. Comparison of the figures in these references with figures 29 and 30 shows that many of the experimentally determined relations are reasonably approximated by members of the family of force-deflection curves considered here. However, experimentally determined curves of the hardening type, similar to figure 27C, do not fall within the scope of this study. It is not known what correspondence exists between force-deflection curves obtained from static testing and those describing the dynamic behavior of structures; therefore, it is not considered appropriate to attempt a detailed fit

of the general force-deflection relation to the results of static tests.

The hysteretic relation formulated here has several advantages over the commonly used elasto-plastic or bilinear hysteretic relations. Principal among these are:

1. It is sufficiently general so that it can be applied to a wide range of structures. Since the linear and elasto-plastic relations are included as limiting cases, the effects of different types of yielding behavior can be studied and where explicit results are obtained the influence of the yielding parameters can be found directly.
2. It is more realistic than the elasto-plastic or bilinear hysteretic yielding relations for many applications because the departure from linearity is continuous and smooth.

There are, of course, some disadvantages to this representation:

1. An explicit expression for the force in terms of the displacement is not possible, which is inconvenient for the presentation and interpretation of the results.
2. In cases where the transient response of yielding structures is studied the formulation of the hysteretic equations is more difficult than for the elasto-plastic or bilinear hysteretic relations.

The first of these disadvantages has been discussed above. The formulation of the hysteretic equations for general dynamic behavior is undertaken in Part IV of the thesis.

D. Steady-State Response by Energy Methods

Energy Dissipated per Cycle

Consider the response of the one degree-of-freedom structure shown in figure 25 to sinusoidal excitation. The force-deflection relation of the structure is given in figure 28 and the hysteresis loop is described by equations 3.4 and 3.5. It is assumed that eventually the response of the structure attains a steady-state.

During steady-state response the hysteresis loop is traced repeatedly and in each cycle the energy dissipated is:

$$E_d = \oint p(x)\, dx \tag{3.10}$$

where E_d is the energy dissipated per cycle. It is convenient to separate this integral into the parts corresponding to the ascending and descending portions of the hysteresis loop and to write dx as (dx/dp) dp:

$$E_d = \int_{-p_o}^{p_o} p(x) \frac{dx}{dp}\, dp + \int_{p_o}^{-p_o} p(x) \frac{dx}{dp}\, dp \tag{3.11}$$

The points (x_o, p_o) and $(-x_o, -p_o)$, the extremes of the hysteresis loop, are assumed to be on the skeleton curve. For the first integral the ascending branch, equation 3.4, applies and it is found that

$$\left(\frac{dx}{dp}\right)_a = \frac{x_y}{p_y}\left[1 + \alpha r \left(\frac{p+p_o}{2p_y}\right)^{r-1}\right] \tag{3.12}$$

Similarly, for the second integral of equation 3.11, equation 3.5 applies and

$$\left(\frac{dx}{dp}\right)_d = \frac{x_y}{p_y}\left[1 + \alpha r\left(\frac{p-p_o}{2p_y}\right)^{r-1}\right] \tag{3.13}$$

Inserting equations 3.12 and 3.13 into equation 3.11 and making a slight change of variable produces

$$\frac{E_d}{\frac{1}{2}x_y p_y} = 2\int_{\frac{-p_o}{p_y}}^{\frac{p_o}{p_y}} \frac{p}{p_y}\left[1 + \alpha r\left(\frac{p+p_o}{2p_y}\right)^{r-1}\right] d\left(\frac{p}{p_y}\right)$$

$$+2\int_{\frac{p_o}{p_y}}^{-\frac{p_o}{p_y}} \frac{p}{p_y}\left[1 + \alpha r\left(\frac{p-p_o}{2p_y}\right)^{r-1}\right] d\left(\frac{p}{p_y}\right) \tag{3.14}$$

The dimensionless energy ratio of the left side of this equation has a convenient interpretation in cases where x_y and p_y represent the maximum values of force and deflection that are linearly related. For example, for the elasto-plastic and bilinear hysteretic force-deflection relations, $E_d/\frac{1}{2}x_y p_y$ is the ratio of the energy dissipated per cycle to the maximum value of the energy that can be stored in the structure without yielding.

Expanding the two integrals of equation 3.14 and letting $y = p+p_o/2p_y$ and $z = p-p_o/2p_y$ yields

$$\frac{E_d}{\frac{1}{2}x_y p_y} = 2\int_{\frac{-p_o}{p_y}}^{\frac{p_o}{p_y}} \frac{p}{p_y}\, d\left(\frac{p}{p_y}\right) + 2\int_{\frac{p_o}{p_y}}^{-\frac{p_o}{p_y}} \frac{p}{p_y}\, d\left(\frac{p}{p_y}\right) \quad +$$

$$+\frac{a\,r}{2^{r-2}}\int_{0}^{2\frac{p_o}{p_y}} y^{r-1}\left(y-\frac{p_o}{p_y}\right)dy+\frac{a\,r}{2^{r-2}}\int_{0}^{-2\frac{p_o}{p_y}} z^{r-1}\left(z+\frac{p_o}{p_y}\right)dz \tag{3.15}$$

The first two integrals of equation 3.15 represent the elastic portion of the work done in the half cycles and are zero. Taking advantage of the fact that r is an odd integer the remaining two integrals can be evaluated to obtain:

$$\frac{E_d}{\frac{1}{2}x_y p_y}=8a\left(\frac{r-1}{r+1}\right)\left(\frac{p_o}{p_y}\right)^{r+1} \tag{3.16}$$

Equation 3.16 gives the energy dissipated in a single cycle as a function of the amplitude of the restoring force. The force amplitude p_o/p_y is related to the amplitude of deflection x_o/x_y by equation 3.1. Although, in general, E_d cannot be expressed explicitly as a function of x_o/x_y approximate expressions for the cases of very small or very large deflections are easily found. For displacements large enough so that the linear term in equation 3.1 can be neglected, the resulting expression can be solved for p/p_y and substitution into equation 3.16 produces the large amplitude approximation:

$$\frac{E_d}{\frac{1}{2}x_y p_y}\simeq\frac{8}{r\sqrt{a}}\left(\frac{r-1}{r+1}\right)\left(\frac{x_o}{x_y}\right)^{\frac{r+1}{r}} \qquad \text{as } \frac{x_o}{x_y}\to\infty \tag{3.17}$$

On the other hand, for deflections small enough so that the nonlinear term of equation 3.1 can be neglected the small amplitude approximation of equation 3.16 is:

$$\frac{E_d}{\frac{1}{2} x_y p_y} \simeq 8a \left(\frac{r-1}{r+1}\right) \left(\frac{x_o}{x_y}\right)^{r+1} \qquad \text{as} \quad \frac{x_o}{x_y} \to 0 \tag{3.18}$$

From equation 3.17 it is seen that for large amplitudes the energy dissipated per cycle is proportional to the displacement amplitude raised to a power which is between one and two, but which approaches one as r increases. Also as r increases, the influence of a diminishes rapidly. Equation 3.18 describes the energy behavior for small amplitudes and it is seen in this case that the energy dissipated per cycle is proportional to a and approaches zero as the displacement to the $r+1^{st}$ power.

By way of comparison, for a linear, viscously damped structure under sinusoidal excitation the energy dissipated per cycle is proportional to the displacement amplitude squared and for an elasto-plastic or bilinear hysteretic structure the energy dissipated is proportional to the amplitude to the first power. This is apparent when it is recalled that E_d is the area of the hysteresis loop. For an elasto-plastic structure

$$\begin{aligned} \frac{E_d}{\frac{1}{2} x_y p_y} &= 8\left(\frac{x_o}{x_y} - 1\right) \qquad \frac{x_o}{x_y} > 1 \\ &= 0 \qquad\qquad \frac{x_o}{x_y} \leq 1 \end{aligned} \tag{3.19}$$

and for a linear, viscously damped structure the energy dissipated per cycle can be written as

$$\frac{E_d}{\frac{1}{2} x_y p_y} = 4\pi n \frac{\omega}{\omega_o} \left(\frac{x_o}{x_y}\right)^2 \qquad (3.20)$$

where ω_o is the natural frequency of the structure, n the fraction of critical damping, and ω the frequency of excitation. It should be noted that (ω / ω_o) and x_o / x_y are not independent.

Figure 32 shows the energy dissipation as a function of the amplitude of vibration for a variety of structures as determined by equations 3.1 and 3.16 for different values of r and for $\alpha = 0.10$. Included in this figure are curves for the elasto-plastic structure described by equation 3.19 and the linear structure for which it has been assumed that $\omega / \omega_o = 1$. Figure 32 illustrates the basic difference in energy dissipation between the elasto-plastic and the linear structure and shows how the behavior of the general structure changes from almost linear to elasto-plastic as r increases.

Energy Input per Cycle

The equation of motion of the general structure in response to sinusoidal excitation is

$$m\ddot{x} + p(x) = F_o \cos \omega t \qquad (3.21)$$

where m is the mass of the structure, F_o the force amplitude, and ω the frequency of the excitation. If it is assumed that the structure has achieved steady-state response under this excitation, the displacement will be periodic in ω and will possess the Fourier expansion

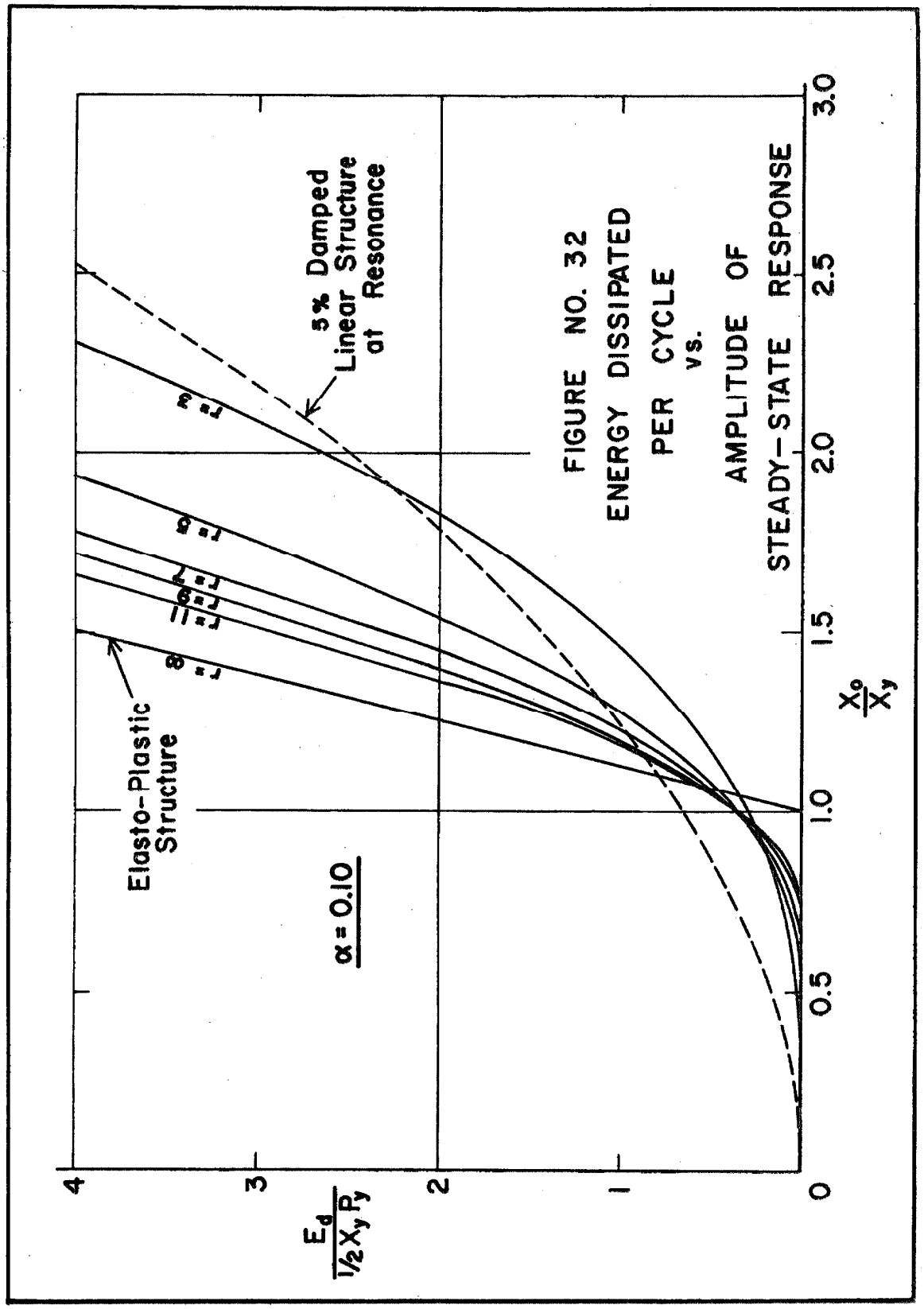
FIGURE NO. 32
ENERGY DISSIPATED
PER CYCLE
vs.
AMPLITUDE OF
STEADY-STATE RESPONSE
5% Damped
Linear Structure
at Resonance
Elasto-Plastic
Structure
α = 0.10
r = 3
r = 2
r = 1.5
r = 1.25
r = 1.1
r = 1
$\frac{E_d}{\frac{1}{2}X_y P_y}$
$\frac{X_o}{X_y}$
0
1
2
3
4
0.5
1.0
1.5
2.0
2.5
3.0

$$x(t) = \sum_{j=1}^{\infty} A_j \cos(j\omega t - \phi_j) \tag{3.22}$$

where ϕ_j is the phase angle and A_j the amplitude of the j^{th} term of the series. The energy supplied to the structure per cycle by the external force is

$$E_c = \oint F(t)dx \tag{3.23}$$

where E_c is the energy input per cycle and $F(t)$ is the external force. Evaluating $dx = \dot{x}dt$ from equation 3.22 yields

$$E_c = -\int_0^{2\pi/\omega} F_o \cos\omega t \left[\sum_{j=1}^{\infty} j\omega A_j \sin(j\omega t - \phi_j)\right] dt \tag{3.24}$$

The interchange of the integration and summation operations is valid in this case so equation 3.24 can be evaluated by use of the orthogonality of the trigonometric functions to obtain:

$$E_c = F_o \pi A_1 \sin\phi_1 \tag{3.25}$$

Therefore, it is seen that for steady-state response to sinusoidal excitation the energy input to the structure depends only on the amplitude and phase angle of the first component of the Fourier expansion of the displacement. Letting β be the ratio of the first Fourier coefficient to the amplitude

$$\beta = \frac{A_1}{x_o} \tag{3.26}$$

equation 3.25 becomes

$$E_c = F_o \pi x_o \beta \sin\phi_1 \tag{3.27}$$

Amplitude of Steady-State Response

When steady-state response is achieved the energy dissipated per cycle must equal the amount of energy input per cycle and from equations 3.16 and 3.27 it follows that

$$\frac{x_o}{x_y} = \frac{4a\left(\frac{r-1}{r+1}\right)\left(\frac{P_o}{P_y}\right)^{r+1}}{\pi\beta \sin \phi_1 \left(\frac{F_o}{P_y}\right)} \tag{3.28}$$

By use of equation 3.1 this result can be expressed in terms of the restoring force amplitude:

$$\frac{F_o}{P_y} = \frac{4a\left(\frac{r-1}{r+1}\right)\left(\frac{P_o}{P_y}\right)^{r}}{\pi\beta \sin \phi_1 \left[1 + a\left(\frac{P_o}{P_y}\right)^{r-1}\right]} \tag{3.29}$$

Equation 3.29 relates the force level of the excitation to the amplitude of steady-state vibrations of the structure. If the phase angle between the excitation and the response could be determined this equation would define response curves for the family of nonlinear structures. This cannot be done in general but the special case of resonance can be investigated. At resonance it is assumed that the excitation and the first Fourier component of the displacement are 90^o out of phase, as they are for a linear structure. From equations 3.21 and 3.22 this implies that $\phi_1 = \pi/2$. If it is assumed also that the ratio β is approximately one, equation 3.29 becomes

$$\frac{F_o}{P_y} = \frac{4a}{\pi}\left(\frac{r-1}{r+1}\right) \frac{\left(\frac{P_o}{P_y}\right)^{r}}{1 + a\left(\frac{P_o}{P_y}\right)^{r-1}} \tag{3.30}$$

It is noted that both of the previous assumptions are true for a linear structure so it is expected that equation 3. 30 will be a good approximation for small amplitudes, gradually worsening as the amplitude is increased. It will be shown later that these assumptions appear to be valid far into the nonlinear range.

By using equations 3. 30 and 3. 1, figure 33 has been constructed to show the relation between resonant steady-state amplitude and the force level of the excitation for several structures including the linear and elasto-plastic. The frequency of the excitation is not a variable in this presentation because the choice of $\sin \phi_1 = 1$ has assured that the resonant frequency is the one considered, though this resonant frequency need not be the same for all the structures. In the case of the elasto-plastic structure the relation between resonant amplitude and excitation level is found from equations 3. 19 and 3. 27 to be:

$$\frac{x_o}{x_y} = \frac{4}{4 - \frac{F_o}{p_y}\pi} \tag{3. 31}$$

It is seen that x_o/x_y is infinite for a certain choice of F_o/p_y. The discussion of infinite resonance will be undertaken in a later section.

Because the resonant amplitude as a function of force level is a measurement that could be made on real structures, figure 33 is of practical interest. The variation of the general structure between the limits of linear and elasto-plastic behavior is clearly seen in the figure. Looking at a particular curve as the force level is increased from zero it is seen that the curve initially steepens and then gradually

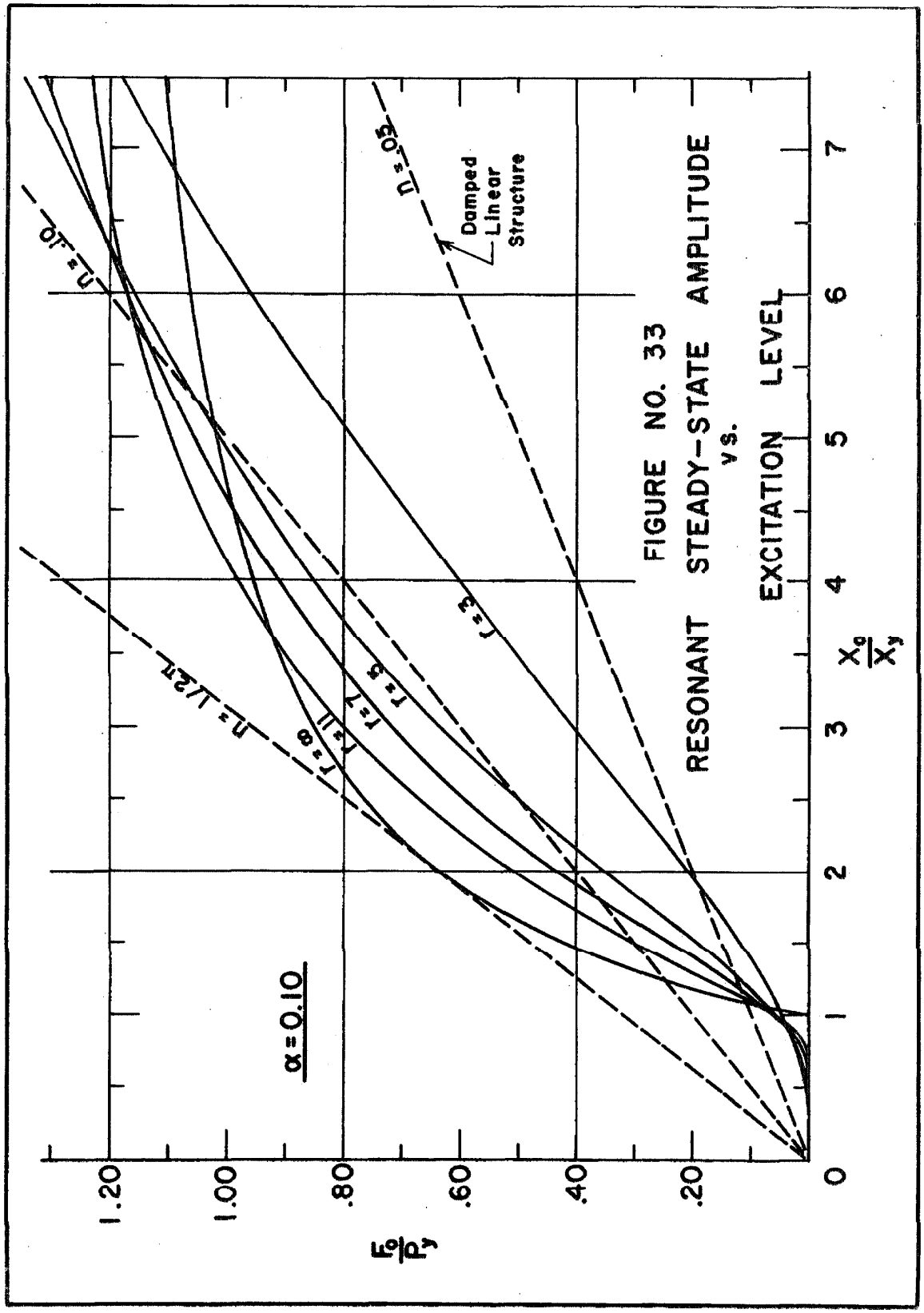
FIGURE NO. 33
RESONANT STEADY-STATE AMPLITUDE
vs.
EXCITATION LEVEL
$\frac{X_0}{X_y}$
$\frac{F_0}{F_y}$
α = 0.10
Damped Linear Structure
Ω = 0.5
Ω = 1/2π
Ω = 0
T = ∞
T = 11
T = 7
T = 5
T = 3
0
.20
.40
.60
.80
1.00
1.20
1
2
3
4
5
6
7

flattens for larger amplitudes. With reference to the linear structures shown in the figure this variation could be considered as a change in the equivalent viscous damping factor as the amplitude is increased.

Equivalent Viscous Damping

An equivalent viscous damping coefficient for the general structure can be found by making an energy balance. For a linear, viscously damped structure at resonance under sinusoidal excitation the energy dissipated per cycle is obtained from equation 3. 20:

$$\frac{E_d}{\frac{1}{2} x_y p_y} = 4n\pi \left(\frac{x_o}{x_y}\right)^2 \qquad (3.32)$$

If the energy dissipated by a linear structure, as given by this equation, is equated to that of the general structure, given by equation 3. 16, an equivalent viscous damping coefficient can be determined with the help of equation 3. 1:

$$n_{eq} = \frac{\frac{2a}{\pi}\left(\frac{r-1}{r+1}\right)\left(\frac{p_o}{p_y}\right)^{r-1}}{\left[1 + a\left(\frac{p_o}{p_y}\right)^{r-1}\right]^2} \qquad (3.33)$$

where n_{eq} is the fraction of critical damping of the linear structure which at resonance will dissipate the same energy as a function of amplitude as the general structure.

As the amplitude of the oscillation approaches zero equation 3. 1 can be used to obtain a small deflection approximation to equation 3. 33:

$$\eta_{eq} \simeq \frac{2a}{\pi}\left(\frac{r-1}{r+1}\right)\left(\frac{x_o}{x_y}\right)^{r-1} \quad \text{as} \quad \frac{x_o}{x_y} \to 0 \tag{3.34}$$

A large amplitude approximation can be found in a similar manner:

$$\eta_{eq} \simeq \frac{2\left(\frac{r-1}{r+1}\right)}{\pi\, \sqrt[r]{a}\left(\frac{x_o}{x_y}\right)^{\frac{r-1}{r}}} \quad \text{as} \quad \frac{x_o}{x_y} \to \infty \tag{3.35}$$

From equations 3.34 and 3.35 it is seen that the equivalent viscous damping factor goes to zero for both small and very large amplitudes. By setting the derivative of η_{eq} with respect to p/p_y equal to zero it is found that the maximum value of η_{eq} occurs when $a(p_o/p_y)^{r-1}=1$ and is

$$\eta_{eq}(\text{Max.}) = \frac{1}{2\pi}\left(\frac{r-1}{r+1}\right) \tag{3.36}$$

For $r=3$ the maximum η_{eq} is 0.0796 and for increasing r it approaches the value 0.159. It is seen that the maximum is independent of a although the amplitude at which it occurs is dependent on both r and a. The maximum occurs when $x_o/x_y = 2(p_o/p_y) = 2/\sqrt[r-1]{a}$. In figure 33 the maximum viscous damping factor is determined by the straight line which is tangent to the curve of the general structure. From equation 3.36 and figure 33 it is concluded that the maximum possible equivalent viscous damping factor for the yielding structures considered here is $1/2\pi$.

The concept of equivalent viscous damping has long been used in structural analysis because of its simplicity. The above discussion indicates that the equivalent viscous damping factors of yielding

structures are strongly dependent on amplitude and should be applied with caution. Furthermore, in view of the generality of the hysteretic relation, it appears unrealistic to attribute coefficients greater than about 16 per cent of critical to the effects of yielding. However, the equivalent viscous damping factor is a variable that can be obtained readily from resonance tests of real structures and if the structure is nonlinear its damping factor should be useful in determining the nonlinear formulation that best describes its dynamic behavior.

E. Steady State Oscillations by the Method of Slowly Varying Parameters

Introduction

In order to characterize the behavior at points other than resonance an investigation of the steady-state response of the general structure by the method of slowly varying parameters was performed. With this method frequency response curves are obtainedwhose maxima agree with the values found in the previous section. The method of slowly varying parameters, attributed to N. M. Krylov and N. N. Bogolyubov, has been applied to bilinear hysteretic structures by T. K. Caughey[28] and the presentation here follows closely that of his study. Another application of the same general method, including higher orders of approximation, can be found in reference 35.

Equations of the Response Curves

The equation of motion of the general structure in response to sinusoidal excitation is

$$m\ddot{x} + p(x) = F_o \cos \omega t \tag{3.37}$$

Introducing the following dimensionless parameters:

$$\omega_o^2 = \frac{p_y}{x_y m}$$

$$\eta = \omega/\omega_o \tag{3.38}$$

$$\tau = \omega_o t$$

where ω_o is the natural frequency of small oscillations, equation 3.37 can be transformed to

$$\frac{d^2}{d\tau^2}\frac{x}{x_y} + \frac{p}{p_y}\left(\frac{x}{x_y}\right) = \frac{F_o}{p_y}\cos \eta\tau \tag{3.39}$$

The solution of equation 3.39 is assumed to be

$$\frac{x}{x_y} = \frac{x_o}{x_y}\cos(\eta\tau + \phi) \tag{3.40}$$

where x_o/x_y and ϕ are slowly varying functions of τ. Taking the derivative of equation 3.40 gives

$$\frac{x}{x_y}' = -\eta\frac{x_o}{x_y}\sin\theta + \frac{x_o'}{x_y}\cos\theta - \frac{x_o}{x_y}\phi'\sin\theta \tag{3.41}$$

where $\theta = \eta\tau + \phi$ and primes denote differentiation with respect to τ. As is done in Lagrange's method of variation of parameters the last two terms are set equal to zero.

$$\frac{x_o'}{x_y} \cos\theta - \frac{x_o}{x_y} \phi' \sin\theta = 0 \tag{3.42}$$

From equations 3.41 and 3.42 it follows that

$$\frac{x''}{x_y} = -\eta^2 \frac{x_o}{x_y} \cos\theta - \eta \frac{x_o'}{x_y} \sin\theta - \eta \frac{x_o}{x_y} \phi' \cos\theta \tag{3.43}$$

Substituting equation 3.43 into equation 3.39 produces

$$-\eta^2 \frac{x_o}{x_y} \cos\theta - \eta \frac{x_o'}{x_y} \sin\theta - \eta \frac{x_o}{x_y} \phi' \cos\theta + \frac{p}{p_y} \left(\frac{x_o}{x_y} \cos\theta \right) = \frac{F_o}{p_y} \cos\eta\tau \tag{3.44}$$

If equation 3.42 is multiplied by $-\eta \cos\theta$ and equation 3.44 by $\sin\theta$ and the results added, one obtains

$$-\eta \frac{x_o'}{x_y} - \eta^2 \frac{x_o}{x_y} \cos\theta \sin\theta + \sin\theta \frac{p}{p_y} \left(\frac{x_o}{x_y} \cos\theta \right) = \frac{F_o}{p_y} \cos\eta\tau \sin\theta \tag{3.45}$$

As x_o/x_y and ϕ are slowly varying parameters the average of equation 3.45 is satisfied instead of the equation itself. Averaging over one cycle gives

$$-2\eta \frac{x_o'}{x_y} + \frac{1}{\pi} \int_0^{2\pi} \frac{p}{p_y} \left(\frac{x_o}{x_y} \cos\theta \right) \sin\theta \, d\theta = \frac{F_o}{p_y} \sin\phi \tag{3.46}$$

where it is noted that no distinction is made between x_o/x_y and ϕ and their averages over a cycle.

Multiplying equation 3.42 by $\eta \sin\theta$ and equation 3.44 by $\cos\theta$ and adding yields

$$-\eta \frac{x_o}{x_y} \phi' - \eta^2 \frac{x_o}{x_y} \cos^2\theta + \cos\theta \frac{p}{p_y}\left(\frac{x_o}{x_y}\cos\theta\right) = \frac{F_o}{p_y} \cos\eta\tau \cos\theta \qquad (3.47)$$

When averaged over one cycle of θ equation 3.47 reduces to

$$-2\eta \frac{x_o}{x_y} \phi' - \eta^2 \frac{x_o}{x_y} + \frac{1}{\pi} \int_0^{2\pi} \frac{p}{p_y}\left(\frac{x_o}{x_y}\cos\theta\right) \cos\theta \, d\theta = \frac{F_o}{p_y} \cos\phi \qquad (3.48)$$

If the integral expressions are defined by

$$C(x_o) = \frac{x_y}{x_o \pi} \int_0^{2\pi} \frac{p}{p_y}\left(\frac{x_o}{x_y}\cos\theta\right) \cos\theta \, d\theta$$

$$S(x_o) = \frac{x_y}{x_o \pi} \int_0^{2\pi} \frac{p}{p_y}\left(\frac{x_o}{x_y}\cos\theta\right) \sin\theta \, d\theta \qquad (3.49)$$

equations 3.46 and 3.48 can be written as

$$-2\eta \frac{x_o'}{x_y} + \frac{x_o}{x_y} S(x_o) = \frac{F_o}{p_y} \sin\phi$$

$$-2\eta \frac{x_o}{x_y} \phi' - \eta^2 \frac{x_o}{x_y} + \frac{x_o}{x_y} C(x_o) = \frac{F_o}{p_y} \cos\phi \qquad (3.50)$$

For steady state response the time derivatives of x_o/x_y and ϕ are zero so equation 3.50 becomes

$$\frac{x_o}{x_y} S(x_o) = \frac{F_o}{p_y} \sin \phi$$

$$\frac{x_o}{x_y} C(x_o) - \eta^2 \frac{x_o}{x_y} = \frac{F_o}{p_y} \cos \phi \qquad (3.51)$$

where henceforth x_o/x_y and ϕ are understood to signify variables of the steady state response. If ϕ is eliminated from equations 3.51 the result is

$$\left[S(x_o)\right]^2 + \left[C(x_o) - \eta^2\right]^2 = \frac{\left(\frac{F_o}{p_y}\right)^2}{\left(\frac{x_o}{x_y}\right)^2} \qquad (3.52)$$

Solving for η^2 the equation for the response curves is obtained.

$$\left(\frac{\omega}{\omega_o}\right)^2 = C(x_o) \pm \sqrt{\left(\frac{F_o}{p_y}\right)^2 \left(\frac{x_y}{x_o}\right)^2 - S^2(x_o)} \qquad (3.53)$$

The response curves can be constructed from equation 3.53 as shown in figure 34 where it is seen that $C(x_o)$ describes the resonant frequency as a function of amplitude.

From equation 3.51 it follows that

$$\tan \phi = \frac{S(x_o)}{C(x_o) - \eta^2} \qquad (3.54)$$

The maximum amplitude of the response curves given by equation 3.53 occurs when the radical is zero; at this point $\eta^2 = C(x_o)$. It can be shown that $S(x_o)$ is negative so from equation 3.51 and 3.54 it follows

FIGURE NO. 34
CONSTRUCTION OF
RESPONSE CURVES
FROM EQUATION 3.53

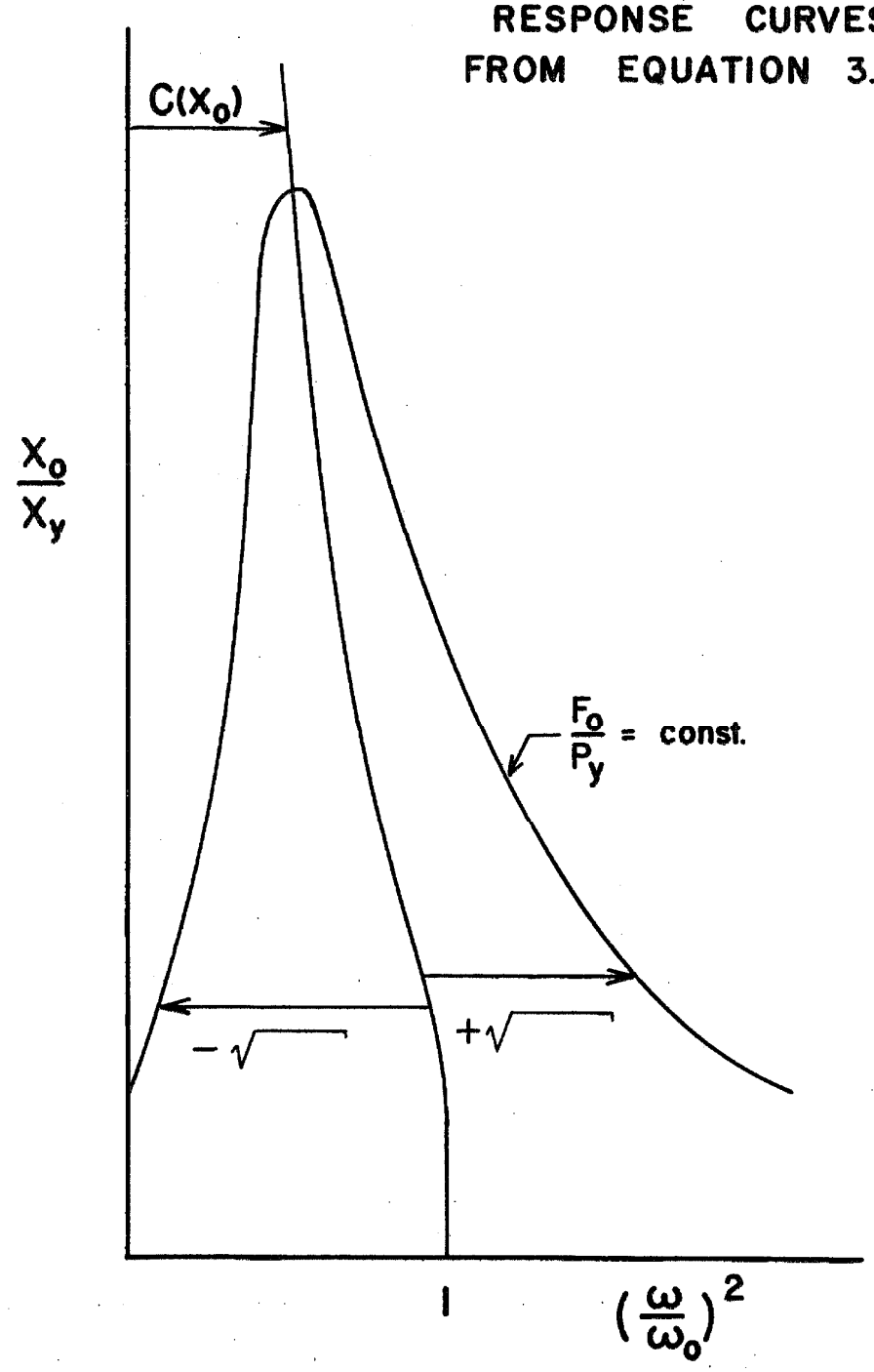

that resonance occurs when

$$\tan \phi = -\infty, \qquad \phi = -\pi/2 \tag{3.55}$$

From equation 3.53 and figure 34 it is seen that the maximum amplitude is determined from

$$\left(\frac{F_o}{p_y}\right)^2 = \left(\frac{x_o}{x_y}\right)^2 S^2(x_o) \tag{3.56}$$

Evaluation of $C(x_o)$ and $S(x_o)$

To help evaluate the integrals of equations 3.49 it is noted that the argument of p/p_y in the integrands is x_o/x_y when $\theta = 0$; $-x_o/x_y$ when $\theta = \pi$; and x_o/x_y when $\theta = 2\pi$. From figure 28 it follows that when θ varies from 0 to π the descending branch of the hysteresis loop is traversed and when θ goes from π to 2π the ascending branch is followed. With the help of figure 28 it can be shown that

$$\frac{p}{p_y}\left[\frac{x_o}{x_y}\cos(\theta + \pi)\right] = -\frac{p}{p_y}\left(\frac{x_o}{x_y}\cos\theta\right) \tag{3.57}$$

The integrals of equation 3.49 can therefore be written as

$$C(x_o) = \frac{2x_y}{\pi x_o}\int_0^{\pi} \frac{p}{p_y}\left(\frac{x_o}{x_y}\cos\theta\right)\cos\theta\, d\theta$$

$$S(x_o) = \frac{2x_y}{\pi x_o}\int_0^{\pi} \frac{p}{p_y}\left(\frac{x_o}{x_y}\cos\theta\right)\sin\theta\, d\theta \tag{3.58}$$

Making the substitution $z = (x_o/x_y)\cos\theta$ equation 3.58 becomes

$$C(x_o) = -\frac{2}{\pi}\left(\frac{x_y}{x_o}\right)^2 \int_{\frac{x_o}{x_y}}^{-\frac{x_o}{x_y}} \frac{z\,\frac{p}{p_y}(z)}{\sqrt{\left(\frac{x_o}{x_y}\right)^2 - z^2}}\,dz \tag{3.59}$$

$$S(x_o) = -\frac{2}{\pi}\left(\frac{x_y}{x_o}\right)^2 \int_{\frac{x_o}{x_y}}^{-\frac{x_o}{x_y}} \frac{p}{p_y}(z)\,dz$$

The integral for $S(x_o)$ is evaluated by letting $dz = \frac{dz}{dp}\,dp$ and proceeding as was done to find equation 3.16 from equation 3.10. It is found that

$$S(x_o) = \frac{-\frac{4a}{\pi}\left(\frac{r-1}{r+1}\right)\left(\frac{p_o}{p_y}\right)^{r+1}}{\left(\frac{x_o}{x_y}\right)^2} \tag{3.60}$$

Applying equation 3.56 and substituting for the value of x_o/x_y from equation 3.1 it is found that the maximum amplitude as a function of force level is described by

$$\frac{F_o}{p_y} = \frac{4a}{\pi}\left(\frac{r-1}{r+1}\right)\frac{\left(\frac{p_o}{p_y}\right)^r}{1 + a\left(\frac{p_o}{p_y}\right)^{r-1}} \tag{3.61}$$

which is identical to equation 3. 30, the result obtained by energy methods.

The integral for $C(x_o)$ in equations 3. 59 can be integrated by parts and then simplified by substituting for z its expression from the descending branch of the hysteresis loop, equation 3. 5. If this is done, after some algebra, the result is:

$$C(x_o) = \frac{8}{\pi}\left(\frac{x_y}{x_o}\right)^2 \int_0^{\frac{p_o}{p_y}} \sqrt{(y+\alpha y^r)\left[\frac{x_o}{x_y} - (y+\alpha y^r)\right]}\, dy \qquad (3.62)$$

The integral for $C(x_o)$ was evaluated on the digital computer for $r = 3, 5, 7, 9$ and 11, and for $\alpha = 0.05, 0.10, 0.15, 0.20$ and 0.25 and the results are presented in graphical form in Appendix II. Equation 3. 58 was used in performing the calculations.

Figure 35 illustrates the behavior of $C(x_o)$ for various values of r including the elasto-plastic case ($r=\infty$) from reference 28. $\sqrt{C(x_o)}$ is the ratio of the resonant frequency to that for small oscillations, so a linear structure is represented by $C(x_o) \equiv 1$. Since the resonant frequency as a function of amplitude could be obtained from tests of actual structures, the tests results could be compared to figures such as 35 to help determine the dynamic force-deflection relations of the structures.

Construction of the Response Curves

If the value of $S(x_o)$ from equation 3. 60 is substituted into equation 3. 53 the equation for the response curves can be written as

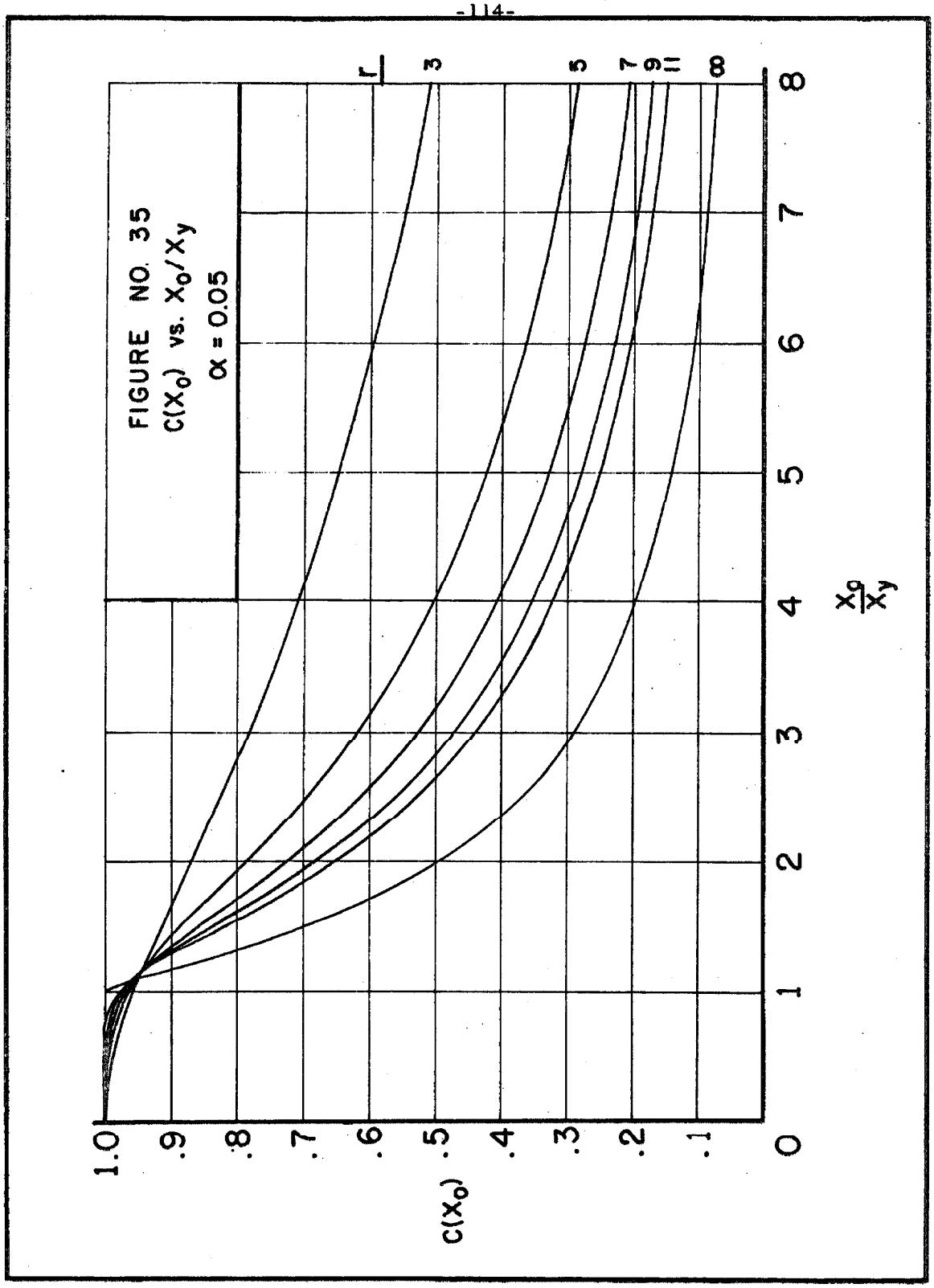
FIGURE NO. 35
C(X0) vs. X0/Xy
α = 0.05
r
3
5
7
9
11
8
1.0
.9
.8
.7
.6
.5
.4
.3
.2
.1
0
1
2
3
4
5
6
7
8
C(X0)
X0/Xy

$$\left(\frac{\omega}{\omega_o}\right)^2 = C(x_o) \pm \frac{\sqrt{\left(\frac{F_o}{p_y}\right)^2\left[1+\alpha\left(\frac{p_o}{p_y}\right)^{r-1}\right]^2 - \frac{16\alpha^2}{\pi^2}\left(\frac{r-1}{r+1}\right)^2\left(\frac{p_o}{p_y}\right)^{2r}}}{\frac{p_o}{p_y}\left[1+\alpha\left(\frac{p_o}{p_y}\right)^{r-1}\right]^2} \qquad (3.63)$$

where equation 3.1 has been used to eliminate x_o/x_y. Using equation 3.63 and values of $C(x_o)$ from Appendix II, the response curves shown in figure 36 were constructed. These curves give the amplitude of steady-state response to sinusoidal excitation as a function of the frequency ratio and of the level of excitation. The curves for $r = \infty$ are from reference 28 and the dashed lines in the figure indicate $C(x_o)$. In figure 36 the variation in dynamic behavior from almost linear to elasto-plastic as r increases is clearly shown. For practical purposes it appears that values of r greater than 11 would rarely be needed.

Verification of Response Curves

As a check upon the results of this section the numerical integration of equation 3.39 was carried out on a digital computer. In essence the procedure was to let the skeleton curve, equation 3.1, describe the force-deflection relation until the velocity first changed sign; thereafter equation 3.3 was used with $(x_i/x_y,\ p_i/p_y)$ being the most recent point at which the velocity changed sign. If steady-state oscillations eventually occur between $(x_o/x_y,\ p_o/p_y)$ and $(-x_o/x_y,\ -p_o/p_y)$ it is seen that equation 3.3 will reduce to equations 3.4 and 3.5 for

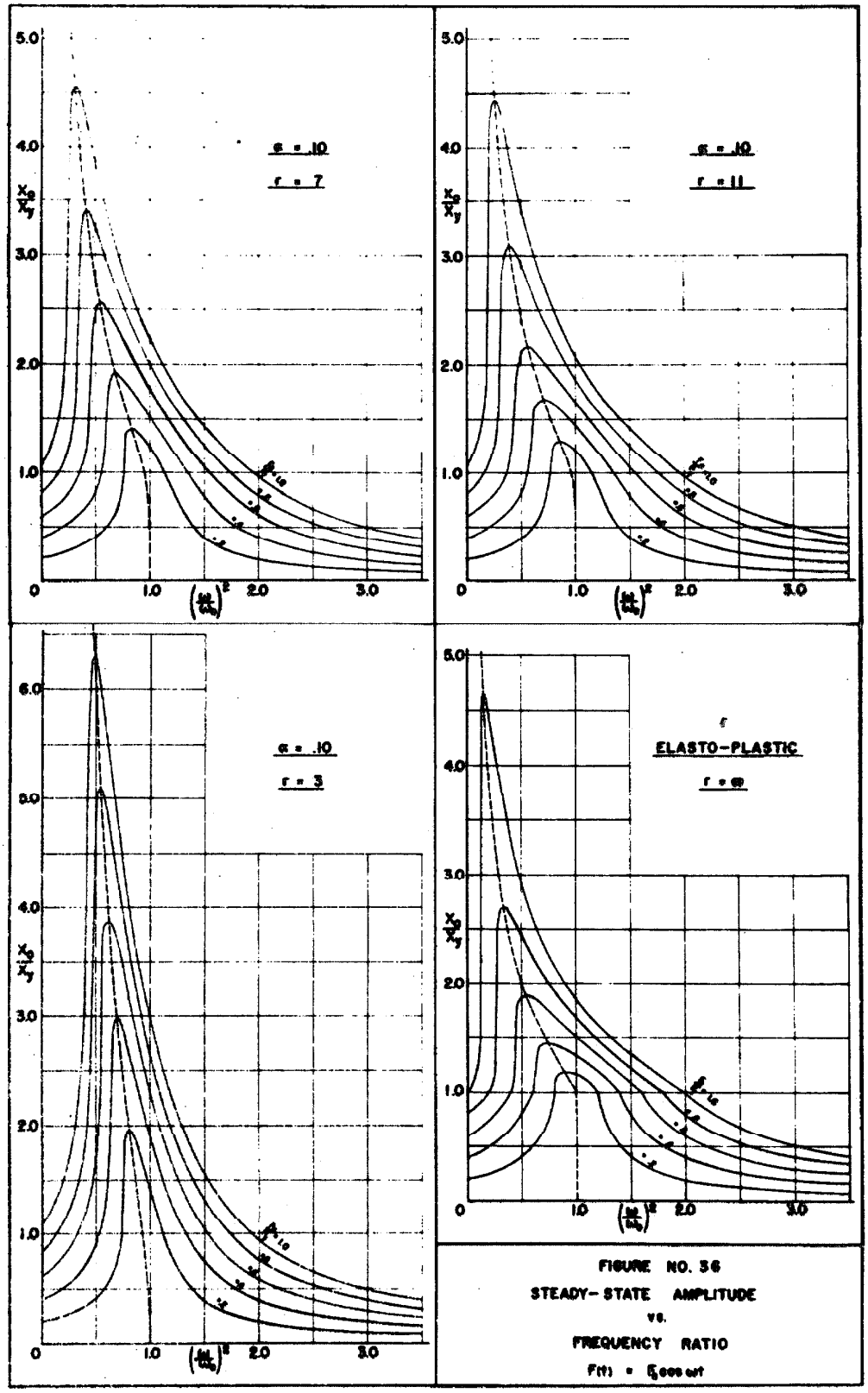

FIGURE NO. 36
STEADY-STATE AMPLITUDE
vs.
FREQUENCY RATIO
F(t) = $F_0 \cos \omega t$

the ascending and descending branches of the hysteresis loop. Convergence to a steady-state was hastened for small amplitudes by supplying the initial conditions that would make a linear oscillator achieve the steady-state immediately. The integration was done using a third order Runge-Kutta method on the Burroughs 220 digital computer at the California Institute of Technology and details are presented in Appendix I.

The results of the verification of the response curves for $r = 7$ and $\alpha = 0.10$ are shown in figure 37. These curves were chosen as typical and were the only ones verified in such detail although occasional points on other curves were obtained. The curves for $r = \infty$ shown in figure 36 have been verified by Caughey[28] and W. D. Iwan[27] on an analog computer. From the agreement of the numerical and analytical results it is concluded that the results of this section describe accurately the steady-state response of the nonlinear structures considered.

The principal assumption made in the theory was that the response was approximately sinusoidal. The numerically calculated steady-state acceleration and displacement corresponding to the peak of the $F_o/p_y = 1$ response curve of figure 37 are shown in figure 38. The hysteresis loop for this amplitude is approximately equal to the largest one shown in figure 31. Although the acceleration is obviously not sinusoidal the displacement is almost indistinguishable from a sine wave. Figure 38 appears to justify the assumption of sinusoidal displacement made in this study and indicates that the

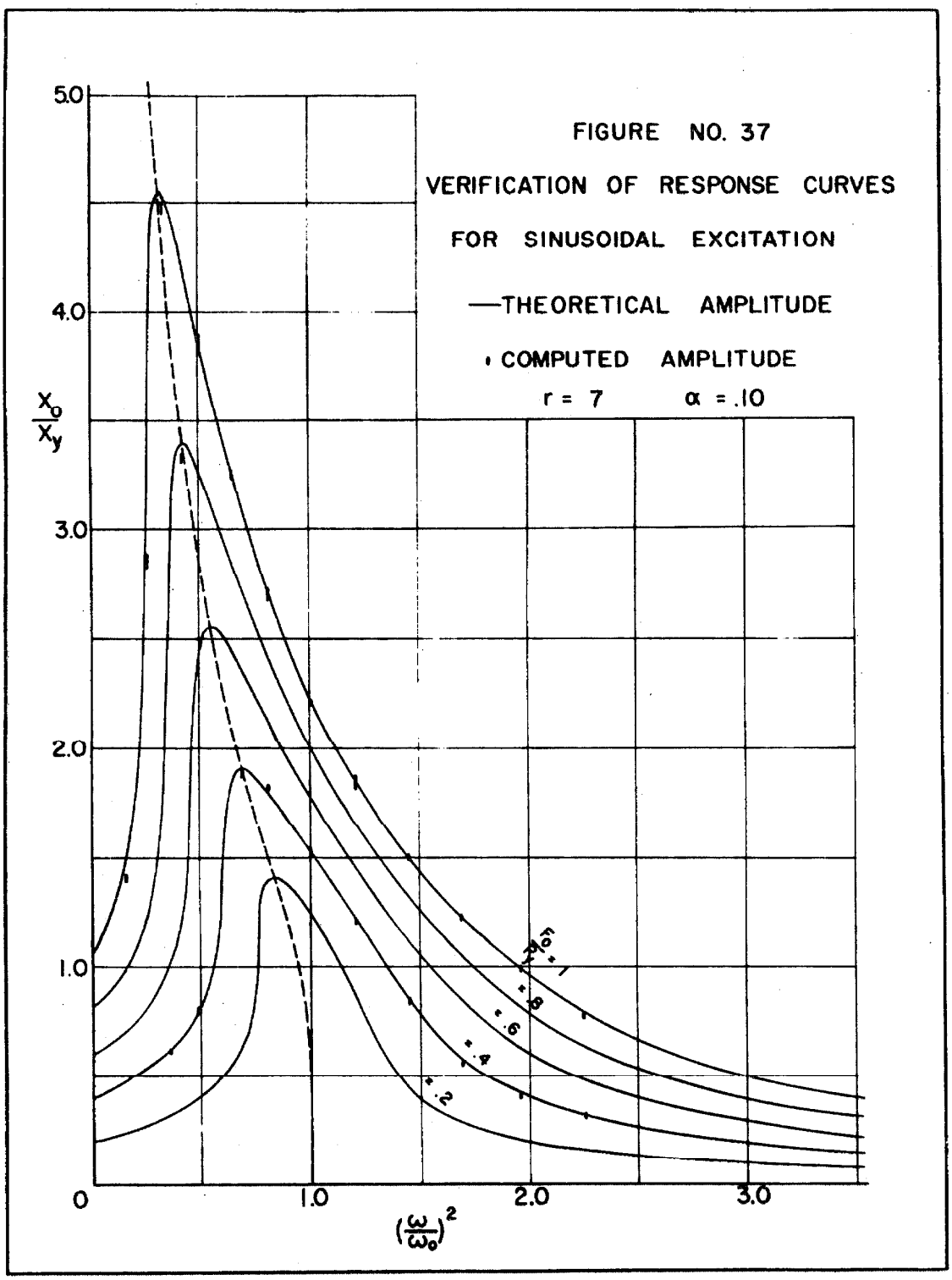

FIGURE NO. 37

VERIFICATION OF RESPONSE CURVES FOR SINUSOIDAL EXCITATION

—THEORETICAL AMPLITUDE

• COMPUTED AMPLITUDE

r = 7 α = .10

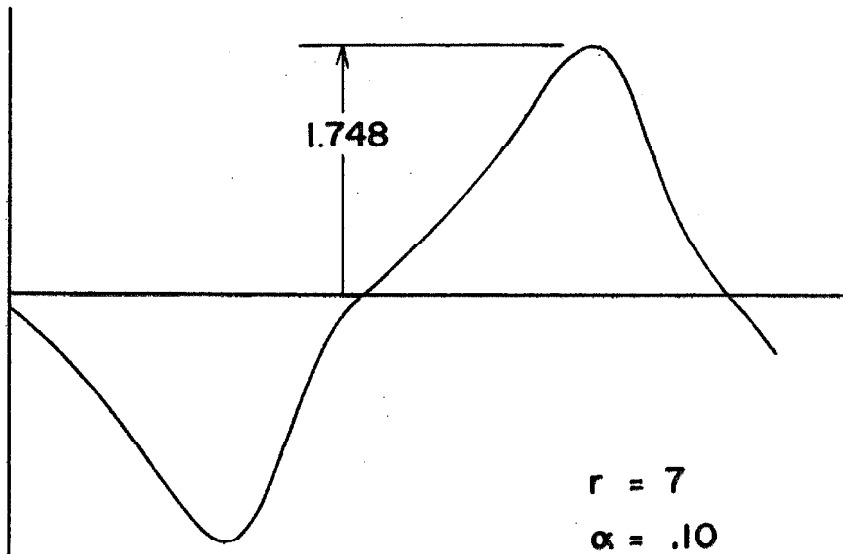

ACCELERATION

$r = 7$

$\alpha = .10$

$\frac{F_0}{P_y} = 1$

$\left(\frac{\omega}{\omega_0}\right)^2 = .325$

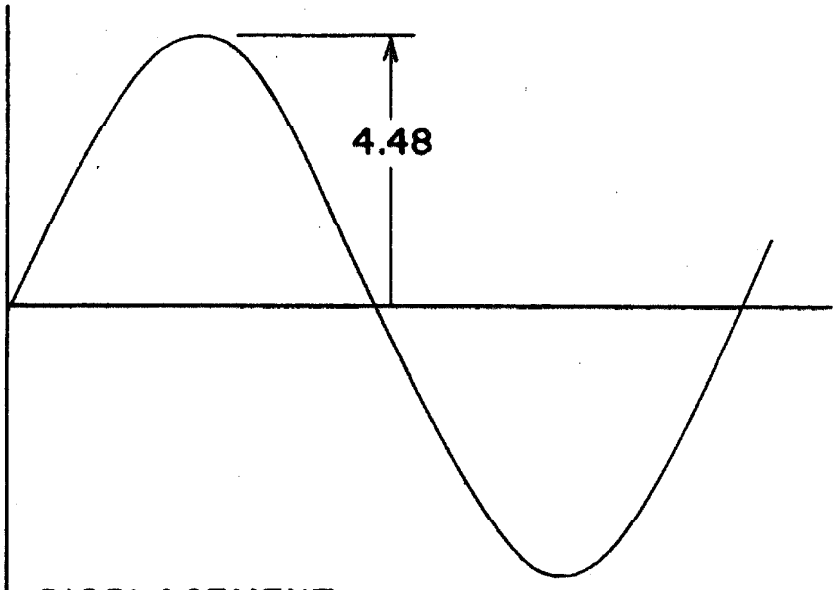

DISPLACEMENT

FIGURE NO. 38
STEADY—STATE RESPONSE

method of slowly varying parameters, originally designed for small nonlinearities, may have wider application in nonlinear response studies.

Infinite Resonance

Since infinite resonance under sinusoidal excitation is indicated at certain excitation levels for the elasto-plastic and bilinear hysteretic structures,[27, 28] it is of interest to see if this phenomenon is possible for any of the nonlinear structures studied here. Equation 3.30 describes the maximum amplitude as a function of the excitation level and to investigate unbounded resonance it is assumed that the displacement is large, postulating whatever exciting force that is necessary to produce this amplitude. For large displacements equation 3.30 approaches

$$\frac{F_o}{p_y} = \frac{4}{\pi}\left(\frac{r-1}{r+1}\right)\frac{p_o}{p_y} \tag{3.64}$$

and neglecting the linear term in equation 3.1, equation 3.64 can be expressed in terms of the displacement amplitude as

$$\frac{x_o}{x_y} = \alpha\left[\frac{F_o}{p_y}\ \frac{\pi}{4}\ \left(\frac{r+1}{r-1}\right)\right]^r \tag{3.65}$$

This equation states that, for any finite value of r, infinite resonance is not possible provided the excitation level is bounded. However, as r tends to infinity the general structure has been shown to approach the elasto-plastic case and equation 3.65 indicates in this instance that unbounded resonance will occur as $r \to \infty$ if

$$\frac{F_o}{p_y} > \frac{4}{\pi} \tag{3.66}$$

This result agrees with that obtained by Caughey.[28]

From this discussion it is concluded that infinite resonance will not occur for any member of the general nonlinear family but that it will occur for the limiting cases of the elasto-plastic and the linear structure.

F. Summary and Conclusions

A general yielding relation for a one degree-of-freedom structure has been proposed and the steady-state response of this structure to sinusoidal excitation has been studied in some detail. Explicit expressions have been obtained for the energy dissipated per cycle, the resonant amplitude, and the equivalent viscous damping factor. With the help of a digital computer the resonant frequency as a function of amplitude and the frequency response curves were calculated. By means of numerical integration the accuracy of the results has been checked and the response was found to be sinusoidal well into the nonlinear range of the structure.

The ability of the general yielding relation to represent a range of hysteretic structures varying in behavior from linear to elasto-plastic has been demonstrated.

If the dynamic force-deflection relation of a real structure can be approximated by the expressions given here, the steady state response can be characterized for amplitudes several times the linear

range of the structure. Many of the results of this study are strongly dependent on p_o/p_y (or x_o/x_y), but weakly dependent on r and α so the approximation should take this into account.

The equivalent viscous damping factor of a yielding structure is seen to be dependent on amplitude, approaching zero for both small and very large amplitudes. The damping factor for the general structure has a maximum dependent only on r; the maximum possible value is for the elasto-plastic structure and is $1/2\pi$. Therefore, it appears unrealistic to attribute viscous damping factors greater than this to the effects of yielding.

The steady-state response to sinusoidal excitation is a result that can be obtained from buildings and other real structures. If the actual structure falls into the general case studied here, it seems that the resonant amplitude as a function of resonant frequency and of excitation level, the equivalent viscous damping, and the frequency response curves would be measurements useful in determining the parameters α, r and x_y (or p_y) needed to characterize the dynamic force-deflection behavior of the structure.

To obtain agreement with test results it may be necessary to extend the theory to include non-integer values of r. It may be necessary also to include a viscous damping coefficient in the steady-state response calculations in order to account for observed energy dissipation at relatively low amplitudes.

Although the force-deflection relation presented here is fairly general and appears to be a reasonable first approximation to nonlinear

dynamic behavior, research into the dynamic behavior of actual structures in the nonlinear range is clearly needed to test its applicability.

IV. RESPONSE OF A SIMPLE NONLINEAR STRUCTURE TO EARTHQUAKE MOTION

A. Introduction

In this chapter the response of a one degree-of-freedom yielding structure to earthquake motion is studied. A class of yielding structures suitable for earthquake response studies is defined. This class includes the linear, the elasto-plastic, and the bilinear hysteretic structures in addition to the general yielding structure of the preceeding chapter. The equation of motion and the energy equation for yielding structures are examined in detail and the yielding structure defined by the parameters $r = 9$ and $\alpha = 0.10$ is subjected to the ensemble of pseudo-earthquakes that were developed in chapter II. The results include the average displacement spectra, the average energy input, the average relative amounts of energy dissipated by yielding and by viscous damping, and averages of the estimated permanent set. Conclusions pertaining to the effects of the strength of the earthquake, the natural period of the structure and the fraction of critical viscous damping upon the response of this particular structure are presented and examples are given to illustrate the application of the results to the analysis of earthquake response.

It is concluded that the class of hysteretic structures that is defined here is broad enough to be useful in dynamic studies and it is thought that the hysteresis law governing the response of this class of structures is a reasonable approximation to the behavior

of many actual structures. It is also concluded that results such as presented here would be useful in predicting the response of one degree-of-freedom yielding structures to earthquake excitation. The results for the structure studied indicate that if the yielding parameters are known the expected values of the response can be determined and estimates of the reliability of these averages can be found.

The notation of this chapter is the same as the previous chapters with the following additions.

Symbol	Explanation or definition
g	acceleration of gravity
k_s	the slope near the origin of the force-deflection curve of a nonlinear structure
q_y	yield level = p_y/m
$\ddot{\bar{y}}$	measure of earthquake acceleration strength
E_p	energy dissipated by yielding
E_s	recoverable strain energy
E_v	energy dissipated by viscous friction
γ	acceleration ratio = $\ddot{\bar{y}}/q_y$
$\sigma(t)$	normalized dimensionless time record of earthquake-type excitation
$\frac{x_I}{x_y}$	intercept of a hysteresis curve on the x/x_y axis
$\frac{x_f}{x_y}$	displacement at end of excitation
$\frac{x_p}{x_y}$	permanent set at the end of the excitation

$\frac{p_f}{p_y}$ restoring force at the end of the excitation

$\left(\frac{x_o}{x_y}, \frac{p_o}{p_y}\right)$ origin of a force-deflection curve

$\left(\frac{x_m}{x_y}, \frac{p_m}{p_y}\right)$ minimum or maximum point on a force-deflection diagram

B. A Class of Nonlinear Structures

In this section a class of nonlinear yielding structures is defined. The set of structures is determined by the geometry of the hysteresis curves and by the hysteresis law governing the yielding behavior. Included in the classification are the elastic, the elasto-plastic and the bilinear hysteretic structures, as well as the general yielding structure discussed in the preceding chapter.

The following definitions are useful for describing the hysteretic response of structures:

1. The minimum curve (min curve) is that ascending curve whose intercept on the x/x_y axis is less than that for all previous ascending curves and whose origin, the minimum point (min point), has a value of x/x_y less than that for all previous ascending curves. The first minimum curve is the skeleton curve with origin and intercept at (0, 0).

2. The maximum curve (max curve) is that descending curve whose intercept on the x/x_y axis is greater than that for all previous descending curves and whose origin, the maximum point (max point), has a value of x/x_y greater than that for all previous ascending curves. The first maximum curve is also the skeleton curve.

3. The upper boundary is the min curve between its least and greatest points of contact with the skeleton curve and is the skeleton curve elsewhere.

4. The lower boundary is the max curve between its least and greatest points of contact with the skeleton curve and is the skeleton curve elsewhere.

When formulating the law governing hysteretic response four criteria were used: 1) The law should apply to a wide range of yielding relations; 2) the law should describe steady-state response and other simple loading situations and prescribe reasonable behavior for more complicated response; 3) the law should be simple and easy to apply; 4) it should not be in contradiction to the general character of the behavior of actual yielding structures.

The set of yielding structures considered is restricted to those softening systems for which the skeleton curve is symmetric about the origin and for which the hysteretic curves are described by the same basic equation as the skeleton curve. The hysteretic curves have parameters scaled to be precisely half those in the equation for the skeleton curve, thus making them geometrically similar to, but twice as large as, the skeleton curve. The class is further restricted to those structures with yielding behavior described by the following law:

> Force-deflection values are given by a hysteretic curve originating from the point of most recent loading reversal until either the upper or lower boundary is contacted. Thereafter the force-deflection values are given by that boundary until the direction of loading again is reversed.

Examination of this class of structures shows that it includes the linear, the elasto-plastic and the bilinear hysteretic force-deflection relations. In the case of the linear structure the upper and lower boundaries are always the same straight line and the

hysteresis law requires that in this instance the force-deflection values be given by this line. For the elasto-plastic and bilinear hysteretic structures the upper and lower boundaries determine a parallelogram which has left and right sides determined by the min curve and max curve, respectively. The upper side of the parallelogram is defined by the min curve and the skeleton curve, and the lower side is determined by the max curve and the skeleton curve. The hysteresis law insures that ascending curves do not cross the upper side of this parallelogram and that descending curves do not cross the lower side. Thus the parallelogram can be extended laterally by following the skeleton curve but its altitude cannot be changed. Consideration will show that these conditions are equivalent to the usual formulation of the elasto-plastic and bilinear hysteretic yielding laws.

In the case of the general yielding structure of the preceeding chapter the skeleton curve is given by equation 3.1:

$$\frac{x}{x_y} = \frac{p}{p_y} + \alpha \left(\frac{p}{p_y}\right)^r \tag{4.1}$$

and other curves are described by equation 3.3:

$$\frac{x-x_i}{2x_y} = \frac{p-p_i}{2p_y} + \alpha \left(\frac{p-p_i}{2p_y}\right)^r \tag{4.2}$$

where $(x_i/x_y,\ p_i/p_y)$ is the point at which the loading was reversed. Since the max and min points are points of loading reversal, equation 4.2 describes the max and min curves.

Figure 39 shows typical upper and lower boundaries for the general structure and figure 40 gives examples of the application of

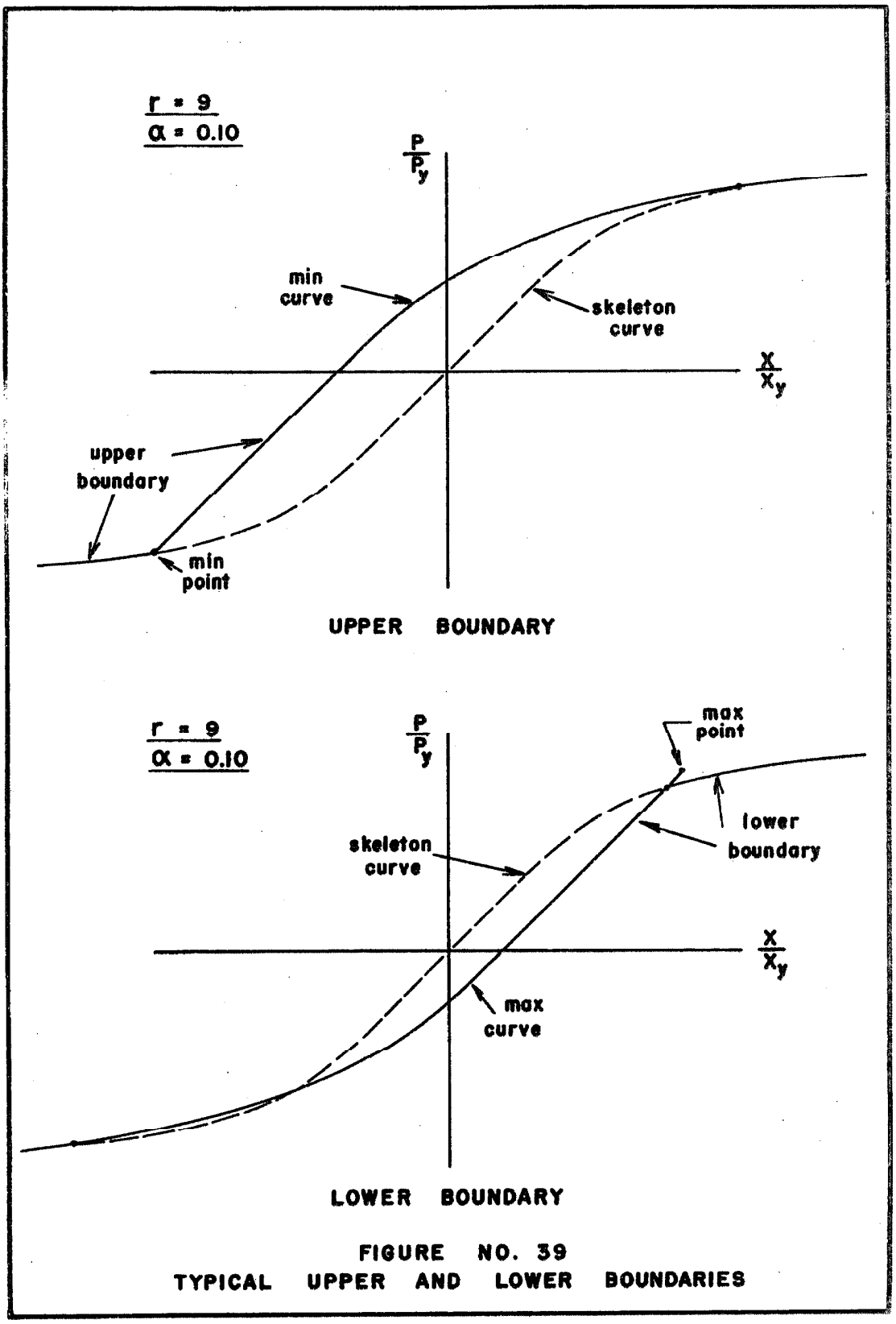

FIGURE NO. 39
TYPICAL UPPER AND LOWER BOUNDARIES

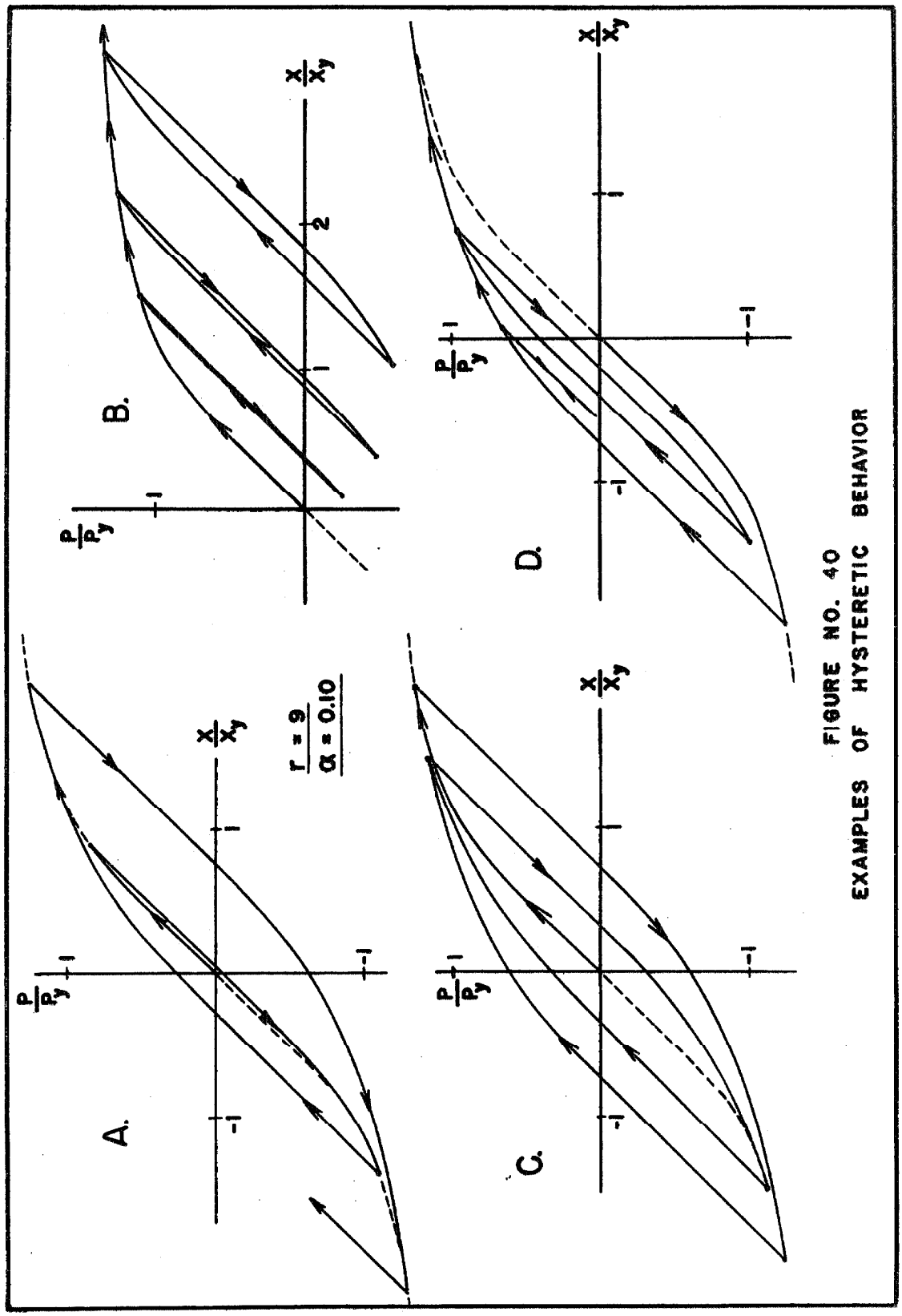

FIGURE NO. 40
EXAMPLES OF HYSTERETIC BEHAVIOR

the hysteresis law to some simple loading situations. Case A of figure 40 shows the response to an alternating load of increasing magnitude, and in case B the load is increased then decreased to less than zero, and then increased beyond its first maximum, etc. Case C shows an example of how the response might reduce to a steady-state in response to periodic excitation. The response to some general excitation is exemplified by case D.

The hysteresis law provides a consistent description of the dynamic behavior of a broad class of yielding structures. It is thought that the law is a reasonable approximation to the behavior of many actual structures but insufficient experimental data are available to verify this. The principal advantage of the hysteresis law postulated here, in addition to its generality, is that it can be readily adapted for use in studies employing digital computers. The main disadvantage in the application of the law to the general yielding structure of chapter III is that the intersections of the min and max curves with the skeleton curve must sometimes be found by iterative techniques.

Application to the General Yielding Structure

Some additional properties of the general yielding structure are needed for the application of the hysteresis law. It was shown in chapter III that equation 4. 2 was capable of describing a closed hysteresis loop whose peaks lay on the skeleton curve. Because of the symmetry of the hysteresis loop, it is easy to show that the closure property is independent of the location of the loop with

respect to the skeleton curve. Consider a descending branch of the hysteresis loop originating at $(x_o/x_y,\ p_o/p_y)$ as shown in figure 41. This curve is described by equation 4. 2:

$$\frac{x-x_o}{2x_y} = \frac{p-p_o}{2p_y} + a\left(\frac{p-p_o}{2p_y}\right)^r \tag{4. 3}$$

At an arbitrary point $(x_i/x_y,\ p_i/p_y)$ the direction of loading reverses and the ascending curve is given by

$$\frac{x-x_i}{2x_y} = \frac{p-p_i}{2p_y} + a\left(\frac{p-p_i}{2p_y}\right)^r \tag{4. 4}$$

The point $(x_i/x_y,\ p_i/p_y)$ must satisfy equation 4. 3 so it follows that

$$\frac{x_i-x_o}{2x_y} = \frac{p_i-p_o}{2p_y} + a\left(\frac{p_i-p_o}{2p_y}\right)^r \tag{4. 5}$$

Evaluating the ascending curve, equation 4. 4, at the force level corresponding to the origin of the descending curve and comparing the resulting equation to equation 4. 5 it is seen that the ascending curve intersects the origin of the descending curve. Thus the closure of the hysteresis loops is established.

It was shown in chapter III that if a branch of the hysteresis loop had its origin at $(x_o/x_y,\ p_o/p_y)$ on the skeleton curve, then the branch was tangent to the skeleton curve at $(-x_o/x_y, -p_o/p_y)$. This fact is useful in characterizing the behavior of curves that do not originate on the skeleton curve. Shown in figure 42 are ascending curves originating from points a and b. Also shown are curves originating from the skeleton curve at the same force and deflection levels. These

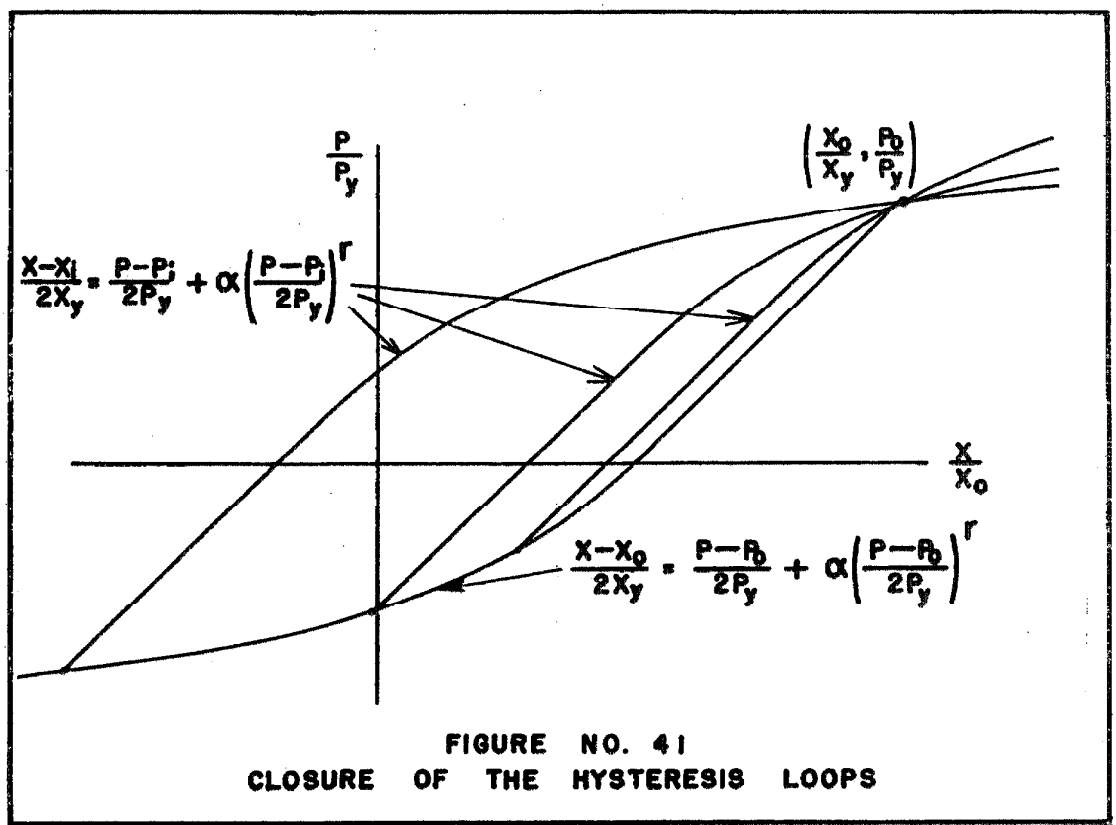

FIGURE NO. 41
CLOSURE OF THE HYSTERESIS LOOPS

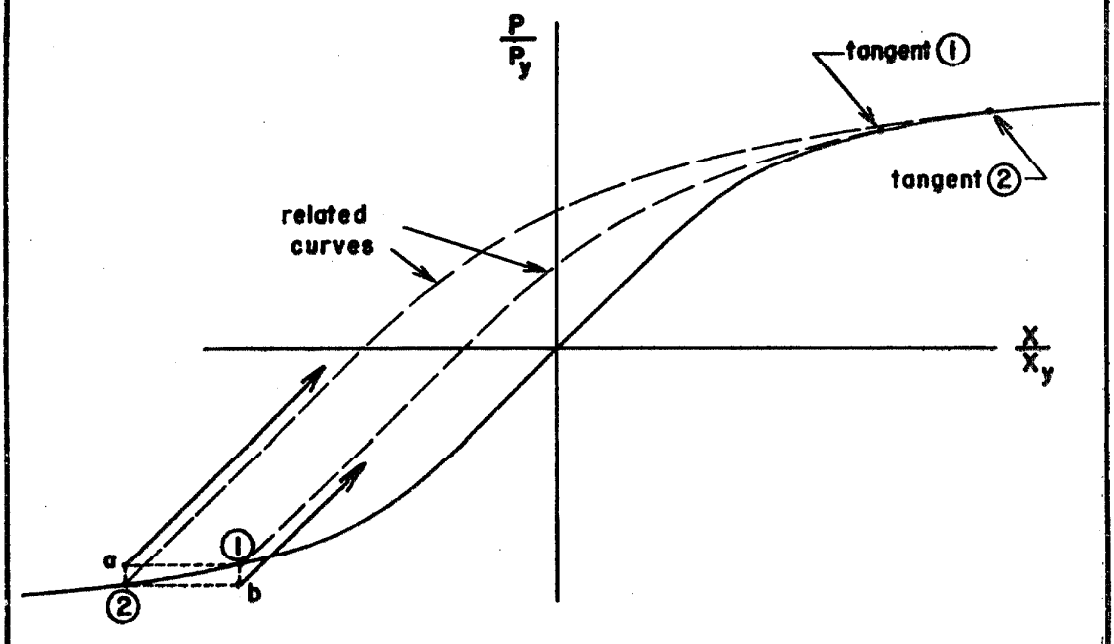

FIGURE NO. 42
RELATED CURVES FOR ASCENDING BRANCHES
OF THE HYSTERESIS LOOPS

related curves are tangent to the skeleton curve as indicated on the figure. With these related curves it is easy to show that the ascending curve from point a does not intersect the skeleton curve, and the curve originating at b will intersect the skeleton curve in three places. It can also be shown with these curves and the closure property that in the application of the hysteresis law ascending hysteretic curves will intersect the upper rather than the lower boundary and that descending curves will intersect the lower boundary.

The application of the hysteresis law to the dynamic response of the general yielding structure is primarily a matter of determining the upper and lower boundaries. To find these boundaries as the structure responds it is necessary to examine each point of loading reversal to ascertain whether or not a new max or min curve has been established. From equation 4.2 the intercept of the curve generated from the point of loading reversal is found to be

$$\frac{x_I}{x_y} = \frac{x_m}{x_y} - \frac{p_m}{p_y} - \frac{\alpha}{2^{r-1}} \left(\frac{p_m}{p_y} \right)^r \qquad (4.6)$$

where $(x_m/x_y\ ,\ p_m/p_y)$ is the point under examination and x_I/x_y is the intercept on the x/x_y axis. If, for an ascending curve, both the intercept given by equation 4.6 and x_m/x_y are less than the values for the existing min curve, a new min curve is established. Likewise, for a descending curve, if the intercept and x_m/x_y exceed the values for the existing max curve, a new max curve is established. The intercept and deflection criteria are independent and both must be used.

To define the boundaries it is necessary to find the points of contact of the max and min curves with the skeleton curve. In the case where the origin of the min or max curve is on the skeleton curve at $(x_m/x_y,\ p_m/p_y)$ there are two points of contact, $(x_m/x_y,\ p_m/p_y)$ and a point of tangency at $(-x_m/x_y, -p_m/p_y)$. For the general case it can be shown that all max curves originate on or above the skeleton curve and all min curves on or below the skeleton curve. Consider the max curve originating above the skeleton curve as shown in figure 43. As is seen in the figure there are three intersections of the two curves, a consequence of the fact that the intercept of the max curve is greater than zero. Equating the skeleton curve of equation 4.1 with the max curve given by equation 4.2 yields

$$\frac{x_m}{x_y} - \frac{p_m}{p_y} + a\left(\frac{p}{p_y}\right)^r - 2a\left(\frac{p-p_m}{2p_y}\right)^r = 0 \qquad (4.7)$$

The required points of intersection, labeled 1 and 2 in figure 43, are the least and greatest roots of equation 4.7. Since the roots are on the skeleton curve the x/x_y values are found from equation 4.1. The intersections of a min curve and the skeleton curve are also given by equation 4.7, so only the max curve is discussed. An example of equation 4.7 is shown in figure 43 and as is easily verified from the equation, points of horizontal tangency occur at $p/p_y = -p_m/p_y$ and $1/3p_m/p_y$.

To find the least and greatest roots of this equation, the iterative method of Newton and Raphson[57] was used. Its application produces the following formula for the $w+1^{st}$ iteration.

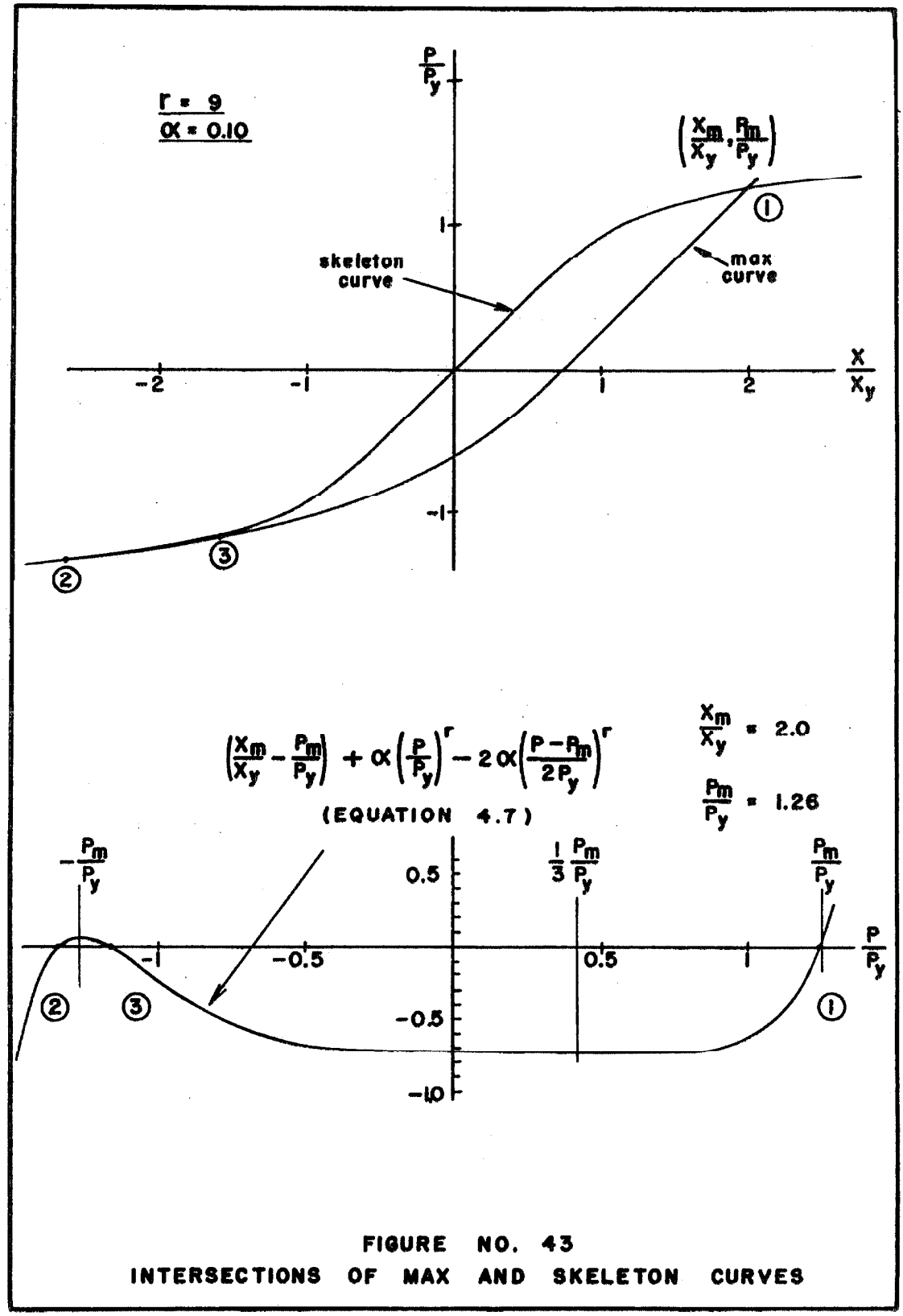

FIGURE NO. 43
INTERSECTIONS OF MAX AND SKELETON CURVES

$$z_{w+1} = \frac{(r-1)z_w^{\,r} - \left[z_w(r-1)+y\right]\left(\frac{z_w-y}{2}\right)^{r-1} + \frac{1}{\alpha}\left(\frac{x_m}{x_y} - y\right)}{r\left[z_w^{\,r-1} - \left(\frac{z_w-y}{2}\right)^{r-1}\right]} \qquad (4.8)$$

where $z = p/p_y$ and $y = p_m/p_y$. It is seen that the denominator vanishes at the points of tangency $-p_m/p_y$ and $1/3p_m/p_y$ so care must be taken in choosing the starting values. To find the intersection nearest the origin of the min or max curve, point 1 of figure 43, the starting point $z_o = p_m/p_y$ was used. The intersection furthest from the origin, point 2 of figure 43, was found by using an initial value beyond the point of horizontal tangency at $-p_m/p_y$. For $r = 9$, $\alpha = 0.10$, the choice $-1.2p_m/p_y$ was used. In using the digital computer the machine limitations occasionally caused convergence trouble when the origin of the min or max curve was very near the skeleton curve and intersection 2 was being sought. In this case the intersection is quite near the point of horizontal tangency at $-p_m/p_y$. In the very few instances where this occurred intersection 2 was taken to be $-p_m/p_y$ and this approximate solution to equation 4.7 was later verified by hand calculation. For the structure used in the earthquake response study ($r = 9$, $\alpha = 0.10$) all the instances when the iteration failed to converge occurred when the behavior of the structure was essentially linear; the maximum p_m/p_y never exceeded 1/3. In all cases the approximation of $-p_m/p_y$ for the root was satisfactory.

The intersections of the max and min curves with the skeleton curve determine the upper and lower boundaries. To implement the hysteresis law during integration of the equation of motion it is

necessary to compare, for the same deflection level, the force value obtained from a curve originating at the point of most recent loading reversal to force values obtained from the upper and lower boundaries. If the value generated by the point of most recent loading reversal is between the boundary values it is used, otherwise the force value from the appropriate boundary is used and further force values are found from this boundary until the direction of loading is reversed.

C. Response of Yielding Structures to Earthquake Motion

Equation of Motion

Consider a one degree-of-freedom structure with viscous damping as shown in figure 44. The restoring force is assumed to be uniquely determined by the displacement and displacement history, but not dependent upon time in any explicit way. It is assumed also that for small deflections the force-deflection relation can be considered linear. The class of yielding structures of the previous section is included in this discussion.

The equation of motion of the structure shown in figure 44 when subjected to earthquake-type excitation is

$$m\ddot{x} + c_d\dot{x} + p(x) = -m\ddot{y}(t) \qquad (4.9)$$

where c_d is the viscous damping coefficient, $p(x)$ the restoring force, $\ddot{y}(t)$ the ground acceleration, and x the relative displacement of the mass m. Dividing through by m and by the characteristic deflection x_y equation 4.9 becomes

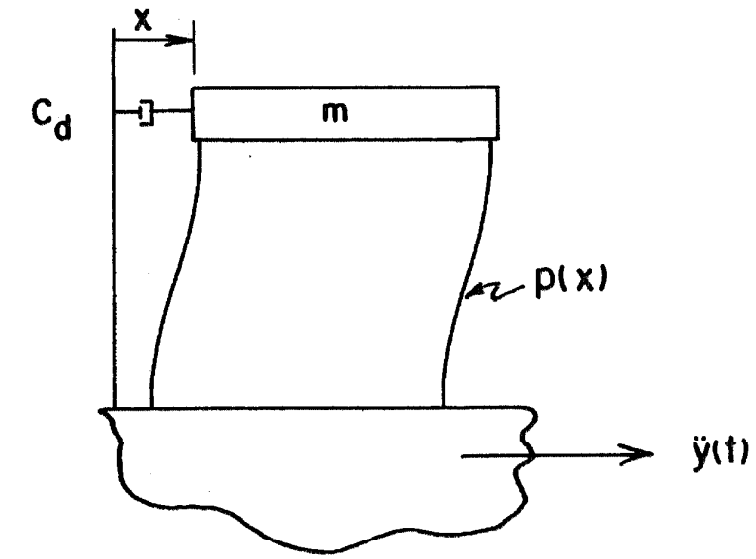

OSCILLATOR

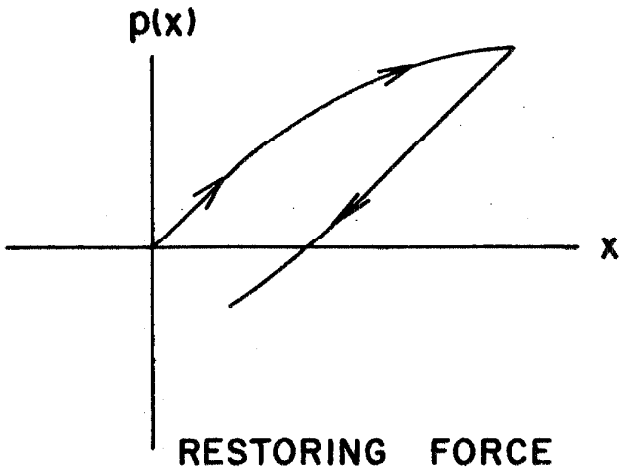

RESTORING FORCE

FIGURE NO. 44

A NONLINEAR OSCILLATOR

$$\frac{\ddot{x}}{x_y} + \frac{c_d}{m}\frac{\dot{x}}{x_y} + \frac{1}{mx_y}\,p(x) = -\frac{1}{x_y}\,\ddot{y}(t) \qquad (4.10)$$

The characteristic restoring force p_y is chosen so that p_y/x_y is equal to k_s, the slope of the force-deflection curve near the origin. It is assumed that the structure can be considered linear for small oscillations, so ω_o, the natural frequency of small oscillations is $\sqrt{k_s/m}$.

$$\omega_o = \sqrt{\frac{p_y}{x_y m}} \qquad (4.11)$$

The fraction of critical damping of small oscillations is denoted by n

$$n = \frac{c_d}{2\sqrt{k_s m}} \qquad (4.12)$$

With the substitution of equations 4.11 and 4.12, equation 4.10 can be rewritten as

$$\frac{\ddot{x}}{x_y} + 2n\omega_o\frac{\dot{x}}{x_y} + \omega_o^2\,\frac{p(x)}{p_y} = -\omega_o^2\,\frac{\ddot{y}(t)}{p_y/m} \qquad (4.13)$$

The ratio p_y/m on the right side of equation 4.13 is the lateral acceleration of the base of the oscillator needed to generate the force p_y in the nonlinear spring. This ratio is denoted by q_y.

$$q_y = p_y/m \qquad (4.14)$$

The earthquake excitation is normalized by letting

$$\ddot{y}(t) = \ddot{\bar{y}}\,\sigma(t) \qquad (4.15)$$

where $\ddot{\bar{y}}$ is a measure of the scale of the excitation (e.g., acceleration r.m.s. or spectrum intensity) and $\sigma(t)$ is the normalized, dimensionless time record of the motion. By means of equations 4.14 and 4.15

equation 4.13 can be written as

$$\frac{\ddot{x}}{x_y} + 2n\omega_o \frac{\dot{x}}{x_y} + \omega_o^2 \frac{p}{p_y}\left(\frac{x}{x_y}\right) = -\omega_o^2 \frac{\ddot{y}}{q_y}\sigma(t) \qquad (4.16)$$

By letting $\tau = \omega_o t$ the frequency dependence of the left side of equation 4.16 is removed yielding

$$\frac{x''}{x_y} + 2n\frac{x'}{x_y} + \frac{p}{p_y}\left(\frac{x}{x_y}\right) = -\frac{\ddot{y}}{q_y}\sigma(\tau/\omega_o) \qquad (4.17)$$

where the primes denote differentiation with respect to τ.

Equation 4.17 is the dimensionless form of the equation of motion of a nonlinear, viscously damped, one degree-of-freedom structure which behaves linearly for small oscillations. For application of this equation to an elasto-plastic or bilinear hysteretic structure p_y and x_y are the force and deflection at which yielding begins. x/x_y then becomes the ratio of the deflection of the structure to its yield deflection and the maximum value of x/x_y that occurs during an earthquake is the "ductility factor" referred to by A. S. Velestos and others.[16, 59] From equation 4.14 it follows that q_y is in this instance the acceleration necessary to produce the yielding force in the springs of the structure; this variable is commonly called the yield level.

When applying equation 4.17 to a structure described by the general yielding relation, p_y and x_y are characteristic force and deflection values subject to the condition that $p_y/x_y = k_s$. If the structure has a well-defined yield point, the value of r is large and

p_y and x_y are values near the yield point of the structure. If the point at which yielding begins is not pronounced, r is not large and p_y (or x_y) can be chosen somewhat arbitrarily. For example, p_y might be chosen as the force level at which the departure from linearity is a certain fraction of the total deflection.

An alternate form of equation 4.17 can be obtained by using equations 4.14 and 4.11 to eliminate the variable q_y. From these equations it follows that

$$q_y = \omega_o^2 x_y \tag{4.18}$$

Substitution of equation 4.18 into equation 4.17 yields

$$\frac{x''}{x_y} + 2n\frac{x'}{x_y} + \frac{p}{p_y}\left(\frac{x}{x_y}\right) = -\frac{\ddot{y}}{\omega_o^2 x_y}\sigma(\tau/\omega_o) \tag{4.19}$$

A comparison of equations 4.17 and 4.19 shows that although the number of symbols is less in equation 4.19, the number of parameters is the same, both equations containing in their right sides a parameter related to the absolute value of the displacement at which yielding begins.

For linear structures equation 4.17 can be simplified, for in this instance $p/p_y = x/x_y$. Since the yield acceleration has no meaning for a linear structure, one simplification is obtained by assigning q_y the value g, the acceleration of gravity. Then from equation 4.18 it is seen that $x_y = g/\omega_o^2$. Letting $z = x\omega_o^2/g$, equation 4.17 reduces to

$$z'' + 2nz' + z = -\frac{\ddot{y}}{g}\sigma(\tau/\omega_o) \tag{4.20}$$

Equation 4. 20 describes the response of a linear structure to earthquake motion. This dimensionless form of the equation also could have been obtained from equation 4. 19 or directly from equation 4. 9.

The influence of the natural frequency of the structure upon the response as measured by x/x_y is illustrated by equation 4. 19. From this equation it is seen that an increase in the natural frequency, with x_y constant, reduces the magnitude of the excitation and spreads out the excitation over a larger range of the time variable τ, i. e., if the excitation lasts 30 seconds then in terms of τ the duration is $30\omega_o$. As ω_o becomes infinite (natural period approaches zero) it is clear that x/x_y goes to zero approximately as $1/\omega_o^2$. As the excitation goes to zero the structure tends toward linear behavior, but the displacement also goes to zero in the linear case since the value of $z = x\omega_o^2/g$ in equation 4. 20 stays approximately constant as ω_o is increased.

The acceleration ratio $\ddot{\bar{y}}/q_y$ is a ratio between a measure of the earthquake acceleration strength and the yield level of the structure. Equation 4. 17 states that doubling the strength of the earthquake will produce the same response in terms of x/x_y as if the yield level had been halved. This implies that nonlinear response studies that have been made using individual earthquakes as excitation[18,17,60,26,13] can be interpreted in a more general manner if the results are measured in terms of x/x_y. A general interpretation is important in view of the fact that the El Centro 1940

earthquake, the strongest recorded ground motion to date and an excitation common to all these studies, has been estimated by G. W. Housner[61] to be only about half as intense as the strongest possible ground motion that might occur.

Earthquake Acceleration Ratios

Table IV has been constructed to help find the range of acceleration ratios that can be expected for response of one degree-of-freedom structures to strong-motion earthquakes. For various values of the yield level q_y, this table gives the acceleration ratio $\gamma = \ddot{\bar{y}}/q_y$. The r. m. s. accelerations were used as measures of earthquake strength; these values were taken from table III.

Energy Equation

Equation 4. 9 is the equation of motion of a nonlinear one degree-of-freedom structure subjected to earthquake excitation and it is the same as the equation for a structure with an immovable base whose mass is excited by the force $-m\ddot{y}(t)$. As the structure moves through an increment of deflection dx energy is supplied to the structure by this force:

$$dE_I = -m\ddot{y}(t)\, dx \tag{4. 21}$$

where E_I is the total energy input to the structure since the excitation began. From equation 4. 9 it follows that

$$E_I = \int_0^x -m\ddot{y}(t)\, dx = m \int_0^x \ddot{x}\, dx + c_d \int_0^x \dot{x}\, dx + \int_0^x p(x) dx \tag{4. 22}$$

TABLE IV

Strong-Motion Earthquake Acceleration Ratios

Earthquake Location and Date	Acc. r. m. s. $\ddot{\bar{y}}$	Acceleration ratio $\gamma = \ddot{\bar{y}}/q_y$			
		$q_y = 0.03g$	$q_y = 0.05g$	$q_y = 0.10g$	$q_y = 0.20g$
El Centro, Calif. 18 May 1940	2.01	2.1	1.2	.62	.31
El Centro, Calif. 30 Dec. 1934	1.35	1.4	.84	.42	.21
Olympia, Wash. 13 April 1949	1.76	1.8	1.1	.55	.27
Taft, Calif. 21 July 1952	1.44	1.5	.89	.45	.22

where it has been assumed that the structure starts from rest. By making use of the substitutions $\ddot{x} = d\dot{x}/dt$ and $dx = \dot{x}\,dt$ equation 4. 22 can be written:

$$E_I(t) = m \int_0^{\dot{x}(t)} \dot{x}\, d\dot{x} + c_d \int_0^t \dot{x}^2(t)\, dt + \int_0^t \dot{x} p(x)\, dt \qquad (4.23)$$

The first integral is readily evaluated and equation 4. 23 is written in a convenient dimensionless form by the use of equations 4. 11 and 4. 12.

$$\frac{E_I(t)}{\frac{1}{2} x_y p_y} = \frac{1}{\omega_o^2}\left(\frac{\dot{x}}{x_y}\right)^2 + \frac{4n}{\omega_o} \int_0^t \left(\frac{\dot{x}}{x_y}\right)^2 dt + 2 \int_0^t \left(\frac{\dot{x}}{x_y}\right) \frac{p}{p_y}\, dt \qquad (4.24)$$

By letting $\tau = \omega_o t$ equation 4. 24 becomes

$$\frac{E_I(\tau)}{\frac{1}{2} x_y p_y} = \left(\frac{x'}{x_y}\right)^2 + 4n \int_0^\tau \left(\frac{x'}{x_y}\right)^2 d\tau + 2 \int_0^\tau \left(\frac{x'}{x_y}\right) \frac{p}{p_y}\, d\tau \qquad (4.25)$$

This is the reduced form of the energy equation for a non-linear structure starting from rest and is in terms of the same variables as the equation of motion, 4. 17.

The left sides of equations 4. 24 and 4. 25 represent the total energy supplied to the structure. The first term on the right sides is the kinetic energy and the second term is the energy dissipated by viscous friction. The third term in these equations is the sum of the potential energy and the energy dissipated by yielding. In the case of a linear structure $p/p_y = x/x_y$ and equation 4. 25 reduces to

$$\frac{E_I(\tau)}{\frac{1}{2} x_y P_y} = \left(\frac{x'}{x_y}\right)^2 + 4n \int_0^{\tau} \left(\frac{x'}{x_y}\right)^2 d\tau + \left(\frac{x}{x_y}\right)^2 \qquad (4.26)$$

where the last term clearly represents the potential energy and x_y can be arbitrarily chosen (e.g., g/ω_o^2) as was done in the derivation of equation 4.20. For nonlinear structures the manner of separation of the potential energy and the energy dissipated by yielding depends on the force-deflection relation. For the type of relations considered here it suffices to evaluate the integrals of equation 4.25 at a value of τ for which all subsequent oscillations can be considered linear. In this case the potential energy is easily determined.

It is noted that the foregoing energy analysis is for a structure whose mass is acted upon by the force $-m\ddot{y}(t)$ rather than for a structure whose base is excited by the acceleration $\ddot{y}(t)$. Therefore, the kinetic energy terms in the previous equations represent the energy of motion relative to the base rather than that due to absolute motion. As it is the relative displacement and velocities that are of primary importance in practice, an energy equation expressed in terms of the relative motion is more meaningful than one expressed in terms of absolute velocities and displacements.

It is seen also that the variables have been manipulated until the integrals are taken with respect to time. This was done to simplify the numerical evaluation of the integrals.

D. Response to Pseudo-Earthquake Excitation

The response of the nonlinear structure described by the parameters r=9 and α =0.10 to the ensemble of eight pseudo-earthquakes was calculated for acceleration ratios of 0.25, 0.50, 0.75 and 1.00. Because the average of the velocity spectra of the pseudo-earthquakes is comparable to that of real earthquakes, it is considered that the average response of a nonlinear structure to the real and pseudo-earthquakes also would correspond closely. Since the average of the pseudo-earthquake spectra are relatively smooth, it was assumed that the average non-linear response spectra also would be relatively smooth and could be defined satisfactorily by relatively few points. The natural periods of small oscillations used in the calculations were 0.5, 1.0, 1.5, 2.0 and 2.5 seconds. To study the influence of viscous damping four values of n were used, 0, 0.02, 0.05, and 0.10. Because of the large amount of computations that would be required, it was not possible to calculate response spectra for different values of r and α and thus obtain results that would exhibit the influence of these yielding parameters upon the response. A limitation had to be made and it was felt that it was more important to study the effect of the earthquake strength as measured by the acceleration ratio γ. The structure given by r=9, α =0.10 was selected as typical; the results of the investigation are intended to indicate some of the average characteristics of the response of a typical yielding structure to earthquakes of various strengths. The skeleton curve for this structure is included in figure 26 and a hysteresis loop is shown in figure 30.

Presentation of Results

Equation 4.17 was used in the numerical integration of the response of the yielding structure to the pseudo-earthquakes. The calculations were done on an IBM 7090 digital computer using a third order Runge-Kutta method which is discussed in Appendix I.

Average displacement spectra were obtained by averaging, over the eight pseudo-earthquakes, the absolute value of the maximum displacement. This average is a function of the acceleration ratio γ and the damping coefficient n, as well as the natural period of small oscillations. The average displacement spectra are shown in figures 45-48. In figure 49 the range of the displacement spectra are shown for the case of zero viscous damping. The bands about the averages in this figure include all the values used to construct the average and give an indication of the dispersion of the data. In the cases where n was not zero an increase in viscous damping resulted in smaller relative dispersion of the spectra than that shown in figure 49. Because only five natural periods were used in the calculations, individual response spectra are not well defined and are not presented.

Equation 4.25 was used to determine the total energy input to the structure during the earthquake. The integration was stopped on or one step after the first velocity sign change after the earthquake was over. At this time the velocity is so small that the kinetic energy can be neglected and equation 4.25 becomes

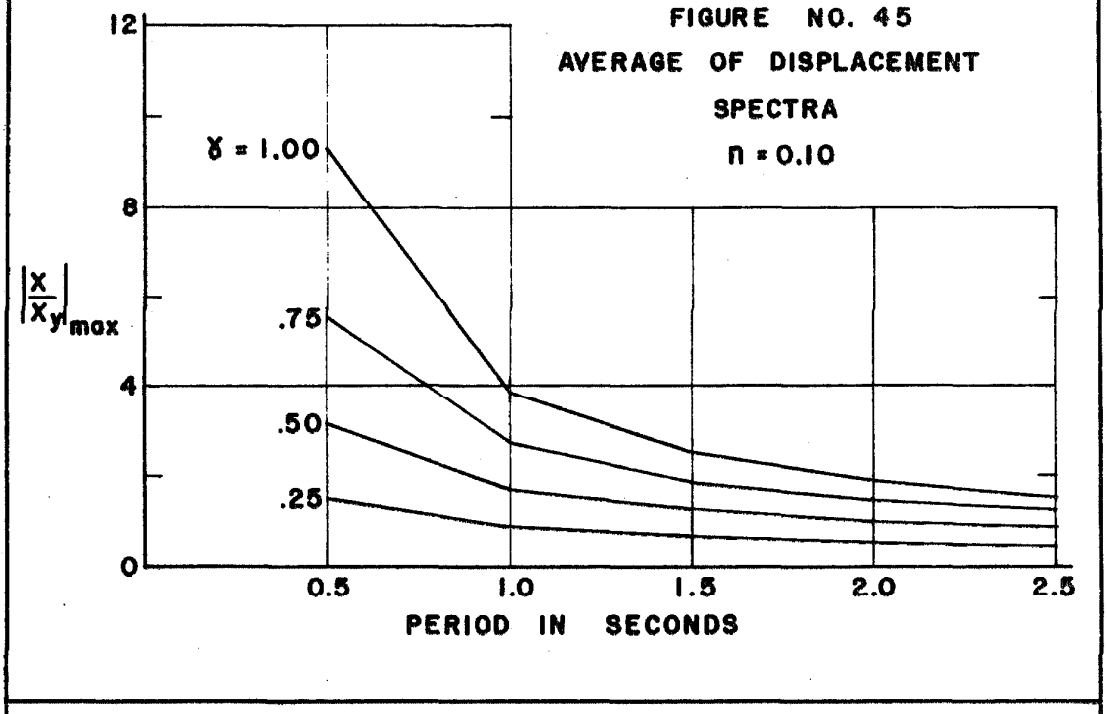

FIGURE NO. 45
AVERAGE OF DISPLACEMENT SPECTRA
n = 0.10

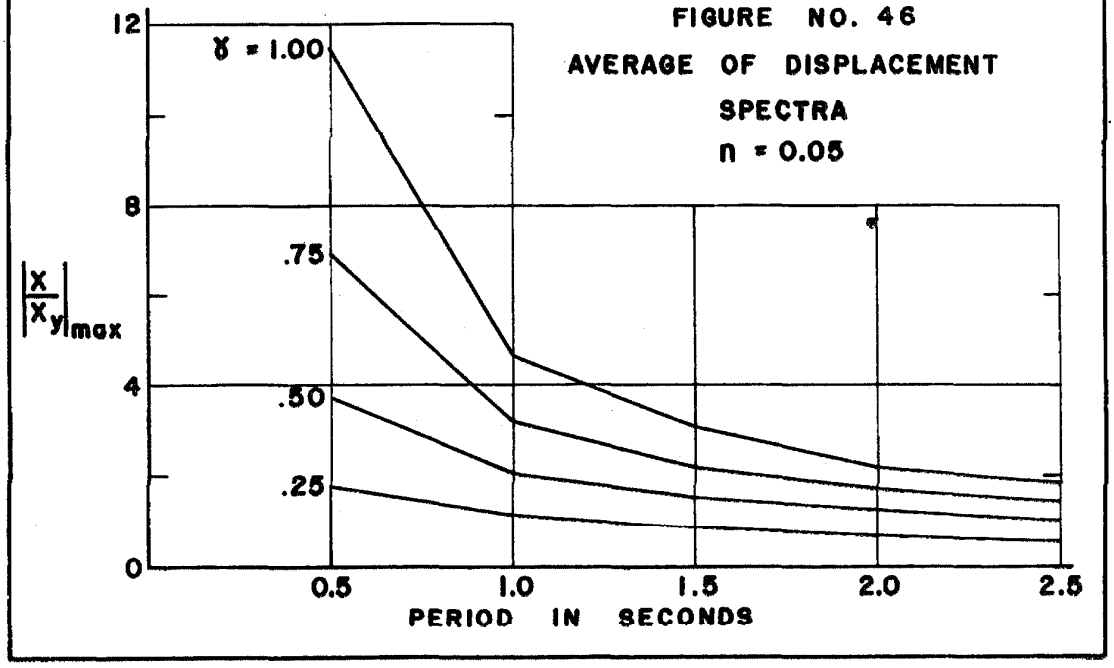

FIGURE NO. 46
AVERAGE OF DISPLACEMENT SPECTRA
n = 0.05

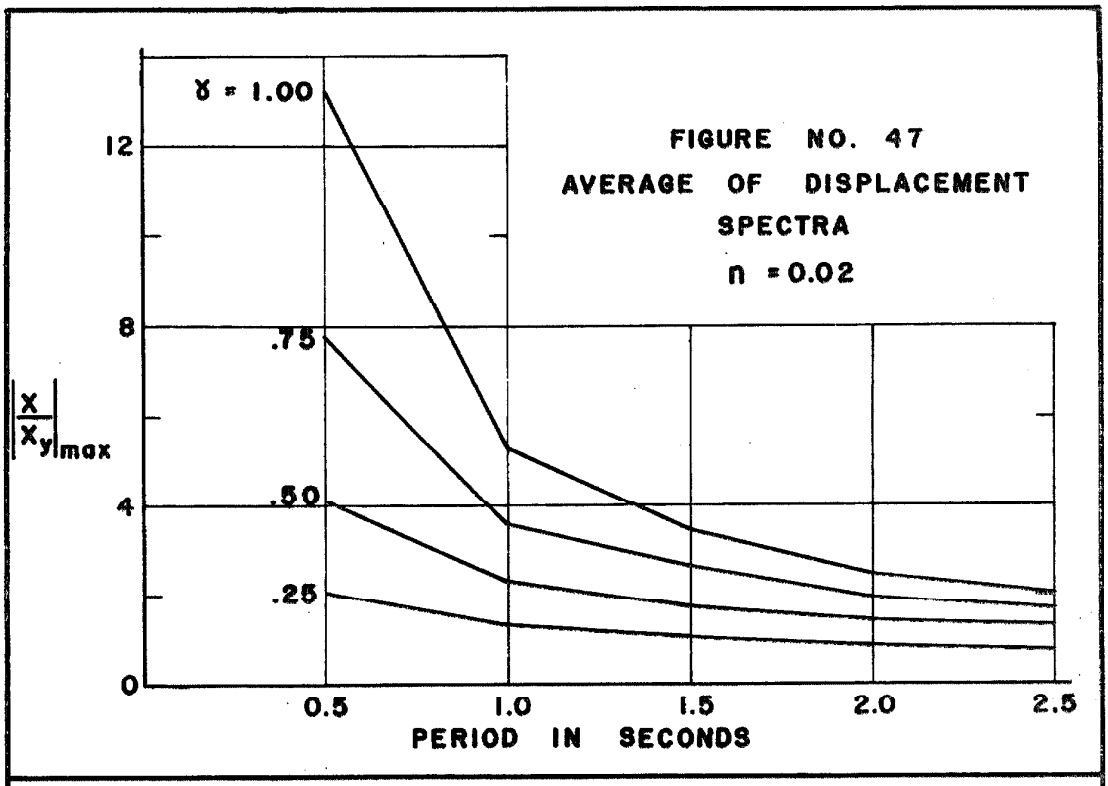

FIGURE NO. 47
AVERAGE OF DISPLACEMENT SPECTRA
n = 0.02

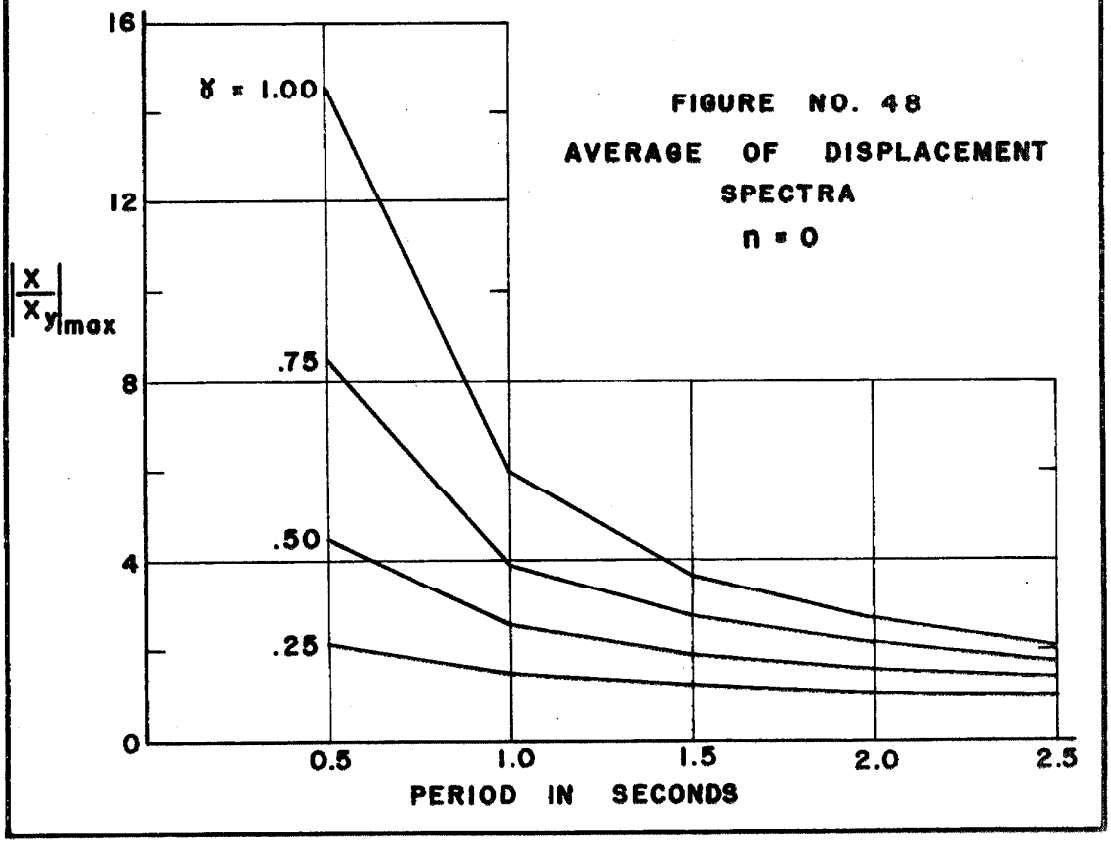

FIGURE NO. 48
AVERAGE OF DISPLACEMENT SPECTRA
n = 0

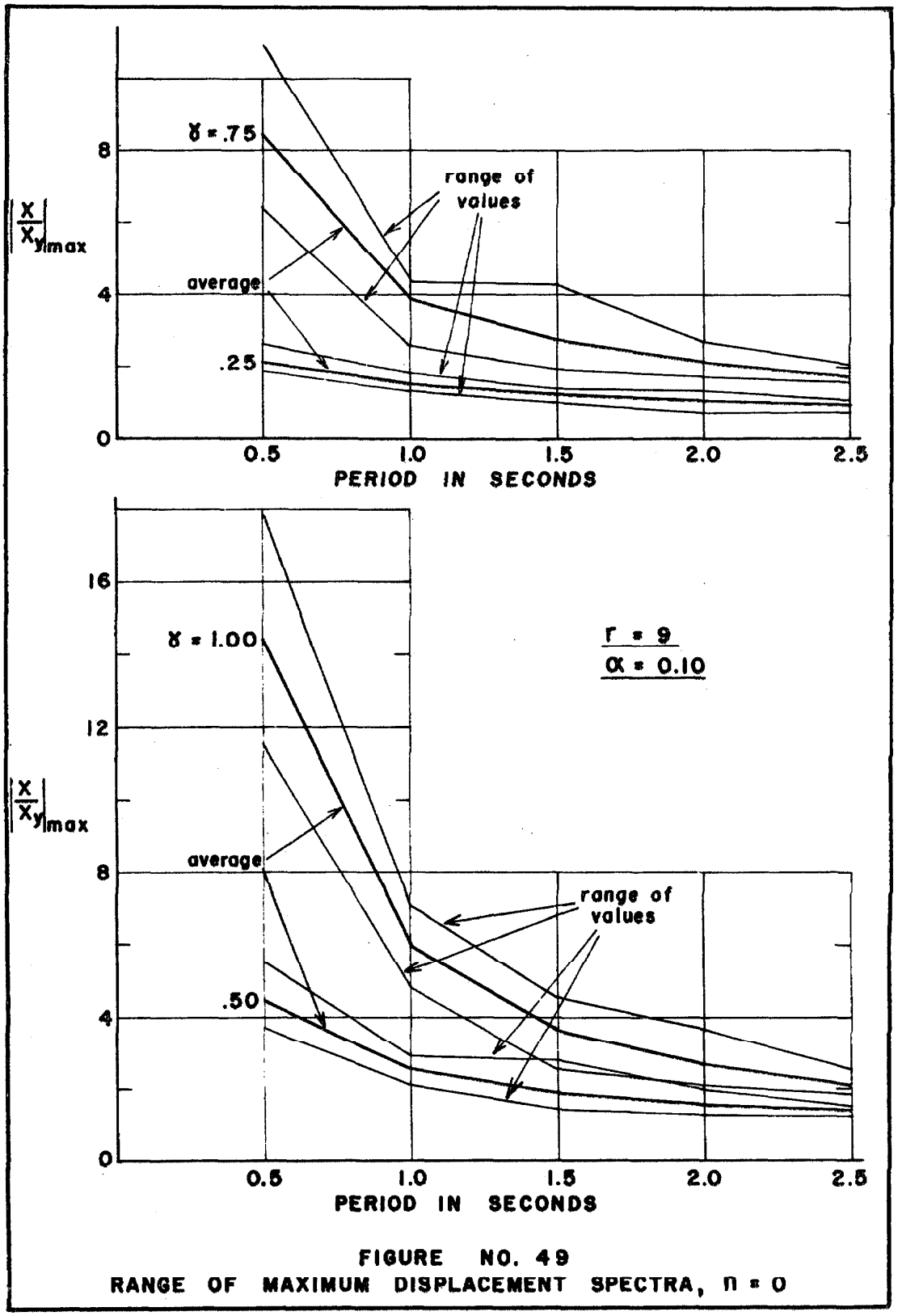

FIGURE NO. 49
RANGE OF MAXIMUM DISPLACEMENT SPECTRA, n = 0

$$\frac{E_I}{\frac{1}{2} x_y p_y} = 4n \int_0^{\tau} \left(\frac{x'}{x_y}\right)^2 d\tau + 2 \int_0^{\tau} \left(\frac{x'}{x_y}\right) \frac{p}{p_y} d\tau \qquad (4.27)$$

The integrals were evaluated by the use of Simpson's Rule;[57] the application is straightforward and requires only that the number of integration steps be an odd number. As the integration step $\Delta\tau$ was about 0.10 the overall error in this integration is on the order of $10^{-4}/90$. The average energy input spectra are shown in figure 50. The heavy lines in this figure represent the mean, for each acceleration ratio, of the energy input averaged over the eight pseudo-earthquakes and over the four values of viscous damping. Associated with the means are bands defining the range of the values producing the means. The averages were taken over n as well as the pseudo-earthquakes because the averages taken across the pseudo-earthquakes varied only slightly with n in a manner which appeared to be a complex function of the period and the acceleration ratio.

Eventually the structure dissipates all the energy supplied to it and a quantity of interest is the relative amount of energy dissipated by viscous damping and by yielding. Although it was not possible to continue the integration until the response was zero the energy dissipated by viscous damping and the energy dissipated by yielding were evaluated at the end of the earthquake. From the first integral of equation 4.27 is seen that the energy dissipated by viscous damping is

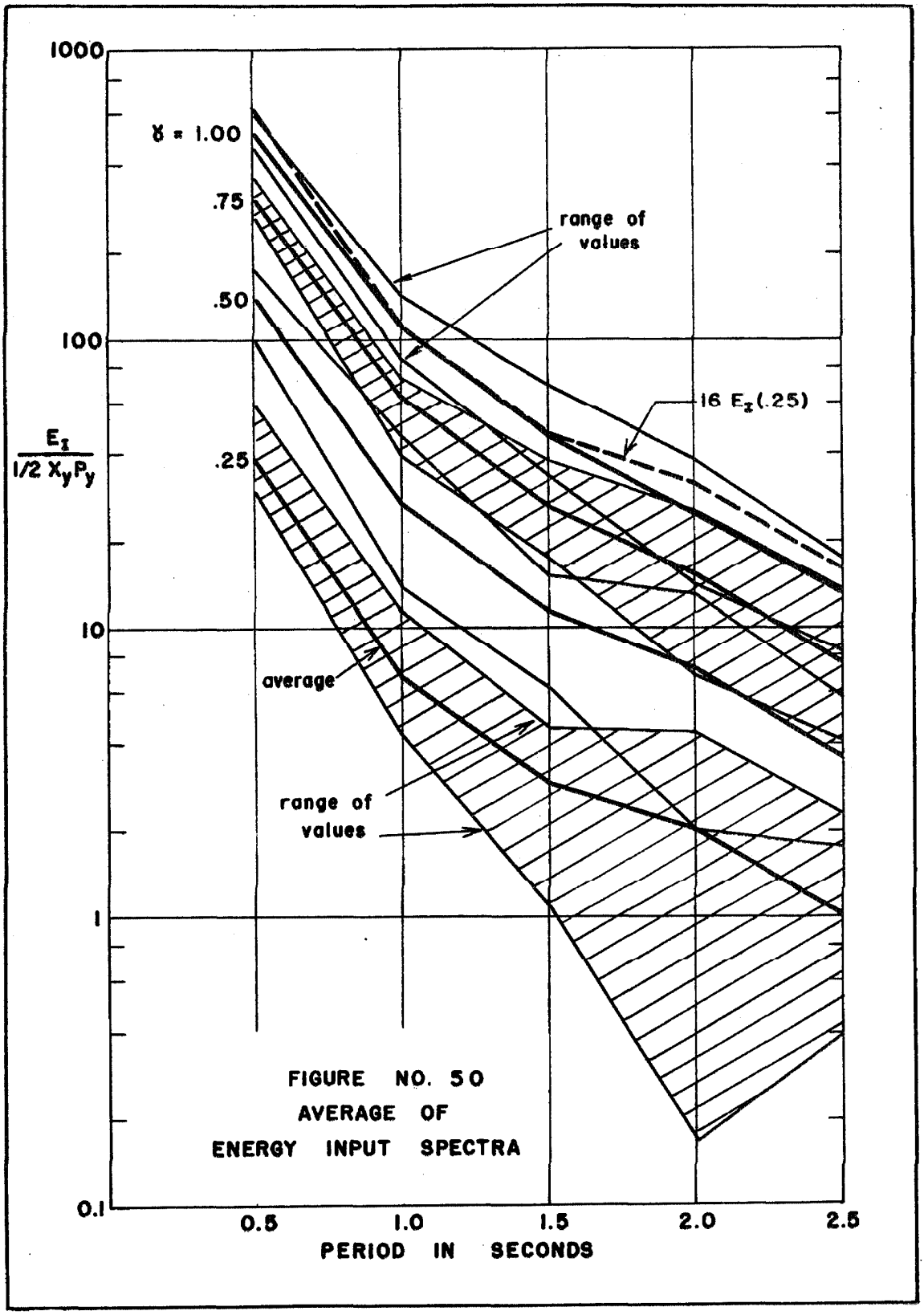

FIGURE NO. 50
AVERAGE OF
ENERGY INPUT SPECTRA

$$\frac{E_v}{\frac{1}{2} x_y p_y} = 4n \int_0^{\tau} \left(\frac{x'}{x_y}\right)^2 d\tau \tag{4.28}$$

where E_v is the energy dissipated by viscous damping. The second integral of equation 4.27 contains both the energy dissipated by yielding and the recoverable strain energy:

$$\frac{E_p + E_s}{\frac{1}{2} x_y p_y} = 2 \int_0^{\tau} \left(\frac{x'}{x_y}\right) \frac{p}{p_y} d\tau \tag{4.29}$$

where E_p is the energy dissipated by yielding and E_s is the recoverable strain energy. Since the integration was stopped near a velocity zero, E_s is generally not zero. At the time the integration is stopped the hysteretic curve is given by equation 4.2 with $(x_i/x_y,\ p_i/p_y)$ being the point of most recent change in sign of the velocity. If $(x_f/x_y,\ p_f/p_y)$ are the final values of force and displacement, the recoverable strain energy is

$$\frac{E_s}{\frac{1}{2} x_y p_y} = -\int_{p_f}^{0} p \frac{dx}{dp} dp \tag{4.30}$$

Equation 4.30 is easily evaluated and with equation 4.29 the energy dissipated by yielding is found to be

$$\frac{E_p}{\frac{1}{2} x_y p_y} = 2 \int_0^{\tau} \left(\frac{x'}{x_y}\right) \frac{p}{p_y} d\tau - \left(\frac{p_f}{p_y}\right)^2 - \frac{8a}{r+1} \left[\left(\frac{p_f - p_i}{2p_y}\right)^r \left(\frac{r p_f + p_i}{2p_y}\right) + \left(\frac{p_i}{2p_y}\right)^{r+1} \right] \tag{4.31}$$

The ratios of the average amounts of energy dissipated by viscous damping and yielding for the four acceleration ratios are shown in figures 51-53. The ranges of the energy dissipation ratios are shown in figures 54 and 55. It was found in the calculations that E_s was usually around one, indicating that by the end of the stronger earthquakes the structure had dissipated nearly all the energy supplied to it. Therefore, to find the amounts of energy dissipated by either mechanism figure 50 can be used along with figures 51-53.

Another variable of interest is the permanent set. As the integration was not continued until the oscillations were so small that the behavior was linear, an estimate of the permanent set was made. The integration was stopped just after the first velocity sign change after the earthquake was over, as is illustrated in figure 56. From this point free oscillations occur and the permanent set is the center of the nest of diminishing hysteresis loops formed in the free vibration. As shown in figure 56 an estimate of the permanent set is found by determining the intercept on the x/x_y axis of the skeleton curve which goes through the point $(x_i/x_y,\ p_i/p_y)$. If p_i/p_y is less than unity, this estimate is exact for all practical purposes, so as the structure approaches linear behavior the permanent set estimate becomes more accurate. The equation of a skeleton curve with origin on the x/x_y axis at x_p/x_y and passing through $(x_i/x_y,\ p_i/p_y)$ can be written as

$$\frac{x_p}{x_y} = \frac{x_i}{x_y} - \frac{p_i}{p_y} - a\left(\frac{p_i}{p_y}\right)^r \qquad (4.32)$$

FIGURE NO. 51

AVERAGE ENERGY DISSIPATION COMPARISON

n = 0.10

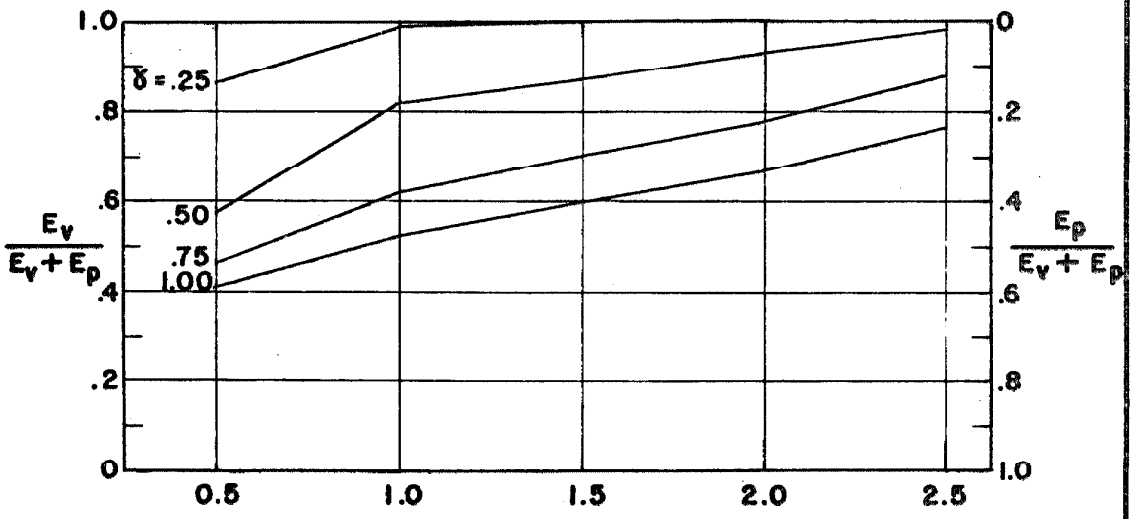

FIGURE NO. 52

AVERAGE ENERGY DISSIPATION COMPARISON

n = 0.05

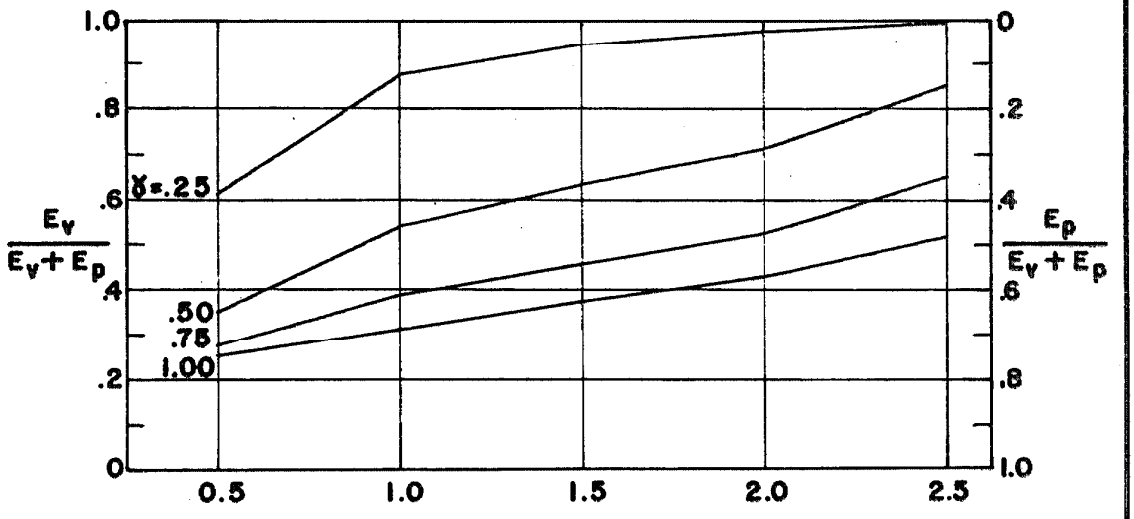

FIGURE NO. 53

AVERAGE ENERGY DISSIPATION COMPARISON

$\eta = 0.02$

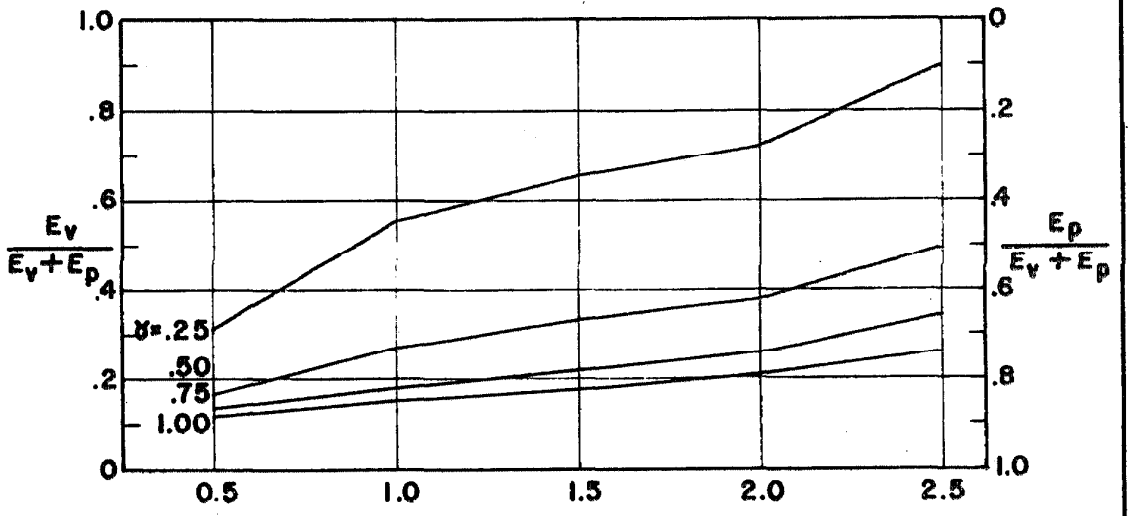

FIGURE NO. 54

RANGE OF ENERGY DISSIPATION RATIOS

$\eta = 0.02$

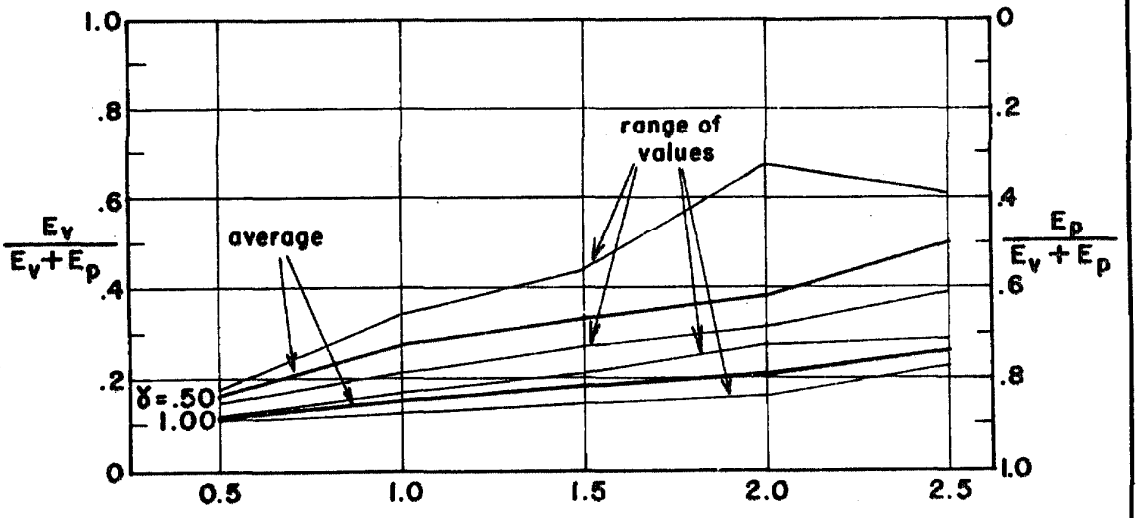

FIGURE NO. 55
RANGE OF ENERGY DISSIPATION RATIOS
$\eta = 0.02$

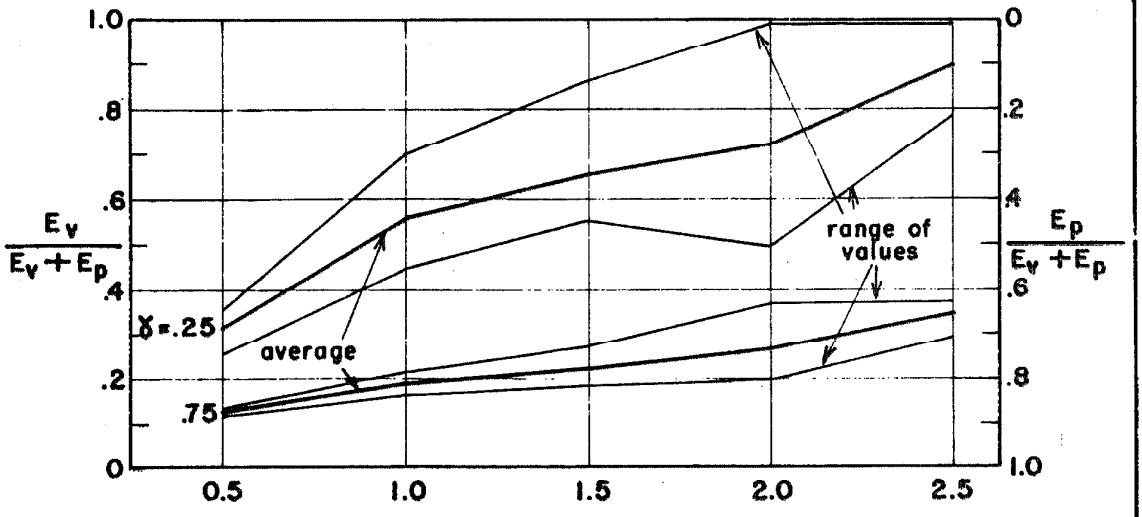

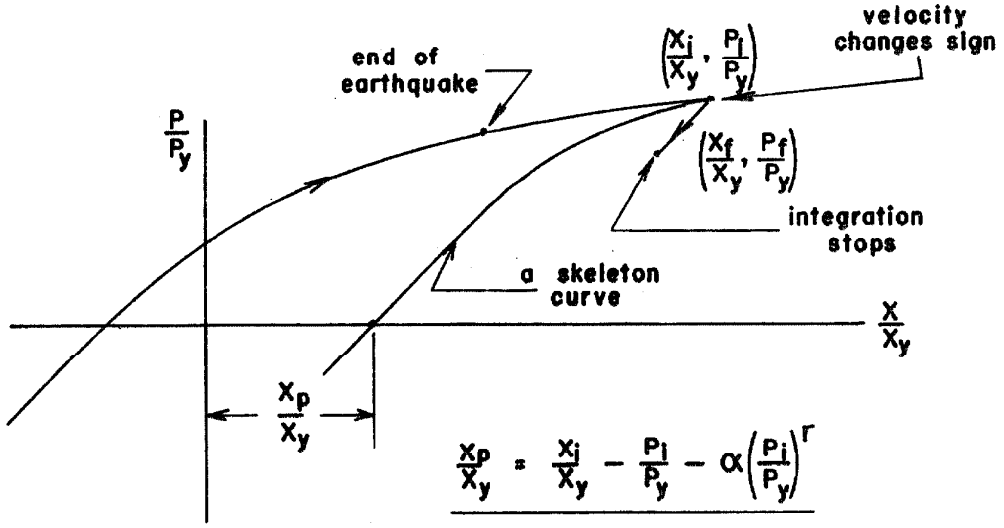

FIGURE NO. 56
PERMANENT SET ESTIMATE

where x_p/x_y is the permanent set and $(x_i/x_y,\ p_i/p_y)$ is the first point of velocity sign change in the free vibration following the earthquake. The average permanent set estimates are shown in figures 57-60, and the range of the estimates is given in figure 61.

To illustrate the response, the displacement as a function of time for $\gamma = 1.00$, $n = 0.02$, pseudo-earthquake 8, and a natural period of small oscillations of 1 second is given in figure 62. This response corresponds to that of a one degree-of-freedom structure with a .06g yield level in response to an earthquake approximately of the strength of the El Centro 1940 shock. A portion of the force-deflection curves which includes the maximum response is shown in figure 63. To provide correlation with figure 62 the times at which the velocity sign changes occur are indicated in figure 63.

Calculation Checks

The calculations were performed using a main program to integrate the equation of motion and using subroutines to evaluate the nonlinear force-deflection relation and to calculate the supplemental information. The numerical integration of the equation of motion employed the same procedure and program that was used to filter white noise to produce the pseudo-earthquakes, to calculate the velocity spectra, and to find the steady-state response of yielding structures to sinusoidal excitation. This program has been checked extensively in these previous calculations.

The subroutine implementing the force-deflection relation was checked by plotting the force against deflection for the response to

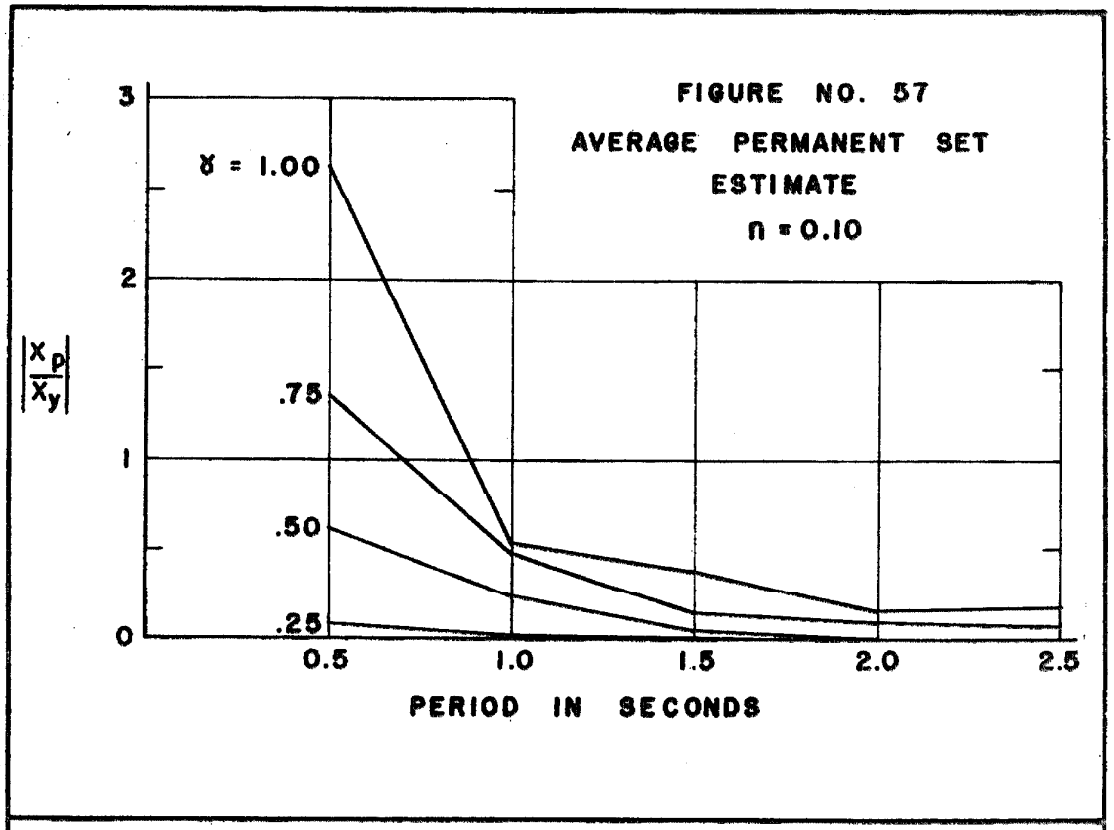
FIGURE NO. 57
AVERAGE PERMANENT SET
ESTIMATE
n = 0.10
γ = 1.00
.75
.50
.25
$\left|\frac{X_p}{X_y}\right|$
3
2
1
0
0.5
1.0
1.5
2.0
2.5
PERIOD IN SECONDS

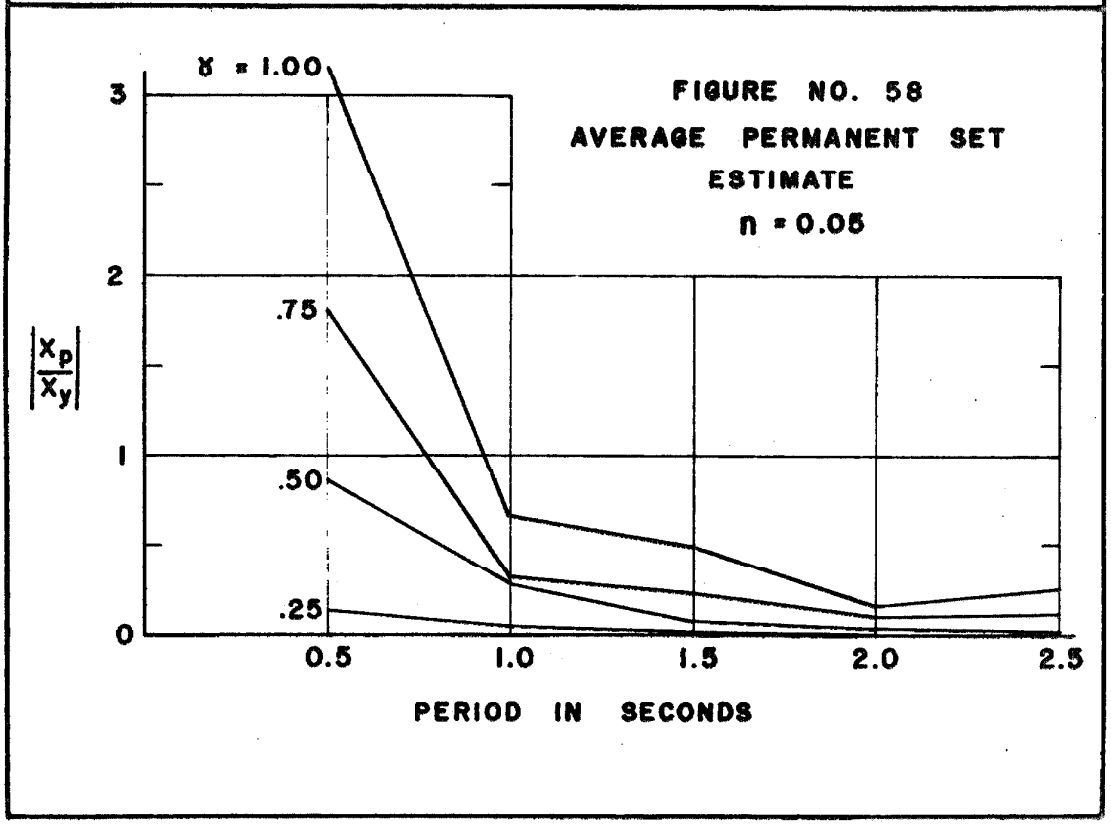
FIGURE NO. 58
AVERAGE PERMANENT SET
ESTIMATE
n = 0.05
γ = 1.00
.75
.50
.25
$\left|\frac{X_p}{X_y}\right|$
3
2
1
0
0.5
1.0
1.5
2.0
2.5
PERIOD IN SECONDS

FIGURE NO. 59

AVERAGE PERMANENT SET

ESTIMATE

$\eta = 0.02$

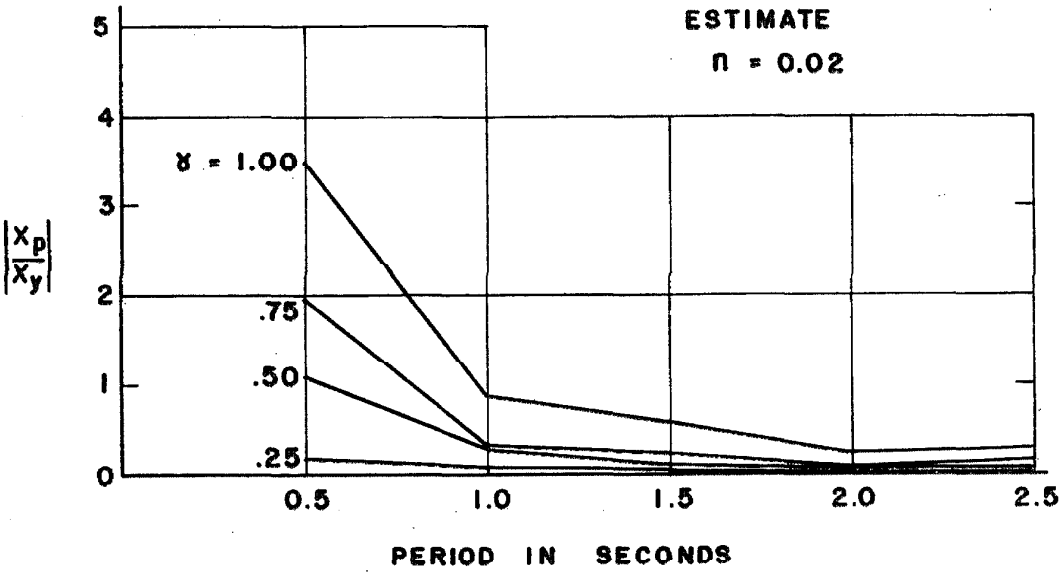

FIGURE NO. 60

AVERAGE PERMANENT SET

ESTIMATE

$\eta = 0$

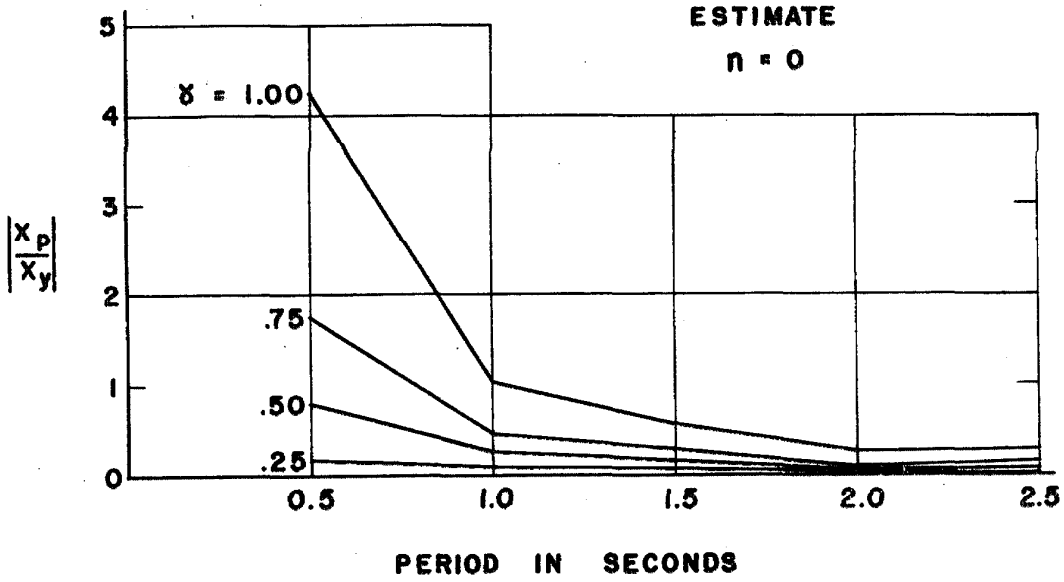

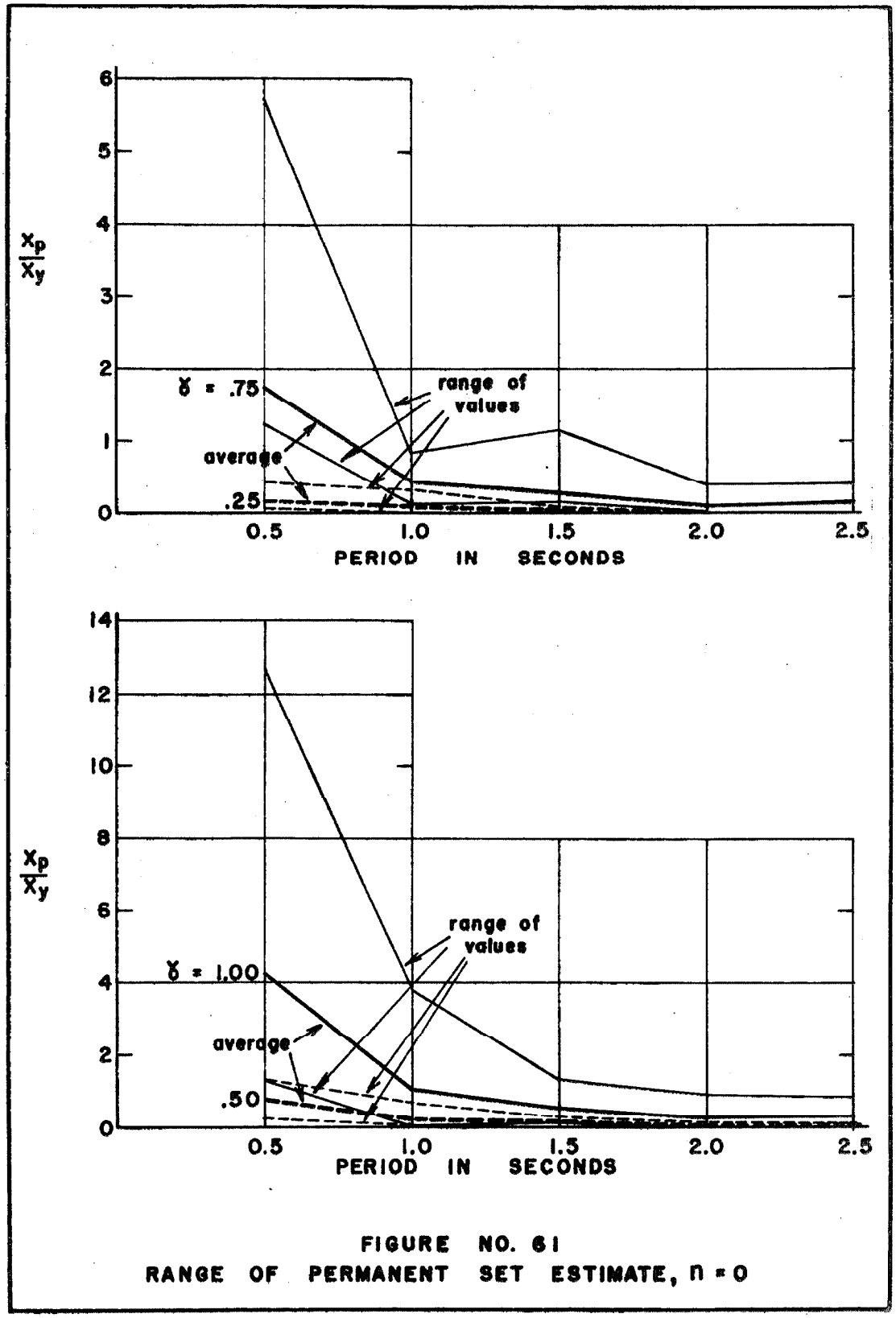

FIGURE NO. 61
RANGE OF PERMANENT SET ESTIMATE, n = 0

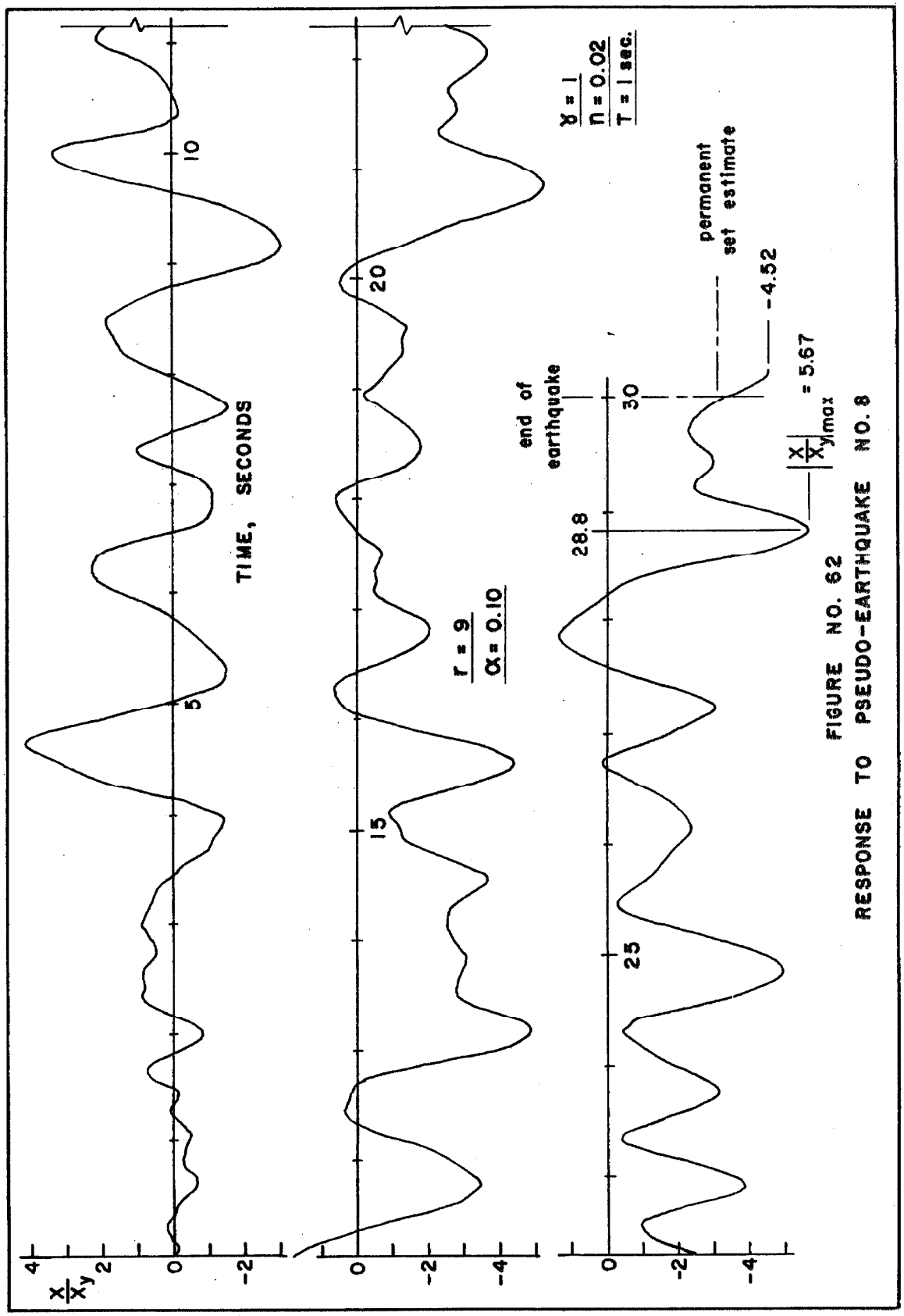

FIGURE NO. 62
RESPONSE TO PSEUDO-EARTHQUAKE NO. 8

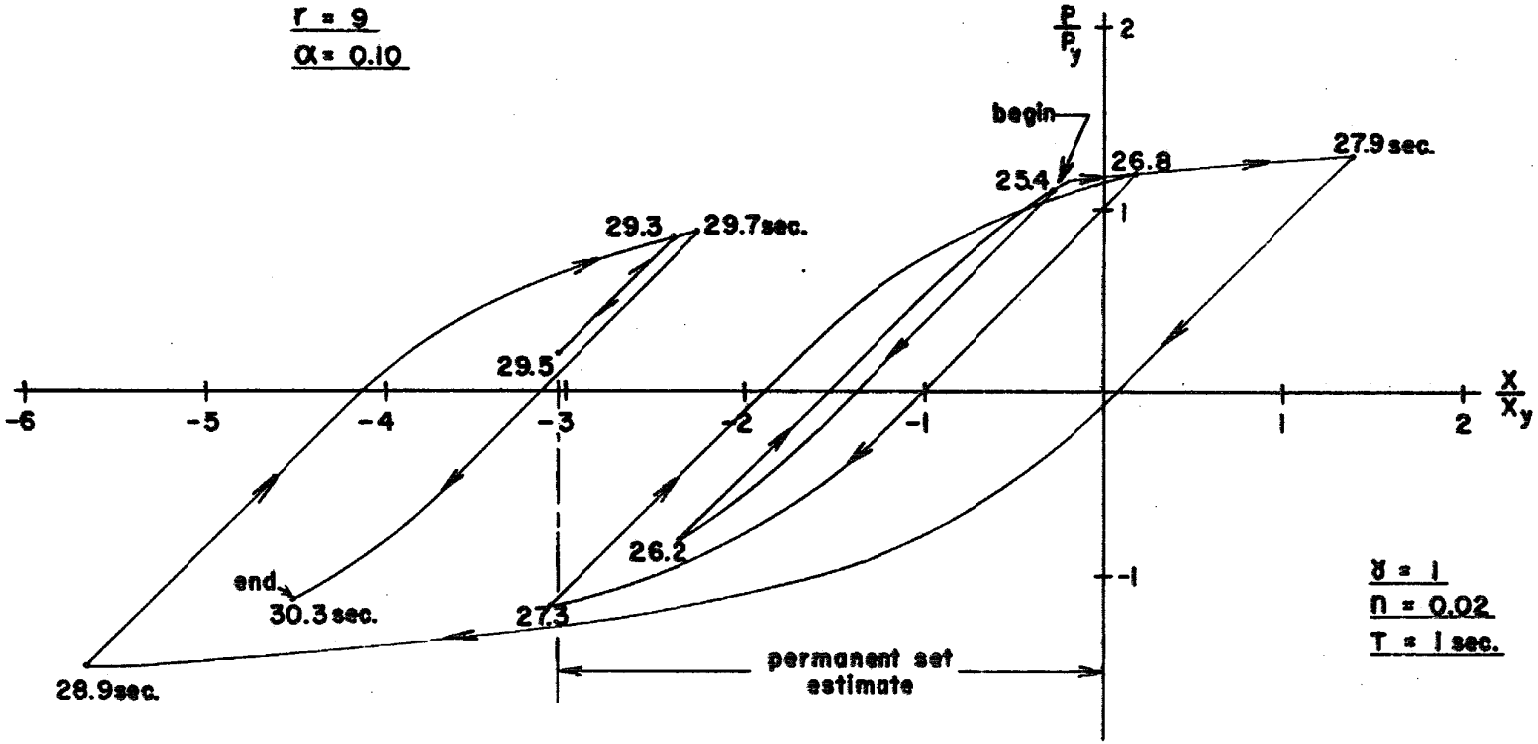

FIGURE NO. 63

A PORTION OF THE HYSTERETIC RESPONSE TO PSEUDO-EARTHQUAKE NO. 8

two pseudo-earthquakes and checking each of the approximately 170 decisions that were made. The subroutine determining the intersections of the min and max curves with the skeleton curve was checked by finding all three intersections for several test cases. A count of the number of iterations necessary for convergence was made to insure that adequate starting values were used and to serve as an error halt in operation of the subroutine.

To check the Simpson's Rule integration for E_v and E_p a short section of an earthquake was analyzed in the usual manner. E_p was evaluated exactly by integrating along the hysteresis curves and the E_v integral was checked by performing a Simpson's Rule computation by hand. The values of the permanent set estimate and E_s were easily verified by hand calculation.

Discussion of Results

Judging from the moderate range of the displacement spectra and the uniform spacing of the averages, it appears that the average of the displacement spectra is determined adequately by the eight pseudo-earthquakes. From these averages it is apparent that for a constant acceleration ratio the expected value of the maximum displacement x/x_y increases with a decrease in period. For earthquake strength $\ddot{\bar{y}}$ constant this implies that for the same yield level q_y, the expected value of the maximum displacement as measured by x/x_y is less for structures with greater periods. Again with $\ddot{\bar{y}}$ constant, it should be noted that if the yield level is constant equation

4.18 states that along a curve of constant q_y the yield displacement $x_y = q_y/\omega_o^2$. Therefore as the period decreases the ratio x/x_y increases but the value of x_y decreases as T^2. If the results are re-examined in terms of the response for constant x_y it will be found that as T goes to zero x/x_y goes to zero as was stated earlier in this chapter.

The effect of viscous damping upon the average displacement spectra is to decrease the magnitude of the average and to decrease the relative dispersion of the data. However, changes in viscous damping do not appear to affect the qualitative nature of the displacement spectra.

Figure 50 gives the average energy input as a function of the natural period of small oscillations. Since the structure can contain elastically only an energy input of about unity, this figure gives the amount of energy that must be dissipated by the structure in response to strong-motion earthquakes of various strengths. The average curves all have the same general shape and it is seen that the relative range of the energy input decreases as the acceleration ratio γ increases. For a linear structure a doubling of γ would increase the energy input 4 times and an interesting comparison is made by multiplying the energy input for $\gamma = 0.25$ by 16 and comparing with the average for $\gamma = 1.00$ as shown in figure 50. Since the behavior of the structure for $\gamma = 0.25$ is close to linear this comparison reinforces G.W. Housner's assumption that the total energy input to a yielding structure is approximately the same as for a linear structure with the same natural period.

The energy dissipation spectra compare the relative amounts of energy dissipated by viscous damping and by yielding. As the strength of the earthquake increases the proportion of energy dissipated by yielding increases, and the same effect is produced by a decrease in viscous damping. From figures 54 and 55 it is seen that a decrease in the acceleration ratio results in an increase in the percentage dispersion of the results. For a constant acceleration ratio it is clearly seen from these figures that an increase in period results in relatively more energy dissipated by viscous damping, i. e., more nearly linear behavior.

The figures for the permanent set x_p/x_y show that eight pseudo-earthquakes were not enough to define the averages well as judged by the inconsistent spacing of the averages and the wide range of the data. As the allowable permanent set is a function of variables besides the yield displacement, figures 57-61 are useful mainly for discussing a particular structure whose permissible permanent set is known. From these figures it can be concluded that a decrease in acceleration ratio rapidly reduces the expected value of the permanent set and the figures indicate that for an acceleration ratio of 0. 50 or less the permanent set is probably not critical.

In all the figures discussed above there is evident a transition from behavior that is essentially linear to that whose character is dominated by the yielding properties of the structure. The point at which the structural behavior might be considered linear is dependent upon the acceleration ratio, the viscous damping, and the natural

period of small oscillations. It is almost certain that the yielding parameters r and α have an effect on this transition also.

To show the application of these curves to the analysis of earthquake response a simple example is presented. It is assumed that a one degree-of-freedom structure is to be analyzed that has yielding properties that can be adequately described by r=9 and α =0.10. The structure has a yield level of 0.10g, a natural period of 1 second, and 2 per cent of critical viscous damping. It is desired to find information about the response of this structure to earthquakes of the strength of the El Centro 1940 shock.

From Table IV the acceleration ratio for this example is 0.62 and from figure 47 it is found that the expected value of the maximum displacement is about three times the yield displacement. Figure 50 indicates that this structure could expect an energy input of $40/\frac{1}{2} x_y p_y$, that is, about 40 times what it can contain elastically. From figure 53 it is found that about 1/4 of this energy would be dissipated by viscous friction and 3/4 by yielding. The expected value of the permanent set is found from figure 59 to be about 1/2 the yield displacement.

Considering the same structure with a period of two seconds, the expected value of the maximum displacement ratio would be 1.6. The expected energy input would be $10/\frac{1}{2} x_y p_y$ and 1/3 of this would be dissipated by viscous damping and 2/3 by yielding. The expected value of the permanent set is about 0.15 times the yield displacement. Comparing the two structures, equation 4.18 implies that the yield

displacement x_y of this second structure is four times that of the first. In terms of the yield displacement of the first structure the expected maximum displacements of the first and second structures are 3 and 6.4 respectively, and the expected permanent sets are .5 and .6.

E. Summary and Conclusions

A class of nonlinear yielding structures that is defined by the geometry of the hysteresis curves and by the law describing yielding response has been presented. The class was seen to include the linear, the elasto-plastic, and the bilinear hysteretic structures. It also contains the general yielding structure presented in chapter III. The application of the hysteresis law to this structure was discussed. The equation of motion and the energy equation for the response of a one-degree-of-freedom yielding structure to earthquake excitation have been derived and discussed in detail. The ratio of the acceleration strength $\ddot{\bar{y}}$ to the yield level q_y of the structure was found to be the parameter measuring the relative magnitude of the excitation and this acceleration ratio γ was estimated for four strong-motion earthquakes using as $\ddot{\bar{y}}$ the r. m. s. of the strong-motion portion of the accelerogram. The response of the yielding structure described by r=9, α=0.10 to the ensemble of eight pseudo-earthquakes was then calculated for four values of γ. Included in the results were the average maximum displacement, the average energy input, the average estimated permanent set, and the average proportion of energy dissipated by viscous damping and by yielding. The results were

discussed and examples given to illustrate the application of the results to earthquake response studies.

It is concluded that results such as presented in this chapter would be useful in analysis of the earthquake response of yielding structures. The results of the study for $r=9$, $\alpha=0.10$ indicate that if the yielding parameters can be determined the average values of the response of the structure can be found and estimates of the reliability of these averages can be made.

The class of yielding structures defined here is considered to be general enough to provide a means for investigating the response of actual structures. It is thought that many real structures exhibit yielding behavior that can be approximated by the hysteresis law given here, but research is clearly needed into the dynamic behavior of actual structures in the yielding range to test the applicability of both the hysteresis law and the general yielding structure. To approximate the hysteresis law governing the response of a particular structure it is necessary that tests include transient as well as periodic response and, if possible, the response to complex or random excitation.

REFERENCES

1. Alford, J. L., Housner, G. W., and Martel, R. R., Spectrum Analyses of Strong-Motion Earthquakes, Pasadena: California Institute of Technology Earthquake Research Laboratory, (1951).

2. Berg, G. V., and Housner, G. W., "Integrated Velocity and Displacement of Strong Earthquake Ground Motion", Bulletin of the Seismological Society of America, Vol. 51, No. 2, (April 1961), pp. 175-189.

3. Hudson, D. E., "Response Spectrum Techniques in Engineering Seismology", World Conference on Earthquake Engineering, Berkeley, California (June 1956).

4. Housner, G. W., "Behavior of Structures During Earthquakes", Proceedings of the American Society of Civil Engineers, Vol. 85, No. EM4 (Oct. 1959), pp. 109-129.

5. Hudson, D. E., "Some Problems in the Application of Spectrum Techniques to Strong-Motion Earthquake Analysis", Bulletin of the Seismological Society of America, Vol. 52, No. 2 (April 1962), pp. 417-430.

6. Goodman, L. E., Rosenblueth, E., and Newmark, N. M., "Aseismic Design of Firmly Founded Elastic Structures", Transactions of the American Society of Civil Engineers, Vol. 120, (1955), pp. 782-802.

7. Rosenblueth, E., "Some Applications of Probability Theory in Aseismic Design", World Conference on Earthquake Engineering, Berkeley, California (June 1956).

8. Caughey, T. K., and Stumpf, H. J., "Transient Response of a Dynamic System Under Random Excitation", Journal of Applied Mechanics, Vol. 28, No. 4, (Dec. 1961), pp. 563-566.

9. Bogdanoff, J. L., Goldberg, J. E., and Bernard, M. C., "Response of a Simple Structure to a Random Earthquake-Type Disturbance", Bulletin of the Seismological Society of America, Vol. 51, No. 2 (April 1961), pp. 293-310.

10. Rosenblueth, E., and Bustamente, J. I., "Distribution of Structural Response to Earthquakes", Proceedings of the American Society of Civil Engineers, Vol. 88, No. EM3, (June 1962), pp. 75-106.

11. Clough, R. W., "On the Importance of Higher Modes of Vibration in the Earthquake Response of a Tall Building", Bulletin of the Seismological Society of America, Vol. 45, No. 4, (Oct. 1955), pp. 289-301.

12. Clough, R. W., "Dynamic Effects of Earthquakes", Proceedings of the American Society of Civil Engineers, Vol. 86, No. ST4, (April 1960), pp. 49-65.

13. Thomaides, S. S., "Effect of Inelastic Action on the Behavior of Structures During Earthquakes", Ph. D. Thesis, University of Michigan, (1961).

14. Tanabashi, R., "Studies on the Nonlinear Vibrations of Structures Subjected to Destructive Earthquakes", Proceedings of the World Conference on Earthquake Engineering, Berkeley, California, (June 1956).

15. Tanabashi, R., "Non-linear Transient Vibration of Structures", Proceedings of the Second World Conference on Earthquake Engineering, Vol. II, Tokyo and Kyoto, Japan, (July 1960).

16. Veletsos, A. S., and Newmark, N. M., "Effect of Inelastic Behavior on the Response of Simple Systems to Earthquake Motions", Proceedings of the Second World Conference on Earthquake Engineering, Vol. II, Tokyo and Kyoto, Japan, (July 1960).

17. Penzien, J., "Dynamic Response of Elasto-Plastic Frames", Proceedings of the American Society of Civil Engineers, Vol. 86, No. ST7, (July 1960), pp. 81-94.

18. Bycroft, G. N., Murphy, M. J., and Brown, K. J., "Electrical Analog for Earthquake Yield Spectra", Proceedings of the American Society of Civil Engineers, Vol. 85, No. EM4, (Oct. 1959), pp. 43-64.

19. Bycroft, G. N., "White Noise Representation of Earthquakes", Proceedings of the American Society of Civil Engineers, Vol. 86, No. EM2, (April 1960), pp. 1-16.

20. Housner, G. W., "Limit Design of Structures to Resist Earthquakes", Proceedings of the World Conference on Earthquake Engineering, Berkeley, California, (June 1956).

21. Housner, G. W., "The Plastic Failure of Frames During Earthquakes", Proceedings of the Second World Conference on Earthquake Engineering, Vol. II, Tokyo and Kyoto, Japan, (July 1960).

22. Berg, G. V., "The Analysis of Structural Response to Earthquake Forces", Ph. D. Thesis, University of Michigan, (1958).

23. Berg, G. V., and Da Deppo, D. A., "Dynamic Analysis of Elasto-Plastic Structures", Proceedings of the American Society of Civil Engineers, Vol. 86, No. EM2, (April 1960), pp. 35-58.

24. Berg, G. V., "Response of Multi-story Structures to Earthquake", Proceedings of the American Society of Civil Engineers, Vol. 87, No. EM2, (April 1961), pp. 1-16.

25. Bycroft, G. N., "Yield Displacements in Multistory Aseismic Design", Bulletin of the Seismological Society of America, Vol. 50, No. 3 (July 1960), pp. 441-453.

26. Penzein, J., "Elasto-Plastic Response of Idealized Multi-story Structures Subjected to a Strong Motion Earthquake", Proceedings of the Second World Conference on Earthquake Engineering, Vol. II, Tokyo and Kyoto, Japan, (July 1960).

27. Iwan, W. D., "The Dynamic Response of Bilinear Hysteretic Systems", Ph. D. Thesis, California Institute of Technology, (1961).

28. Caughey, T. K., "Sinusoidal Excitation of a System with Bilinear Hysteresis", Journal of Applied Mechanics, Vol. 27, No. 4, (Dec. 1960), pp. 640-643.

29. Caughey, T. K., "Random Excitation of a System with Bilinear Hysteresis", Journal of Applied Mechanics, Vol. 27, No. 4, (Dec. 1960), pp. 649-652.

30. Muto, K., et. al. (Response Analyzer Committee), "Non-linear Response Analyzers and Application to Earthquake Resistant Design", Proceedings of the Second World Conference on Earthquake Engineering, Vol. II, Tokyo and Kyoto, Japan, (July 1960).

31. Ando, N., "Non-linear Vibrations of Building Structures", Proceedings of the Second World Conference on Earthquake Engineering", Vol. II, Tokyo and Kyoto, Japan, (July 1960).

32. Jacobsen, L. S., "Dynamic Behavior of Simplified Structures Up to the Point of Collapse", Proceedings of the Symposium on Earthquake and Blast Effects on Structures, Los Angeles, California, (June 1952).

33. Jacobsen, L. S., "Damping in Composite Structures", Proceedings of the Second World Conference on Earthquake Engineering, Vol. II, Tokyo and Kyoto, Japan, (July 1960).

34. Tanabashi, R., and Kaneta, K., "On the Relation Between the Restoring Force Characteristics of Structures and the Pattern of Earthquake Ground Motion", Proceedings of Japan National Symposium on Earthquake Engineering, Tokyo, Japan, (1962).

35. Pisarenko, G. S., Vibrations of Elastic Systems Taking Account of Energy Dissipation in the Material, Technical Documentary Report No. WADD TR 60-582, (February 1962).

36. Kobayashi, H., "Seismic Coefficients of Buildings Determined by Frequency of Earthquakes", Proceedings of Japan Symposium on Earthquake Engineering, Tokyo, Japan, (1962). (In Japanese with English Summary).

37. Okamuto, S. and Hakuno, M., "On the Elastic-Plastic Vibration of the Ground", Ibid. (In Japanese with English Summary).

38. Hisada, T., Nakagawa, K., and Izuma, M., "Earthquake Response of Structures Having Various Restoring Force Characteristics", Ibid., (In English).

39. Muto, K., et. al., "A Study of the Earthquake Response of an Actual Building by the Analog Computer 'SERAC' ", Ibid., (In English).

40. Housner, G. W., "Characteristics of Strong-Motion Earthquakes", Bulletin of the Seismological Society of America, Vol. 37, No. 1, (Jan. 1947), pp. 19-31.

41. Housner, G. W., "Properties of Strong Ground Motion Earthquakes", Bulletin of the Seismological Society of America, Vol. 45, No. 3 (July 1955), pp. 197-218.

42. Bendat, J. S., Principles and Applications of Random Noise Theory, New York: John Wiley & Sons, Inc. (1958).

43, Davenport, B. D., Jr., and Root, W. L., An Introduction to the Theory of Random Signals and Noise, New York: Mc-Graw-Hill Book Company, Inc., (1958).

44. Crandall, W. H., et. al., Random Vibrations, New York: The Technology Press and John Wiley & Sons, Inc., (1958).

45. Wax, N., ed., Selected Papers on Noise and Stochastic Processes, New York: Dover Publications (1954).

46. Harris, C. M., and Crede, C. E., eds., Shock and Vibration Handbook, Vol. I, Chapter 11, New York: McGraw-Hill Book Company, Inc., (1961).

47. Laning, J. H., Jr., and Battin, R. H., Random Processes in Automatic Control, New York: McGraw-Hill Book Company, Inc., (1956).

48. Tajima, H., "A Statistical Method of Determining the Maximum Response of a Building Structure During an Earthquake", Proceedings of the Second World Conference on Earthquake Engineering, Vol. II, Tokyo and Kyoto, Japan, (July 1960).

49. Kanai, K., "Semi-empirical Formula for the Seismic Characteristics of the Ground", Bulletin of the Earthquake Research Institute, University of Tokyo, Vol. 35, (June 1957), pp. 309-325.

50. Franklin, J. N., "Deterministic Simulation of Random Processes", Mathematics of Computation, Vol. 17, No. 81, (Jan. 1963), pp. 28-59.

51. Franklin, J. N., "Digital Computer Simulation of Random Processes", Solid Mechanics Seminar at the California Institute of Technology, Nov. 20, 1962.

52. Ramberg, W., and Osgood, W. R., "Description of Stress-Strain Curves by Three Parameters", NACA TN 902, (July 1943).

53. Ang, A. H., "Analysis of Frame with Non-linear Behavior", Proceedings of the American Society of Civil Engineers, Vol. 86, No. EM3, (June 1960), pp. 1-24. Discussion by Wilson, E. L., Ibid., Vol. 86, No. EM6 (Dec. 1960), pp. 97-99.

54. Eppink, R. T., et. al., Experimental Study of Effects of Repeated Blast Loadings on Structural Elements, Pasadena, California: National Engineering Science Co. (May 1962).

55. Welding Research Council and the American Society of Civil Engineers, Commentary on Plastic Design in Steel, ASCE Manual of Engineering Practice No. 41, (1961).

56. Popov, E. P., and McCarthy, R. E., "Deflection Stability of Frames Under Repeated Loads", Proceedings of the American Society of Civil Engineers, Vol. 86, No. EM1, (Jan. 1960), pp. 61-78.

57. Hildebrand, F. B., Introduction to Numerical Analysis, New York: McGraw-Hill Book Company, Inc., (1956).

58. Lazard, A., "The effect of Plastic Yield in Bending on Mild Steel Girders", Structural Engineering, Vol. 32, No. 49, (1954).

59. Blume, J. A., Newmark, N. M., and Corning, L. H., Design of Multistory Reinforced Concrete Buildings for Earthquake Motions, Chicago: Portland Cement Association, (1961).

60. Berg, G. V., and Thomaides, S. S., "Energy Consumption by Structures in Strong-Motion Earthquakes", Proceedings of the Second World Conference on Earthquake Engineering, Vol. II, Tokyo and Kyoto, Japan, (July 1960).

61. Housner, G. W., "Intensity of Ground Motion During Strong Earthquakes", Second Tech. ONR Report, California Institute of Technology Earthquake Research Lab., (Aug. 1951).

APPENDIX I

Numerical Integration of Equations 2. 21, 2. 26, 3. 39 and 4. 17.

In the course of the thesis work it was necessary to integrate numerically the following differential equations

$$\ddot{z} + 2bc\dot{z} + c^2 z = -\sqrt{a}\, N(t) \tag{2.21}$$

$$\ddot{z} + 2n\omega\dot{z} + \omega^2 z = -\ddot{y}(t) \tag{2.26}$$

$$\frac{x''}{x_y} + \frac{p}{p_y}\left(\frac{x}{x_y}\right) = \frac{F_o}{p_y}\cos(\eta\tau) \tag{3.39}$$

$$\frac{x''}{x_y} + 2n\frac{x'}{x_y} + \frac{p}{p_y}\left(\frac{x}{x_y}\right) = -\frac{\ddot{y}}{q_y}\sigma(\tau/\omega_o) \tag{4.17}$$

These equations are of the form

$$w'' + 2jw' + kp(w) = -mF(q\tau) \tag{I-1}$$

where w is the integration variable; p is a function of w; j, k, m and q are constants; and $F(q\tau)$ is the excitation. The primes indicate differentiation with respect to τ which is a constant times t.

The numerical procedure used to integrate equation I-1 is a third order Runge-Kutta method attributed to Heun and is discussed in reference 57, pp. 233-239. This method was chosen because of its long-range stability, its self-starting feature, and because it can be adapted readily to cases where the excitation is not defined at regular intervals. It has the disadvantage of being slower than other less flexible methods of comparable accuracy. Letting $y = w'$ equation I-1 becomes

$$w' = y$$

$$y' = -mF(q\tau) - kp(w) - 2jy \tag{I-2}$$

The Runge-Kutta formulae for the $s+1^{st}$ integration step are

$$w_{s+1} = w_s + \frac{1}{4}(K_o + 3K_2) \qquad \text{(I-3)}$$

$$y_{s+1} = y_s + \frac{1}{4}(M_o + 3M_2)$$

where

$$K_o = \Delta\tau y_s$$

$$K_1 = \Delta\tau(y_s + 1/3M_o)$$

$$K_2 = \Delta\tau(y_s + 2/3M_1)$$

$$M_o = -\Delta\tau\left(mF(q\tau_s) + kp(w_s) + 2j\,y_s\right) \qquad \text{(I-4)}$$

$$M_1 = -\Delta\tau\left(mF\left[q(\tau_s + 1/3\Delta\tau)\right] + kp(w_s + 1/3K_o) + 2j(y_s + 1/3M_o)\right)$$

$$M_2 = -\Delta\tau\left(mF\left[q(\tau_s + 2/3\Delta\tau)\right] + kp(w_s + 2/3K_1) + 2j(y_s + 2/3M_1)\right)$$

By simplifying equations I-3 and I-4 one obtains

$$w_{s+1} = w_s + w_s'\Delta\tau + 1/2M_1\Delta\tau$$

$$w'_{s+1} = w_s' + 1/4(M_o + 3M_2) \qquad \text{(I-5)}$$

and

$$M_o = -\Delta\tau\left(mF(q\tau_s) + kp(w_s) + 2jw_s'\right)$$

$$M_1 = -\Delta\tau\left(mF\left[q(\tau_s + 1/3\Delta\tau)\right] + kp(w_s + 1/3w_s'\Delta\tau) + 2j(w_s' + 1/3M_o)\right)$$

$$M_2 = -\Delta\tau\left(mF\left[q(\tau_s + 2/3\Delta\tau)\right] + kp(w_s + 2/3w_s'\Delta\tau + 2/9M_o\Delta\tau) + 2j(w_s' + 2/3M_1)\right) \qquad \text{(I-6)}$$

For application to equation 4.17 equation I-6 becomes

$$M_o = -\Delta\tau\left[\frac{\ddot{\bar{y}}}{q_y}\,\sigma\left(\frac{\tau_s}{\omega_o}\right) + \frac{p}{p_y}\,(w_s) + 2nw_s'\right]$$

$$M_1 = -\Delta\tau\left[\frac{\ddot{\bar{y}}}{q_y}\,\sigma\left(\frac{\tau_s + 1/3\Delta\tau}{\omega_o}\right) + \frac{p}{p_y}\,(w_s + 1/3w_s'\Delta\tau) + 2n(w_s + 1/3M_o)\right]$$

$$M_2 = -\Delta\tau\left[\frac{\ddot{\bar{y}}}{q_y}\,\sigma\left(\frac{\tau_s + 2/3\Delta\tau}{\omega_o}\right) + \frac{p}{p_y}\,(w_s + 2/3w_s'\Delta\tau + 2/9M_o\Delta\tau) + 2n(w_s' + 2/3M_1)\right] \qquad (I\text{-}7)$$

To integrate for the velocity spectra using equation 2.26, equation 2.26 was first transformed by letting $\tau = \omega t$ and $w = z\omega^2/g$. This equation then becomes:

$$w'' + 2nw' + w = \frac{1}{g}\,\ddot{y}(\tau/\omega) \qquad (I\text{-}8)$$

The velocity spectrum value is given by

$$S_v = \frac{g}{\omega}\left|w'\right|_{max} \qquad (I\text{-}9)$$

For the integration of equation I-8

$$M_o = -\Delta\tau\left[\frac{1}{g}\ddot{y}\left(\frac{\tau_s}{\omega}\right) + w_s + 2nw_s'\right]$$

$$M_1 = -\Delta\tau\left[\frac{1}{g}\ddot{y}\left(\frac{\tau_s + 1/3\Delta\tau}{\omega}\right) + (w_s + 1/3w_s'\Delta\tau) + 2n(w_s + 1/3M_o)\right]$$

$$M_2 = -\Delta\tau \left[\frac{1}{g} \ddot{y} \left(\frac{\tau_s + 2/3\Delta\tau}{\omega} \right) + (w_s + 2/3 w_s' \Delta\tau + 2/9 M_o \Delta\tau) + 2n(w_s' + 2/3 M_1) \right] \quad \text{(I-10)}$$

The application of the method to equations 2. 21 and 3. 39 is similar to that for equation 4. 17. Because only one value of c was used in equation 2. 21 it was not transformed as was equation 2. 26.

As noted in the text, the pseudo-earthquake accelerograms and the approximate white noise were defined at intervals of Δh = 0. 025 sec. and it was assumed that the records were straight lines between these points. It was felt that it would be desirable for the integration interval $\Delta\tau$ to be compatible with the interval of the excitation, and in particular $\Delta\tau$ should be chosen so that the corresponding $\Delta t = \Delta\tau / \omega$ would never exceed Δh. To insure this Δt was taken as a fraction of Δh which implies that

$$\Delta\tau = \frac{\omega \Delta h}{K} \quad \text{(I-11)}$$

where K is an integer. With the integration step chosen in this manner the closest possible following of the excitation record is achieved and the integer K is the number of integration steps used to span the basic interval of the excitation. The integration steps must satisfy one other condition as the truncation error involved in this integration method is order of $(\Delta\tau)^4$. To make this error sufficiently small the additional requirement

$$\Delta\tau \leq 0.15 \quad \text{(I-12)}$$

was imposed and where feasible $\Delta\tau$ was usually less than 0.10. Using equations I-11 and I-12 sets of natural frequencies and integration steps were chosen for each calculation and are given in the following tables. The natural periods to three significant figures and the values of K are also given. For integration of equation 3.39 a correspondence between integration steps and excitation intervals was not needed and $\Delta\tau$ was taken as not greater than $\pi/25$ and usually as $\pi/50$.

TABLE I-1

Natural Frequencies and Integration Steps for Equation 2.21

($\Delta h = 0.025$)

$\omega = c$	$T = \frac{2\pi}{\omega}$	$\Delta\tau$	K
15.56	.404	.09725	4

TABLE I-II

Natural Frequencies and Integration Steps for Equation 2.26 (Δh=0.025)

ω	$T = \frac{2\pi}{\omega}$	$\Delta\tau$	K
60	.105	.15	10
30	.209	.15	5
20	.314	.10	5
16	.393	.10	4
12	.524	.10	3
10	.628	.125	2
9	.698	.1125	2
8	.785	.10	2
7	.898	.0875	2
6.3	.997	.07875	2
5.2	1.21	.065	2
4.5	1.40	.1125	1
3.9	1.61	.0975	1
3.5	1.80	.0875	1
3.1	2.03	.0775	1
2.9	2.17	.0725	1
2.6	2.42	.065	1
2.4	2.62	.06	1
2.2	2.86	.055	1
2.1	2.99	.0525	1

TABLE I-III

Natural Frequencies and Integration Steps for Equation 4.17 (Δh=0.025)

ω (8 figs.)	$T = \frac{2\pi}{\omega}$	$\Delta\tau$	K
12.566371	.50	.10471976	3
6.2831853	1.00	.078539816	2
4.1887902	1.50	.10471976	1
3.1415927	2.00	.078539816	1
2.5132741	2.50	.062831853	1

APPENDIX II

Graphs of $C(x_o)$ vs. x_o/x_y

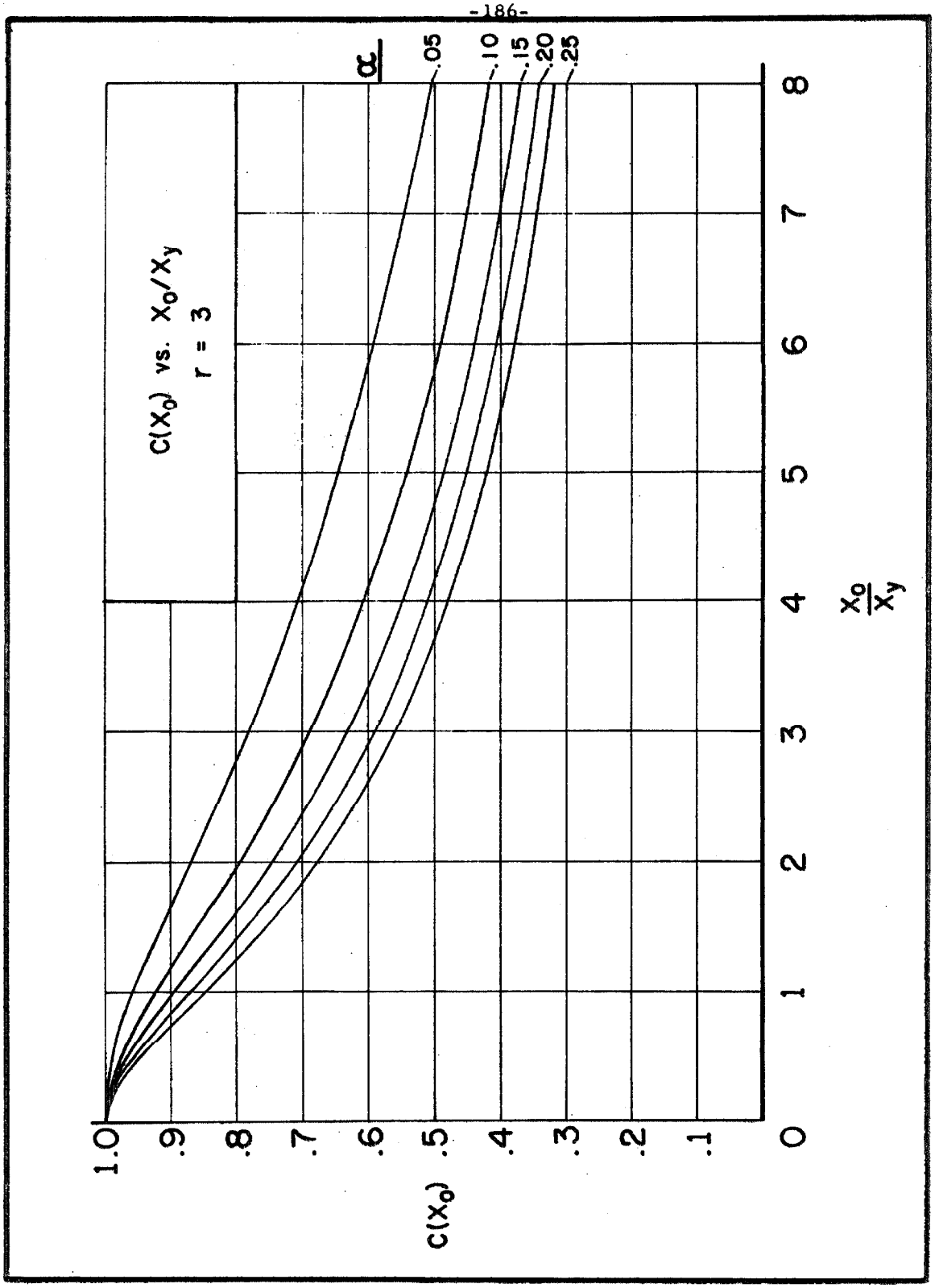
C(X₀) vs. X₀/Xy
r = 3
α
.05
.10
.15
.20
.25
C(X₀)
1.0
.9
.8
.7
.6
.5
.4
.3
.2
.1
0
1
2
3
4
5
6
7
8
X₀/Xy

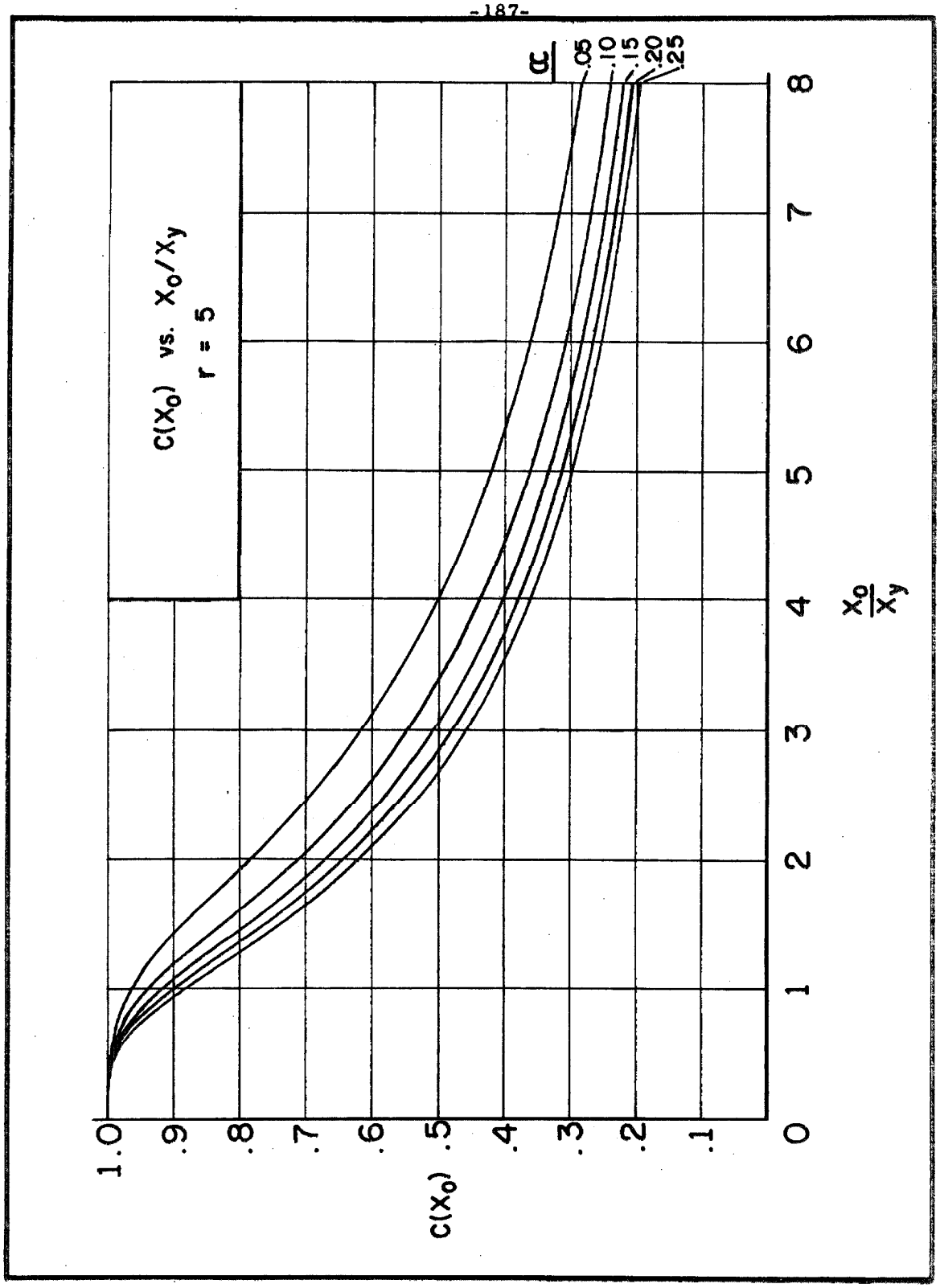
$C(X_o)$ vs. X_o/X_y
r = 5
α
.05
.10
.15
.20
.25
$C(X_o)$
1.0
.9
.8
.7
.6
.5
.4
.3
.2
.1
0
1
2
3
4
5
6
7
8
$\frac{X_o}{X_y}$

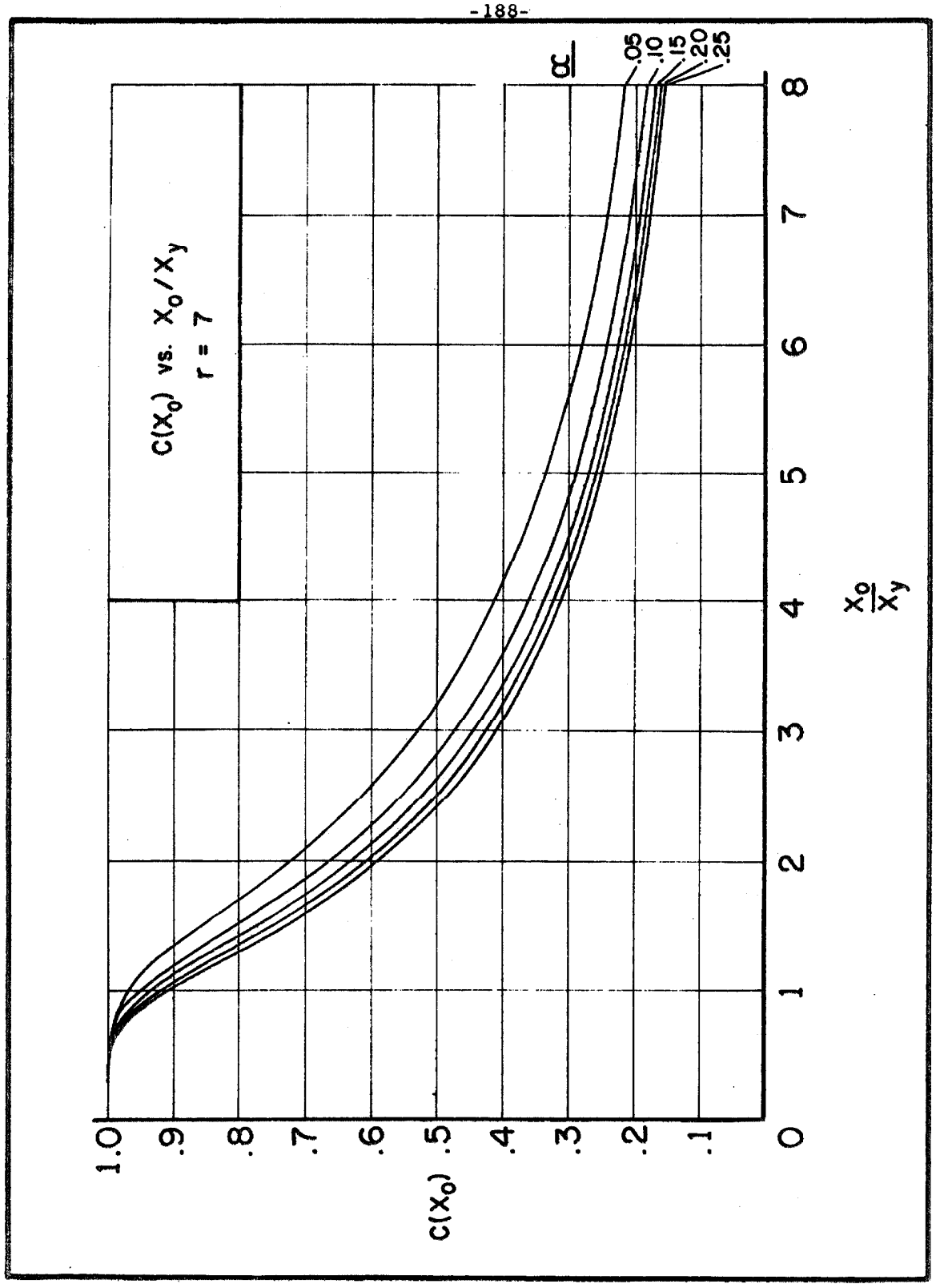
C(X0) vs. X0/Xy
r = 7
α
.05
.10
.15
.20
.25
C(X0)
1.0
.9
.8
.7
.6
.5
.4
.3
.2
.1
0
1
2
3
4
5
6
7
8
X0/Xy

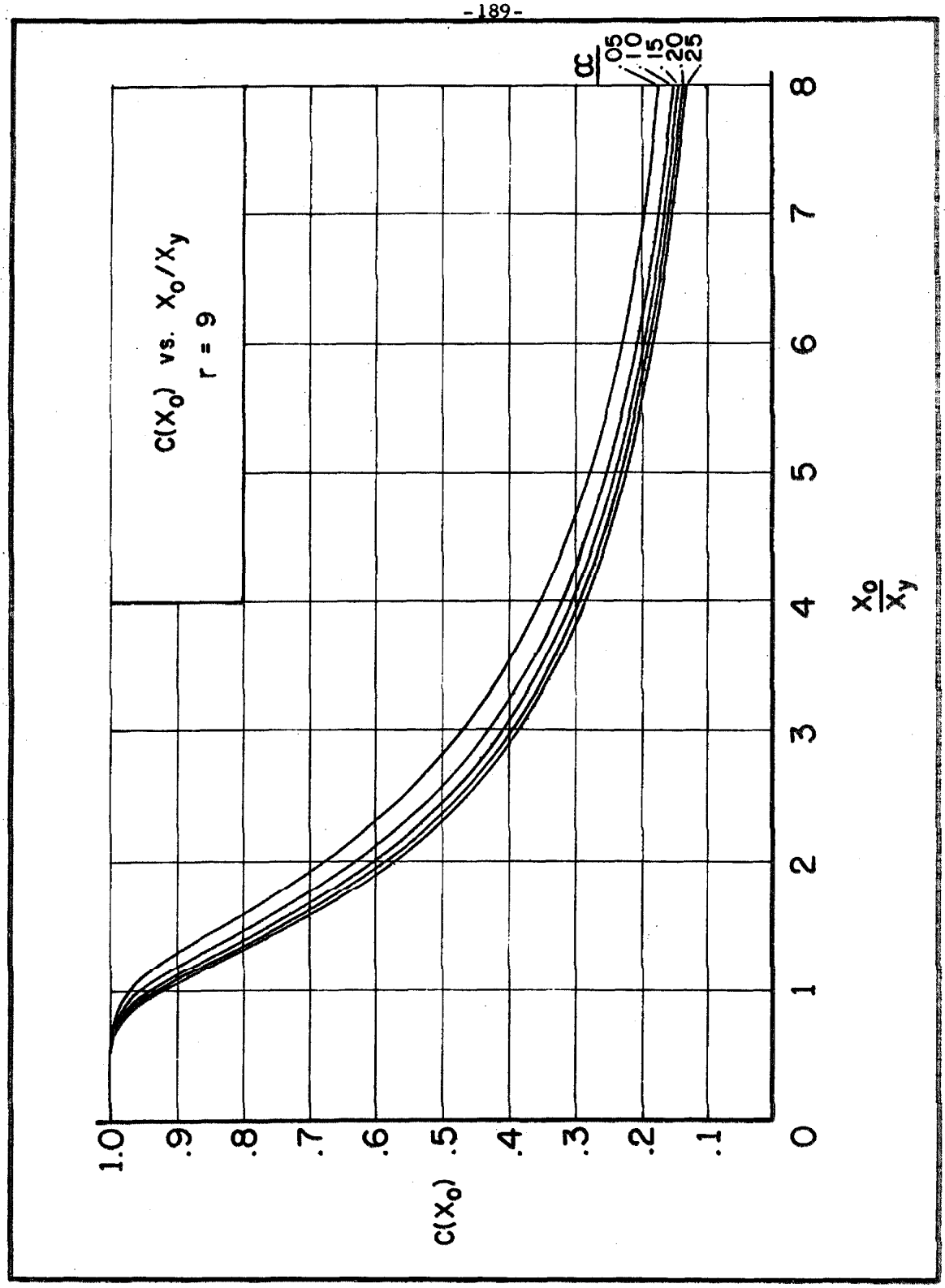
C(X_o) vs. X_o/X_y
r = 9
α
.05
.10
.15
.20
.25
C(X_o)
1.0
.9
.8
.7
.6
.5
.4
.3
.2
.1
0
1
2
3
4
5
6
7
8
X_o/X_y

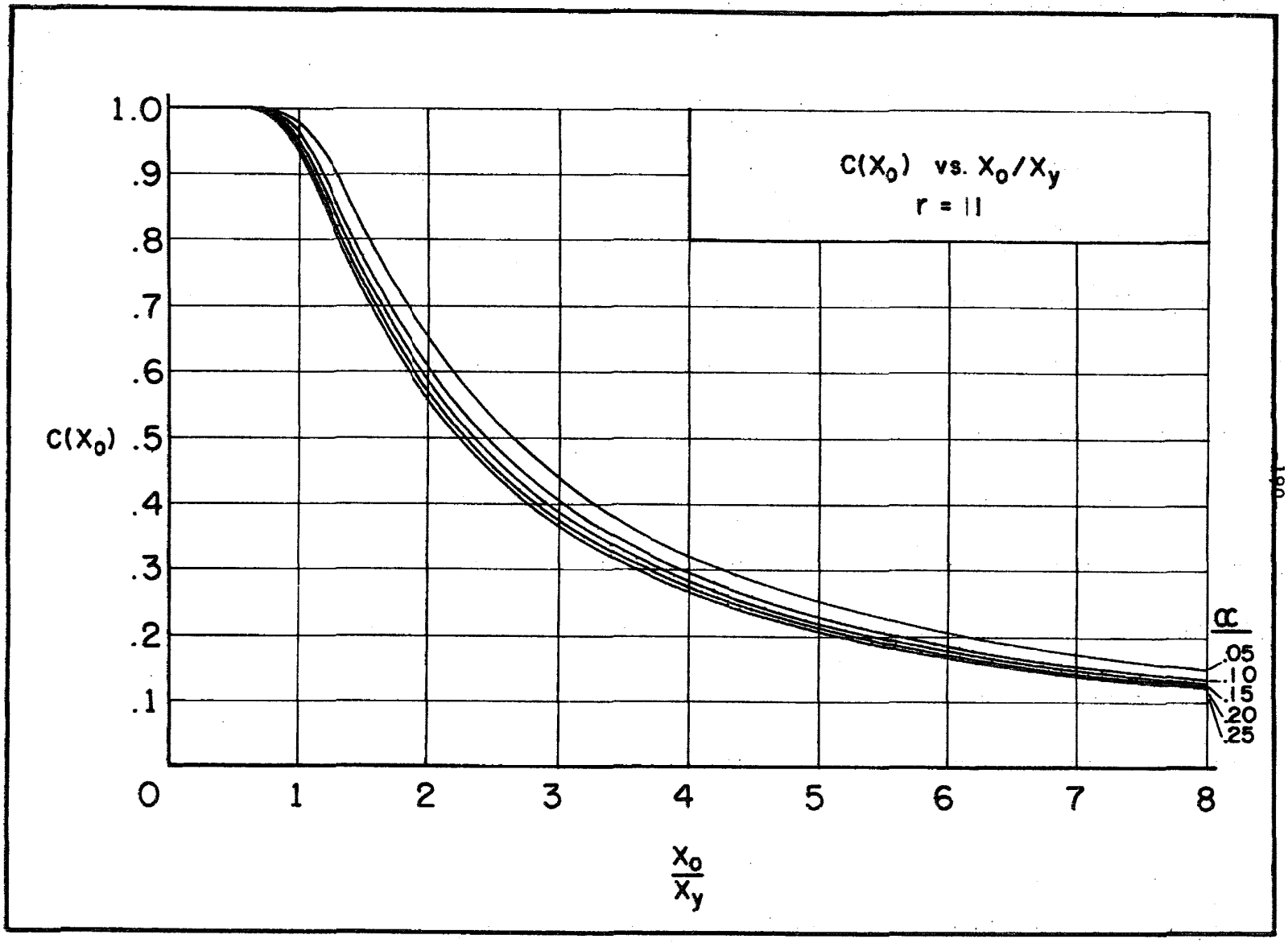
C(X0) vs. X0/Xy
r = 11
C(X0)
1.0
.9
.8
.7
.6
.5
.4
.3
.2
.1
0
1
2
3
4
5
6
7
8
X0/Xy
α
.05
.10
.15
.20
.25